High efficiency blazed gratings in resonance domain

Dissertation

zur Erlangung des akademischen Grades
Doktor-Ingenieur (Dr.-Ing.)

Friedrich-Schiller-Universität Jena

seit 1558

vorgelegt dem Rat der Physikalisch-Astronomischen Fakultät
der Friedrich-Schiller-Universität Jena

von M. Sc.-Engineer Maria Oliva

geboren am 09.01.1980 in Caltanissetta

Gutachter:

1. Prof. Dr. Andreas Tünnermann, Friedrich-Schiller-Universität Jena

2. Prof. Dr. Hartmut Bartelt, Friedrich-Schiller-Universität Jena

3. Prof. Dr. Toralf Scharf, Ecole Polytechnique Fédérale de Lausanne

Tag der Disputation: 04.12.2014

If you cannot explain it simply,
you do not understand it
well enough.

A.Einstein

Contents

Introduction

> *"It is difficult to point to another single device that has brought more important experimental information to every field of science than the diffraction grating. The physicist, the astronomer, the chemist, the biologist, the metallurgist, all use it as a routine tool of unsurpassed accuracy and precision, as a detector of atomic species to determine the characteristics of heavenly bodies and the presence of atmospheres in the planets, to study the structures of molecules and atoms, and to obtain a thousand and one items of information without which modern science would be greatly handicapped."* [1].

This statement of Sir Harrison perfectly points out the importance of diffraction gratings and it explains the reason why after almost 200 years from the first experiment of Joseph von Fraunhofer [2], diffraction gratings are still an attractive research field. Nowadays, diffraction gratings can be found in several industrial applications. For example, they are used as dispersing elements in spectrometers, beam-splitting elements, imaging system [3], pulse-compression gratings for the manipulation of ultrashort laser pulses.

In the family of diffraction gratings, the *blazed gratings* have a key role for their property to redirect the incident light highly efficient in only one diffraction order. Such gratings can operate both in reflection and in transmission. Typically, transmission diffraction gratings are preferred because of their higher flexibility in being used in different optical setups.

However, in resonance domain (i.e. grating period close to wavelength), where the highest dispersion of light can be achieved, the transmission blazed gratings are still not widely used. The reason is because in the past the technology was not capable to fabricate such elements with sufficient quality. In 1997 Lowen and Popov wrote "Transmission gratings are excluded from high dispersion application...because of the impossibility to manufacture small period grating (600gr/mm)[1]..." [4]; and also ten years later Gross still affirmed that the technology to manufacture such blazed structures was not available [5]. For these reasons, in many applications, transmission gratings have been replaced by reflection ones (due the reduced depth required). Furthermore, the most optical setups have been build up in Littrow or close to Littrow configuration[2] in order to achieve the higher efficiency possible with binary gratings.

[1] gr/mm: grooves/millimeter

[2] In Littrow configuration the angle of the diffracted order coincides with the incidence one

In the last years, the improvements in resolution and accuracy of the lithographic technologies, allow to reconsider such statements and to open the possibility to fabricate highly dispersive transmission blazed gratings. The further development in this field is now based on a close synergy between design and fabrication capabilities.

Aim and structure of this thesis

The scope of this work is to design and develop suitable fabrication technologies for high efficient 1D transmission blazed gratings in the resonance domain. The gratings have to work at normal or close to normal incidence, additionally the area of the elements has to be large enough to be used in industrial applications. The normal incidence is required in complex optical setups in order to build up compact or easy-to use systems [6, 7].
Due to the industrial application purpose, the work is focused on monolithic fused silica transmission gratings. The choice of fused silica as grating material, is related to its good transmission properties in the visible spectral region and to the goal to fabricate gratings [8] with a good homogeneity on relative large area ($> 10mm^2$). Even if 15 years ago in [9] Lalanne wrote that there was no way to fabricate binary blazed gratings in glass, nowadays the fused silica microstructuring is actually a mature and reliable technology.
Furthermore, new kind of multilevel blazed structures can be optimized and fabricated by means of technological approaches adapted to the peculiar grating profile.

This thesis is structured as follows:
In Chapter 1 the blazed gratings are introduced with emphasis on design and fabrication solutions for gratings working in resonance domain.
In Chapter 2, two grating configurations are analyzed. The optimized designs are discussed and physical interpretation for the high diffraction efficiency performances are provided.
The Chapter 3 is dedicated to the technology for the fabrication of multilevel structures. The standard approach with its limitations is first discussed, and new technological approaches are proposed in order to over come such limitations.
In Chapter 4, the results of fabrication of both designed gratings by means of different technological approaches is presented and discussed.

1 Blazed diffraction gratings

The first chapter contains an overview about blazed transmission diffraction gratings.
The physical properties, the design concepts, and the available fabrication techniques are discussed, with emphasis on resonance domain.
The two main design options available in this domain are presented and discussed in more detail, i.e. the binary blazed gratings and the multilevel gratings.
In the final part of the chapter, the technologies to fabricate such grating profiles in fused silica are introduced.

1.1 Diffraction gratings

One of the most general definitions of a diffraction grating is given by Born and Wolf [10], defining a diffraction grating as any arrangement which imposes a periodic variation of amplitude or phase, on an incident wave. Typically, however, this arrangement is periodic itself, therefore, the common definition of a diffraction grating is that of a periodic optical structure, which diffracts the light incident on its surface.
Each period of the grating can be considered as a source for the reflected and/or transmitted light. The light scattered from each single *source* interferes constructively only in determinate angular directions, depending exclusively on the illumination wavelength and period of the grating. This simple optical functionality gives to the diffraction grating its fundamental role in Physics experimentation [11].
The optical structures belonging to this definition are very copious and heterogeneous. Their classification is based on several criteria, according to geometry, material, efficiency behavior, operating bandwidth, application, and fabrication method. A quite exhaustive classification of gratings can be found in [4, 5, 12]; the classification includes classical grating types, as echelle gratings or ruled gratings, and relative novel types, such as effective medium gratings [13–15].
This thesis, as already discussed in the introduction, is focused on 1D (fused-silica) surface relief transmission gratings, consequently the discussion about diffraction gratings in this introduction chapter is focused on such kind of gratings. Considering, for example, the binary gratings schematically shown in Fig. 1.1. The different directions θ_m, in which the incident light is diffracted, namely diffraction orders, are for given illumination determined by the period of the

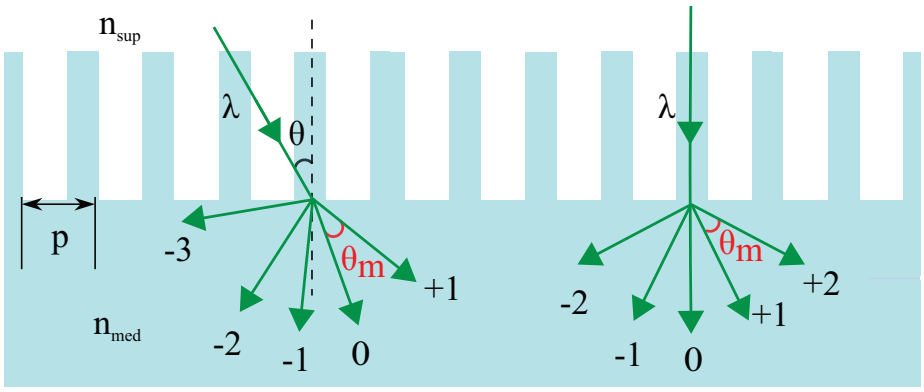

Figure 1.1: 1D transmission-diffraction grating: light redistribution for a incidence angle θ=30°, normal incidence. The figure is a schematic representation for a fused transmission grating. The period is 1 μm. The grating is illuminated from air by λ= 650 nm . (For the clarity of the representation, the reflection orders are not drawn.)

structure. For a one-dimensional grating, they can be calculated by the *grating equation*

$$sin(\theta_m) = \frac{1}{n_{med}}(-n_{sup}sin(\theta) + m\frac{\lambda_0}{p}) \quad , \tag{Eq.1.1}$$

where m is the the diffraction order considered, n_{med} the refractive index of the propagation medium, n_{sup} the refractive index of the superstrat, λ_0 the illumination wavelength in vacuum, θ the incidence angle, and p the period of the grating, respectively.

The number of the diffraction orders, physically possible, is related to the ratio between the illumination wavelength λ_0 and period p, as easily derivable from Eq.1.1.

If the incident light is in air (n=1) and the diffraction orders are propagating in air as well, the grating equation Eq.1.1 can be written as

$$sin(\theta_m) = (-sin(\theta) + m\frac{\lambda_0}{p}) \quad . \tag{Eq.1.2}$$

In case of normal incidence, the equation becomes

$$sin(\theta_m) = m\frac{\lambda_0}{p} \quad . \tag{Eq.1.3}$$

If the angle of the diffracted order coincides with the incidence one (θ=θ_m), in the so called Littrow configuration, the grating equation Eq.1.1, can be written as

$$2sin(\theta_L) = (m\frac{\lambda_0}{p}) \quad , \tag{Eq.1.4}$$

and θ_L is the Littrow angle for the mth diffraction order.

The Littrow configuration is well known and used in several optical setups, because binary gratings achieve an extremum of the efficiency in this mounting, due to a symmetry condition

[16]. The efficiency, i.e. the redistribution of the energy of the incident light between the diffraction orders can be calculated by scalar or rigorous diffraction theory [5, 17], depending on the dimensions of the diffractive structure with respect to the wavelength. The diffraction efficiency is related to the profile of the grating [18–20].

1.2 Blazed diffraction gratings

A blazed grating is a diffraction grating, which through its profile can efficiently redirect the incident light into only one single diffraction order. The direction of this order is called blazing direction. The blazed order can be a low or high diffraction order, but, if not differently specified, it is referred to the first order. Traditionally, the typical profile associated with a blazed grating is a sawtooth-shaped profile with a linear slope within the grating period.
The ratio between the grating period p and the illuminating wavelength λ determines the domain, scalar or resonance, where the grating is working and influences the optimal structure profile. The structure profiles are designed and optimized to redirect the light for a specific wavelength usually in the blazing direction with the highest achievable efficiency. In resonance domain, i.e. for ratio $\lambda/p \leq 10$, rigorous methods are required for the calculation of the efficiency.
Also for blazed gratings, the efficiency depends on the grating profile [21]. In theory, a properly designed surface relief phase grating (i.e. a linear sawtooth profile with the appropriate depth) can achieve in the scalar domain 100% efficiency in the first diffraction order [22]. In the resonance domain, the sawtooth profile grating is not the most efficient solution, but other kind of structures can accomplish the blazing effects, as for example, the lamellar gratings [23].
In the following sections, the scalar and resonance domain and the respective grating design solutions for maximizing the diffraction efficiency are discussed.

1.2.1 Blazed diffraction gratings in scalar domain

The domain where the scalar theory of diffraction [10] is valid, is called scalar domain. This required, in general that the lateral dimensions of the optical component under considerations are much larger than the operating wavelength. The fundamental assumption on which the scalar approximation is based is that the light vectorial field components do not interacts and mix each others, and thus it is sufficient for the light-structure interaction to consider one scalar field component only. Consequently, the polarization effects can be neglected for the calculation of the efficiency.
Following this assumption, in the scalar domain, the far field distribution of an incident plane wave on a grating is given by the Fourier transform of the transmittance function of the grating itself [22].

The transmittance function characterizes a grating, containing information about its profile and period. It describes how the optical component modifies the amplitude and the phase of a wavefront propagating through the component and can be approximated by the TEA (thin element approximation).
As example, the simplest case to analyse, among the blazed element family, is a linear sawtooth blazed grating with period p and depth d, as schematically shown in Fig. 1.2.

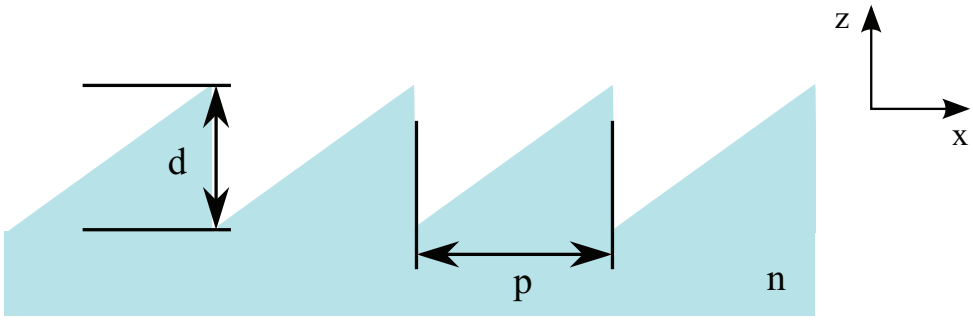

Figure 1.2: Linear blazed grating profile: p is the period, d the depth and n the refractive index of the structure, respectively.

For this linear blazed profile, the transmittance function in the usual Fourier Optics complex notations [17], can be expressed as

$$t(x) = exp(i2\pi\beta x) rect\frac{x}{p} * comb\frac{x}{p} \quad , \tag{Eq.1.5}$$

with $\beta = (n-1)d/\lambda p$.
The efficiency for the mth diffraction order, has been calculated by Swanson [22], as:

$$\eta_m = \left[sinc^2(\pi p(\beta - \frac{m}{p})) \right] \tag{Eq.1.6}$$

with $sinc(x) = \frac{sin(\pi x)}{\pi x}$.
The maximum blazing efficiency for a grating operating in the first diffraction order is obtained for a phase accumulation through the grating of 2π, and the corresponding depth is

$$d = \frac{\lambda}{(n-1)} \quad . \tag{Eq.1.7}$$

Theoretically, the blazed diffraction efficiency of a linear sawtooth grating can reach 100% in transmission; in practice, considering the Fresnel losses at the interface air-grating, in case of glass, this maximum efficiency achievable is reduced by approx. 4%.

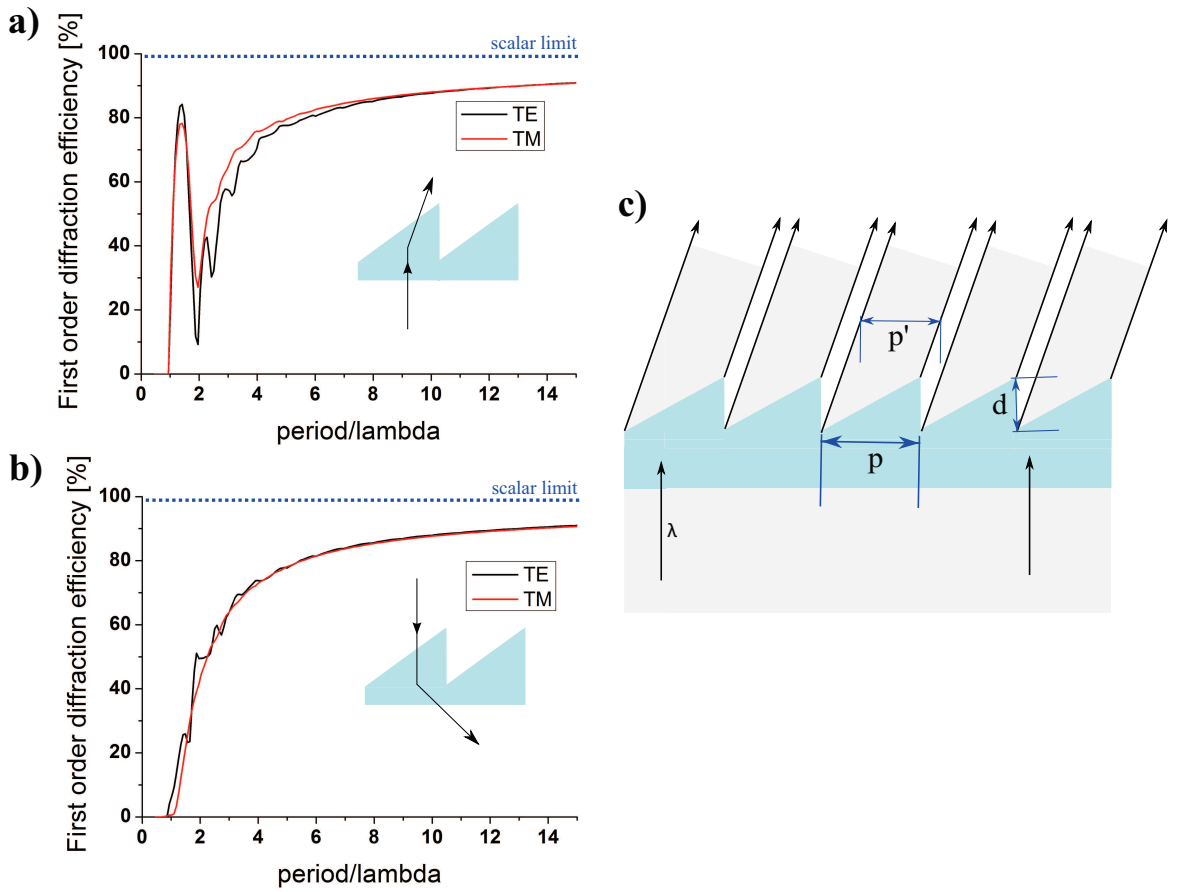

Figure 1.3: Linear sawtooth blazed grating. Blazed efficiency vs. period/lambda : a) and b) with incident light incoming through substrate and from air, respectively. The simulations for both linear polarization state of the light are shown, Tranverse Electric (TE) and Transverse Magnetic (TM) mode, respectively (in resonance domain the achieved efficiency is different for the two polarizations); c) Schematic view of the shadowing effect. The effective grating period is reduced to p'.

However, in reality the achieved efficiency of such a linear blazed profile decreases with decreasing period over wavelength ratio, as shown in the Fig. 1.3 a), b), with a substantial drop in the resonance domain (especially for ratio $\lambda/p < 3$).

An explanation of such a behavior based on simple ray-optical considerations, consists in the so called *shadowing effect* [24]. As shown in Fig.1.3 c), there is an area of the blazed profile which does not contribute to the re-direction of the incident light. This area, the shadowing zone, can be geometrically calculated by ray tracing consideration of the propagation through the grating [24].

For smaller periods, the light shadowing zone becomes more significant for the diffraction performance of the grating, and it cannot be neglected as in case of larger periods. The shadowing effect has also been rigorously calculated by Sandfuchs for the resonance [25] and intermediate regime [26].

Furthermore, the efficiency is usually also reduced by inaccuracies in the fabricated continuous profiles, related to the manufacturing methods (presented in section 1.3) [20, 27]. An alternative

to the continuous profile blazed grating is the multilevel blazed grating [22, 24], which consist in a stepwise approximation of the linear sawtooth profile. The linear continuous profile is approximated by discrete steps, as shown in Fig. 1.4 resulting in a multilevel structure.

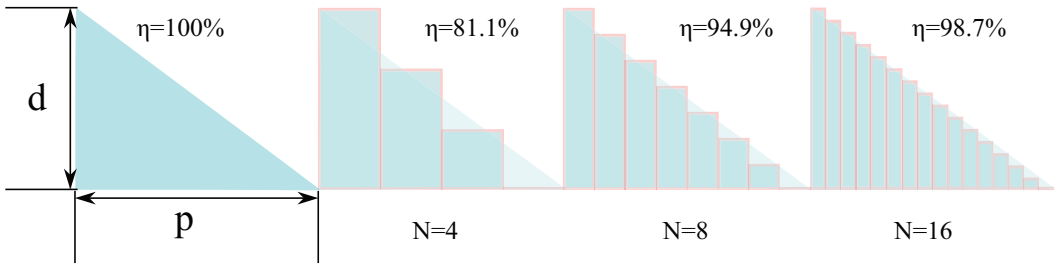

Figure 1.4: Multistep approximation of a linear blazed grating. Continuous profile approximation with different number of levels N and achievable efficiency.

If N is the number of levels which approximate the structure, each level has a width equal to w_N=p/N and a depth d_N=d/N-1, where p and d are the period and the total depth of the continuous grating profile, respectively.
The diffraction efficiency can be calculated assuming that the transmittance function is obtaining as summation of the transmittance of the single levels [24].
The diffraction efficiency of the first order is given by:

$$\eta_1^N = \left[sinc^2(\frac{\pi}{N})\right] * \eta_1 \quad . \tag{Eq.1.8}$$

The higher the number of levels, the higher the achieved efficiency. With a 4-level approximation the achieved efficiency is about 81%, but with a 16-level profile the efficiency is already close to 99% (ignoring the Fresnel-loss at grating-air interface).
In general, the scalar diffraction theory is accurate with an error $\epsilon < 5\%$ when the grating period is greater than $20 * \lambda$. It can be extended by an approach, introduced by Swanson [24], called *Extended Scalar theory*, taking into account the p/λ diffraction efficiency dependency. An additional hybrid model which combines fully vectorial and scalar theories has been presented in [28] for gratings working in the intermediate region ($5 < p/\lambda < 20$). Rigorous calculation of the Maxwell's equations are required in the resonance domain ($p/\lambda \leq 5$).

1.2.2 Blazed diffraction gratings in resonance domain

The resonance domain is defined as the region where the transverse dimension of the grating, i.e. period and lateral feature size, are comparable to the illuminating wavelength. In this region, the simplifications of scalar diffraction theory are not valid, and the rigorous electromagnetic theory must be used to calculate the diffraction behavior of the optical elements [29].
Several numerical methods for the analysis of resonance domain gratings are available, but the two most frequently used approaches are the rigorous coupled-wave analysis (RCWA) and the modal method (MM) approach. Both approaches do not employ approximations and their results are equivalent [30].
The calculations of diffraction efficiency presented in this work are based on the RCWA method. In particular the calculations have been implemented using the numerical methods proposed by Moharam [31] and Li [32, 33].
In the previous paragraph, it has been mentioned that the standard linear blazed grating profile achieves low efficiency in the resonance domain. Different grating designs have been proposed in order to achieve higher efficiency in the first diffraction order. The most successful and flexible solutions, i.e. binary blazed gratings and the parametrically optimized multilevel gratings are discussed in the following.
For a special incidence angle, the Bragg-angle (i.e. Littrow angle) or close to Bragg-angle, also in resonance domain optimized continuous or trapezoidal profiles achieve high efficiencies [34, 35].

1.2.2.1 Binary blazed gratings

An alternative approach for the achievement of a blazing function consists in the generation of a so called effective-medium index structure [36, 37].In this case the modulation of the refractive index inside a period is not related to the variation of the depth of the structure, but is artificially synthesized through sub-wavelength structures inside the grating period [38]. The structure profile is calculated using the effective medium theory [39].
The artificial synthesis of the refractive index can be achieved by different design concepts, that lead to different kind of grating geometries, as it will be discussed in the following paragraphs.

Effective-medium binary gratings

The classical approach for the synthesis of such binary gratings has been suggested by Lalanne [9] and Haidner [40, 41]. The grating period is first sampled in sub-period intervals. The sub-periodicity of the grating is chosen in order to have only non-propagating evanescent orders. Each sub-period contains a sub-wavelength structure characterized by a specific width. The depth is the same for each sub-period. The duty cycle for each sub-period is determined in order that the incident light experiences the same phase accumulation of the corresponding point of

a standard sawtooth blazed grating (see Fig. 1.5).

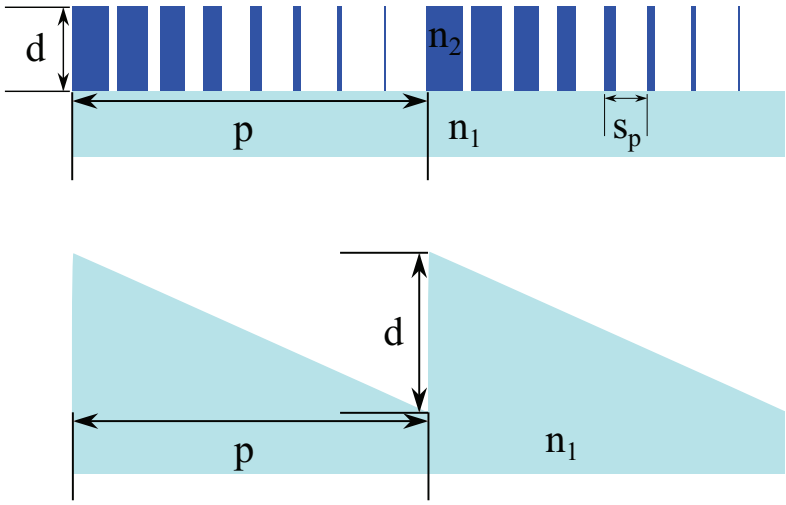

Figure 1.5: Effective-medium binary blazed grating. The grating period p is divided into sub-periods S_p. For sake of clarity a standard blazed sawtooth grating with the same period is drawn. n_1 and n_2 are the respective refractive indices, here $n_2 > n_1$.

The diffraction behavior of the binary blazed gratings is very interesting in resonance domain because the rectangular shape of the groove exhibits no shadowing effect, resulting in very high efficiency achievable [3, 42, 43]. The high blazed efficiency has been explained by wave guiding effects of the incident light through the sub-wavelength features by Lalanne [44].

The binary blazed gratings, as 1D (ridge) or 2D (pillar) structures, have been manufactured in high index materials, in order to reduce the required depth [45]. The achieved efficiency is high in comparison with the standard continuous blazed profile and they show better performance over the incidence angle [45] and incidence wavelength [46].

The achievable efficiency can be maximized by parametric optimization of the structure width of each sub-period, as suggested in [47–49]. Furthermore, the synthesis of a continuous blazing phase through simple binary structures could be a successful approach in order to achieve high efficiency also in the scalar domain, as it has been theoretically proven in [50]. Additionally, the technological effort of the fabrication of a binary grating is reduced with respect to multilevel profiles, as it will be discussed in the section 1.3.2.

However, typically binary blazed gratings exhibit aspect ratio (AR) structures, i.e. the ratio of depth to lateral feature size, considerably larger than 5. Thus, this approach becomes no longer suitable when the illumination wavelength is so short that the minimum feature size of the subwavelength structures is below the technological capabilities of the fabrication process. For structure geometries close to the technology capabilities, it is not possible to avoid efficiency losses due to fabrication deficiencies resulting in unwanted propagating diffraction orders within the grating [51].

Area-coded effective medium structures

An alternative design solution can be found in the so-called area-coded effective medium structures (ACES), proposed by Kleemann at al. in [52]. The basic idea consists in the use of large contiguous structures, instead of thin ridges as in 1D binary gratings or thin pillars as in 2D binary gratings. The structure geometry depends on the optical function. In case of blazed structures, the ACES is specifically called BLACES (a schematic view of a BLACES grating is shown in Fig. 1.6). Such kind of design approach avoids the challenging fabrication of high aspect ratio structures. In fact, the 2D grating structures are continuous planar periodic structures; they are characterized by an additional sub-wavelength periodicity w in the transverse direction of the grating.

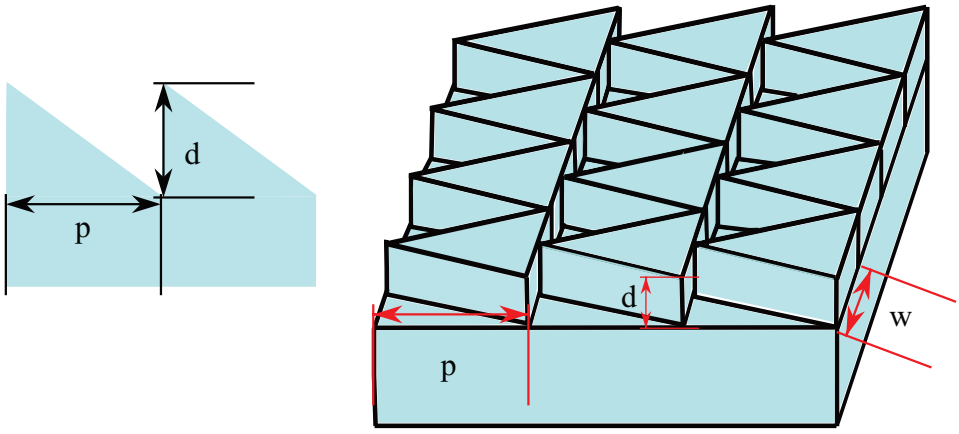

Figure 1.6: Example of a BLACES structure. Grating period p, transverse period w. For sake of clarity a standard blazed sawtooth grating with the same period is drawn.

Considering the conventional direction of the grating, the ACES acts as a ordinary 1D diffraction grating, where the required phase variation is obtained by the local variation of the fill factor of the transversely encoded structure. The depth is consequently not varying within the grating period, therefore a single-step lithographic process can be used to manufacture these area coded structures.

In literature experimental results obtained with BLACES structures are reported in [53], but the efficiencies achieved are not very high (74%). The fabrication of such kind of structure in fused silica has not been very successful because of the sharp tip of the triangular profile.

It is worth to note that despite the promising theoretical results, the effective-medium binary blazed gratings, based on sub-periods, and the BLACES have not yet been used in any large area grating for real applications. The reason probably lies on the difficulty inherent to the lithographic process, or transferring the etching technology of high index materials to larger area.

Parametrically optimized binary gratings

The parametrically optimized binary gratings are the successful alternative approach for large area gratings. This approach, especially developed for fused silica structures, avoids the sub-periodicity within a grating period, and it consists in the simple parametric optimization of ridges (1D) [54] or pillars (2D), or a combination of both [55].

Despite the larger grating depth due to the comparable low refractive index of fused silica, this approach relaxes the critical dimension of the sub-wavelength structures, because the number of pillars/ridges is not imposed by the sub-periodicity of the grating as in the Lalanne approach, but it can be decided in view of the technological capabilities.

The smaller the grating period is, the smaller the number of sub-wavelength structures will be. Furthermore, the optimization can already take into account the fabrication constrains [56], not allowing extremely fine structure widths. The possibility to combine 1D and 2D features in the same grating increases the design flexibility.

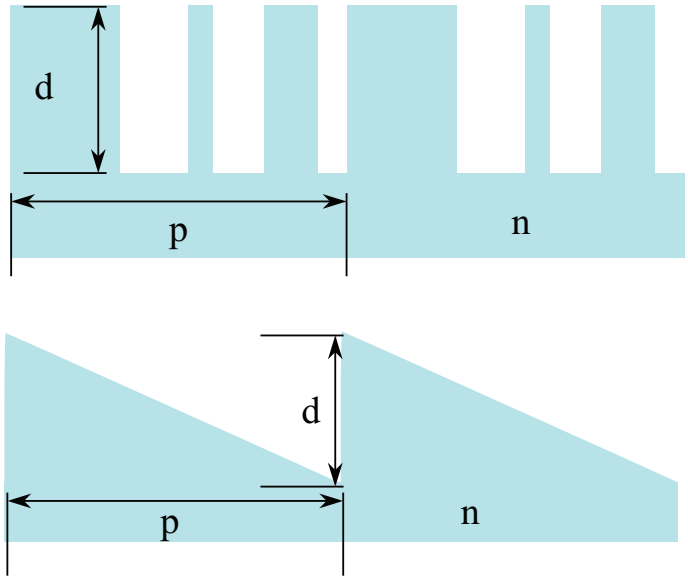

Figure 1.7: Parametrically optimized binary gratings. Schematic view of a three-ridges blazed binary grating. For sake of clarity a standard blazed sawtooth grating with the same period is drawn. n is the refractive index.

The high efficiencies achieved by such kind of binary gratings can be explained by the analysis of the propagation of the light through the structure based on the Floquet-Bloch theory [57]. In fact, high efficiencies are achieved only if the number of propagating Bloch-modes inside the grating structure is small and well adapted to transform the input field into the desired output field [47, 58].

Such binary gratings have been manufactured on large areas in fused silica and the optical performances achieved enable the use in space applications [59].

The parametrically optimized fused silica binary gratings are a valid alternative solution to accomplish the blazing function in resonance domain. Nevertheless, there is a limit in the use of such gratings: the maximum efficiency cannot be achieved for arbitrary incidence angles, but only close to the Littrow angle, due to the approximate symmetry of the binary profile [16, 45].

1.2.2.2 Parametrically optimized multilevel gratings

Another option to achieve high efficiency for blazed gratings in resonance domain has been proposed by Noponen in [60], and it is based on the parametric optimization of multilevel structures [61–63].
The idea is to add degrees of freedom in the optimization of each level of the grating. In the standard multilevel approximation of scalar blazed grating, the levels have all the same width and the same depth. Noponen suggested instead to optimize the width and the depth of each single level. By means of such parametric optimization, the achieved efficiency is comparable to the efficiency obtained in the scalar domain.

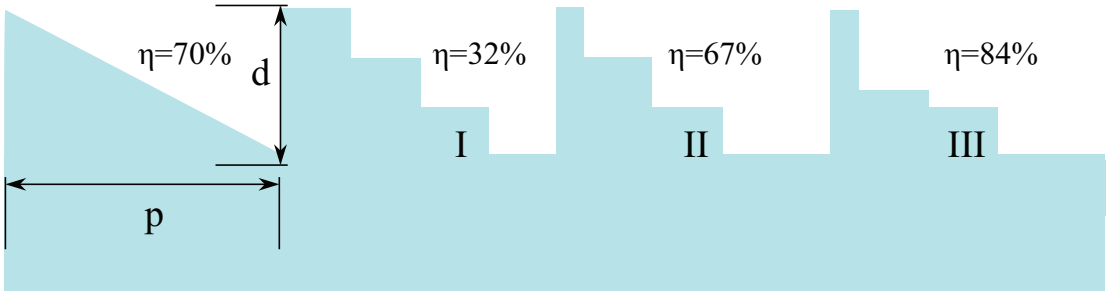

Figure 1.8: Multilevel blazed gratings: standard (I) and parametrically optimized 4-level profiles (II, III). The period of grating is p= 4*λ, normal incidence condition through the substrate. Fabrication constrains (minimum feature size >100 nm) have been taken into account during the optimization. In the grating II only the width of the levels are optimized, in grating III both width and depth.

Furthermore, the high efficiency is not related to the higher number of levels, as in the scalar domain. In resonance domain, actually an optimized three-level grating is sufficient to achieve high efficiency (>90%). This simplifies the technological effort for the fabrication of multilevel profiles in resonance domain, especially for applications in the UV-VIS[1] spectral region, where the lateral feature size becomes very demanding. Furthermore, it is possible to optimize the grating profile for each arbitrary incidence angle. This property is fundamental for normal incidence grating applications.
As example, in Fig. 1.8 a comparison between classical and optimized four-level gratings in

[1] UV: ultraviolet; VIS: visible

resonance domain is shown. The period is $p = 4 * \lambda$, the light is coming through the substrate at normal incidence. The efficiency of the optimized grating is more then 2x higher with respect to the equidistant multilevel approximation of the linear profile.

1.3 Fabrication technologies

The technologies for the fabrication of blazed gratings are diverse and of different kind [20]. In general it is possible to distinguish between mechanical and lithographic methods. Both methods can be used to fabricate the grating in itself, or a master for replication processes.
The choice of the appropriate technique depends on the profile (continuous, multilevel, binary), period, lateral feature size, and material of the blazed grating [64].

1.3.1 Continuous profile grating fabrication methods

Direct machining techniques

The traditional mechanical methods include mechanical ruling and diamond turning, but also the more recent technique of FIB (Focused Ion Beam) milling [65] is considered as direct machining method. The main characteristic of such techniques is that the optical microstructures are directly fabricated through the removal of the optical material.
In particular, the mechanical ruling uses a sharp stylus tip to remove the material in a well controlled way, allowing the fabrication of high quality gratings [66]. But the profile smoothness is limited by the finite size of the tip.
Another direct technique traditionally used for the diffractive optic fabrication, is Single-Point Diamond Turning (SPDT) [67]. In this method, a diamond tip is brought in contact with a rotating substrate. Also in this case, the quality of the grating profile is limited by the shape of the diamond tip, and additionally the technique works best for radially symmetric pattern.
Other techniques, considered as direct machining, are FIB milling and laser ablation [68, 69]. These techniques can be used for arbitrary pattern generation. Nevertheless, they are not suited for large area elements due to the slowness of the process.

Lithographic techniques

The lithographic techniques commonly used for the fabrication of blazed gratings include direct writing, interferometric exposure, and half-tone mask lithography. Differently from the direct machining techniques, by lithographic processes the grating geometry is first transferred into photo- or e-beam sensitive material (resist). The developed pattern is then transferred into the substrate through an etching step, that can be a dry process (RIE, IBE, Reactive Ion and Ion Beam etching) [70] or a wet etching process [71].

The direct writing consists in the exposure of the continuous profile into the resist by modulating the intensity of the exposure source. The intensity is varied in order to achieve the right local depth of the structure in resist (after the chemical development process). The source for the exposure of diffractive components can be e-beam [72–75] or laser [76, 77]. The two direct writing techniques achieve of course different resolution. Typically, the laser writing is used for optical elements working in scalar domain, and the e-beam for resonance domain gratings, where high resolution is essential.
But also in scalar domain, the optical performances of blazed gratings fabricated by means of laser direct writing are reduced by fabrication artifacts due to the limited resolution (i.e. finite laser spot-size).
Another well-established technique for the fabrication of blazed gratings is the interference lithography. It allows to fabricate especially sinusoidal or sawtooth profiles. Here, the resist is exposed by a stationary interference fringe pattern generated by coherent wave fronts. This technique is used also for elements working in resonance domain [78]. It can also be considered as direct writing because no mask is used for the lithographic exposure of the pattern geometry.
A further lithographic method for the fabrication of diffractive optics is the half-tone lithography. In this approach, the continuous grating profile is generated by the resist exposure through a lithographic mask with a spatially varying transmission profile, usually called half (or gray)-tone mask. The quality of the grating depends on the quality of the half-tone mask. This approach allows to generate continuous profiles as in the direct writing, but it is faster because it works parallel on large areas.
Another approach that allows to fabricate diffractive gratings at wafer level has been adapted from the microelectronic industry and is called *Binary Optics* approach [79–81]. This fabrication method allows to fabricate binary structures and multilevel profile by a multistep approach.
The following paragraphs are dedicated in particular to the Binary Optics technology, because it is the core technology used in this work.

1.3.2 Binary Optics Technology

Binary Optics technology is an approach devoted to the fabrication of multilevel grating profiles. It is based on planar lithographic techniques for the fabrication of integrated circuits in microelectronics. Binary Optics is actually a technology adapted from the semiconductor industry to the fabrication of micro-optical elements [79, 82].
By the use of this lithographic technique, it is possible to realize optical elements with large dimensions but characterized by binary sub-micron features. This approach has been successfully used already in the 1970s [83, 84] for the fabrication of thin film lenses in the scalar domain; and later for the manufacturing of optical elements working in regions close to the resonance domain [79, 85, 86].

The fabrication technique is based on consecutive repetition of the planar binary lithographic steps. The multilevel profile actually can be ideally considered as a superimposition of several binary structures. The number of the binary lithographic steps required depends on the number of levels of the grating. With M binary fabrication steps, it is possible manufacture a N=2^M level structure; but with only M independent level heights.

For the singular binary lithographic step, the fabrication process starts with the exposure of the binary geometry pattern into the resist. The binary lithographic process can be direct, by using laser or e-beam source [87], or carried out by photo-lithography using a photo-mask.

The binary resist pattern has to be transferred into the grating material in the final phase of the overall process.

The grating material depends on the kind of application and on the wavelength the grating is designed for and it also influences the details of the fabrication process.

In the Fig. 1.9 the fabrication flow for a binary fused silica grating is schematically illustrated, as example to explain the fabrication process. The choice of a fused silica grating is related to the subject of this thesis.

A fused silica substrate is first coated with a chromium layer, on the top of which an e-beam resist layer is deposited (see Fig. 1.9(I)). The resist layer is tempered, and afterwards lithographically exposed. The exposed resist is then developed, resulting in a binary profile (see Fig. 1.9(II)). The resist pattern is then used as a mask to transfer the binary geometry into the chromium layer through a RIE (Reactive Ion Etching) process [88] (see Fig. 1.9(III)). The resist is then removed from the top of the chromium structures (see Fig. 1.9(IV)). The patterned chromium layer (see Fig. 1.9(V)) acts as a hard mask to transfer the geometry into the substrate material [89]. After removing the chromium layer (see Fig. 1.9(VI)), the binary grating profile is present in fused silica.

To obtain a multilevel profile, the binary lithographic process has to be repeated on the top of the already microstructured substrate. In the Fig. 1.10, the fabrication process for a four-level fused silica grating is schematically illustrated. Only two binary lithographic steps are required. Each single fabrication step is carried out in the same way as previously described, but precise alignment between the different binary layers is additionally required in order to avoid fabrication artifacts in the grating profile [90]. Especially, in the resonance domain, such artifacts can affect the optical performances of the grating dramatically, because their dimensions become comparable to the features size and they cannot be neglected. A detailed discussion about this is provided in chapter 3.

In general, the described *Binary Optics* fabrication process can be also used for the fabrication of gratings in other different materials. The process flow needs to be adapted, for example by skipping some steps in case of polymer optics where the exposure and development of the polymer are the only necessary steps; or a different material (instead of chromium) will be used

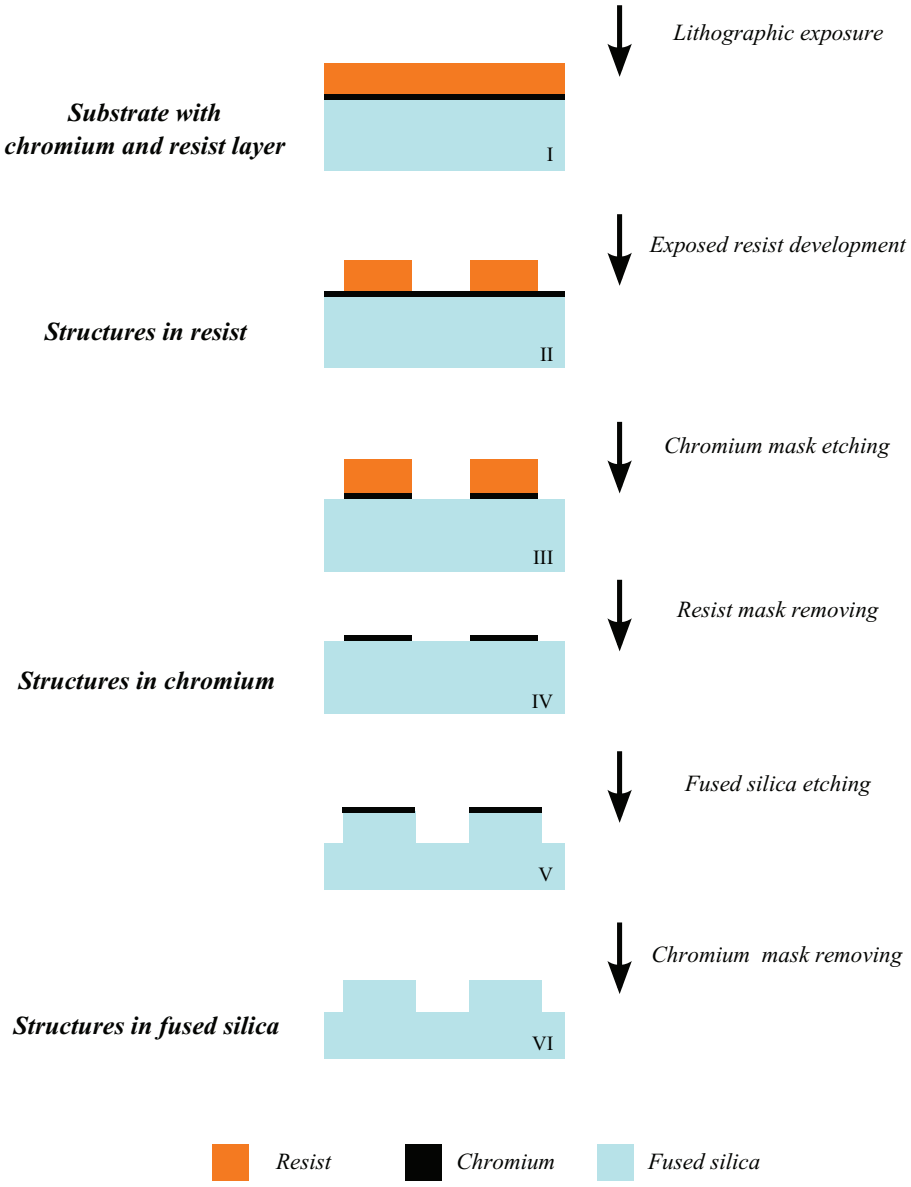

Figure 1.9: Binary Optics Technology: fused silica binary grating fabrication flow scheme.

as a mask to transfer the geometry into the substrate.

The limits of the binary optics technology are in fact not due exclusively to the misalignment between diverse binary exposures, but also to the resolution achievable in the exposed material and to the etch selectivity between mask and substrate. The first factor limits the minimum achievable lateral feature size, the second factor the achievable aspect ratio (AR) of the grating. The problems related in particular to the etching of high AR structures in fused silica, will be discussed in detail in chapter 3.

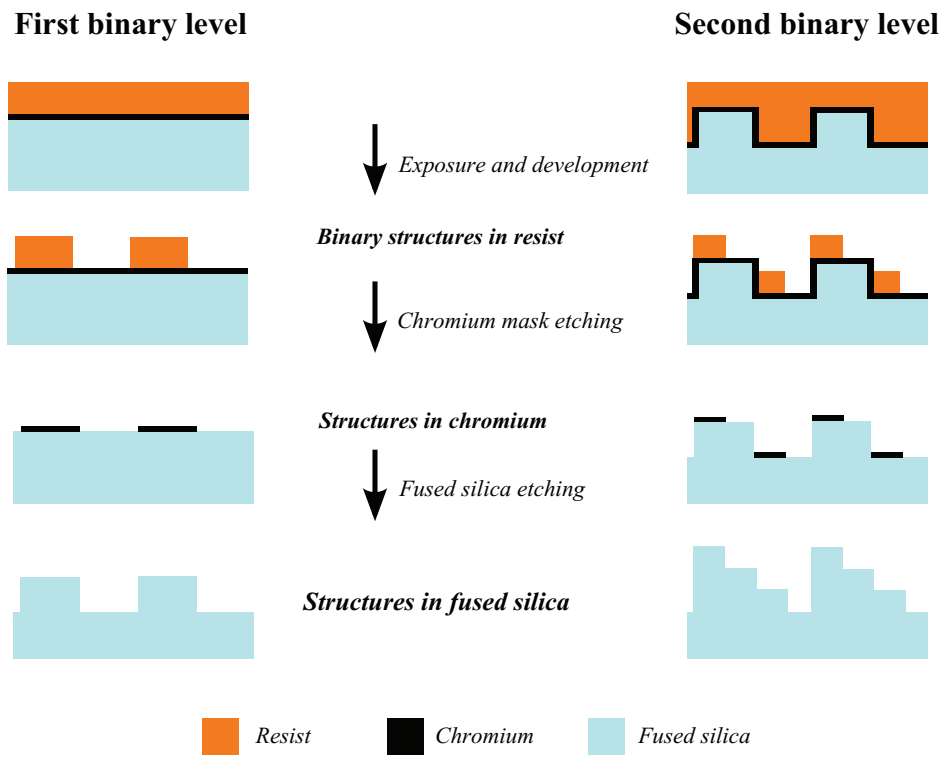

Figure 1.10: Binary Optics Technology: four-level fused silica grating fabrication flow scheme.

Chapter summary

In this first chapter, a brief introduction about blazed transmission gratings has been presented. The efficiency behavior of the classical sawtooth profile (echelette) has been analyzed in scalar and resonance domain.

In particular, in the resonance domain, the binary gratings and the parametric multilevel gratings have been discussed as alternatives to achieve high efficiency.

The technologies for the fabrication of the blazed gratings have been discussed, with particular emphasis on the binary optics technology.

2 Design and novel analysis concept of blazed gratings in resonance domain

In this chapter the design of two fused silica blazed multilevel gratings operating in resonance domain is presented. Both gratings are optimized for visible light at normal incidence. In particular, a three-level grating is proposed as a high efficiency solution for the case of light incident through the substrate [91]; as well as a so-called effective medium enhanced three-level grating, as a solution for the light incident from air [92].
The optimized designs and tolerance analysis are discussed. Physical interpretation of the high efficiencies are provided for both gratings. The interpretation is based on a three beam interferences mechanism for the three-level grating and on the modal analysis for the effective medium enhanced three-level grating.

High dispersive blazed gratings in resonance domain

The aim of this research work is the design and fabrication of high efficient monolithic fused silica blazed gratings, working at normal incidence in resonance domain for visible wavelengths. The choice of fused silica as material for the diffractive structures is related to the operation wavelength and technological constrains for large area gratings. The comparable low refractive index of fused silica restricts the design options in resonance domain to the parametrically optimized binary and multilevel gratings, as discussed in the section 1.2.2. The normal incidence, as the condition to optimize the blazing efficiency, penalizes the binary gratings because of their symmetry. However, the parametrically optimized multilevel gratings theoretically can fulfill all specifications.
For the optimization the fabrication constraints have to be taken into account, and this can lead to different grating profiles. As a consequence, the optimum grating profile is a compromise between design specification and fabrication capabilities.
In the following paragraphs, the two different optimum solutions for the two directions of the incident light are discussed.

2.1 Three-level grating (substrate to air)

The first blazed grating considered in this work is a fused silica grating with a period p= 1.266 μm, illuminated through the substrate at normal incidence with a λ= 633 nm TE polarized light. The ratio between period and wavelength is two, consequently the grating is working in the region of the resonance domain that exhibits the minimal efficiency for the linear blazed gratings, as shown in Fig. 1.3.

Here, different kinds of gratings have been optimized for the maximum efficiency at normal incidence. The optimized gratings have been compared to find a design that can be successfully fabricated. The optimization has taken into account the actual limits of the technology available at the Fraunhofer-IOF [93] in Jena. The minimum width for a level has been set to 100 nm, and its aspect ratio (AR) is not allowed to be larger than 10. Such technological limitations, together with the small period (1.266 μm), restrict the range of binary fabricable structures to two-ridges gratings. For the multilevel gratings, three or four levels are enough to achieve high efficiency in resonance domain, as suggested by Noponen [60].

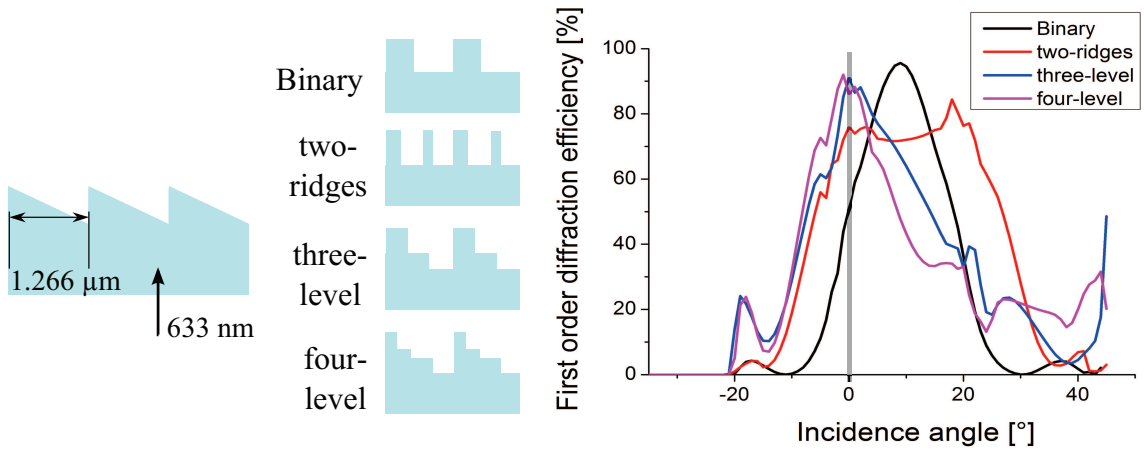

Figure 2.1: First order efficiency of different kinds of optimized fused silica gratings versus the incidence angle; normal incidence optimization for three-level, four-level as well as two-ridges binary grating; one-ridge binary grating is optimized for the Littrow angle; λ= 633 nm, TE polarization, p= 1.266 μm.

The results of the optimizations are presented in Fig. 2.1. As shown, the simple binary element achieves really high efficiency exclusively at Littrow angle ($\approx 9°$), while at normal incidence the efficiency drop to $\approx$ 50%. At normal incidence also a two-ridges binary grating achieves only a modest efficiency of 74%. In contrast, both optimized multilevel structures reach efficiencies close to 90%. The technological effort to realize a three or a four-level grating is similar, because two lithographic steps are needed. Nevertheless, the optimized three-level grating is characterized by wider lateral dimensions with respect to the optimized four level element. The

three level design, therefore, is considered more practical from a technological point of view.

2.1.1 Design

The three-level blazed grating has been optimized as suggested by Noponen [60], by means of free optimization of width and depth of each level.
As expected by the parametric optimization, the result is a non-linear step height and width variation within the period.

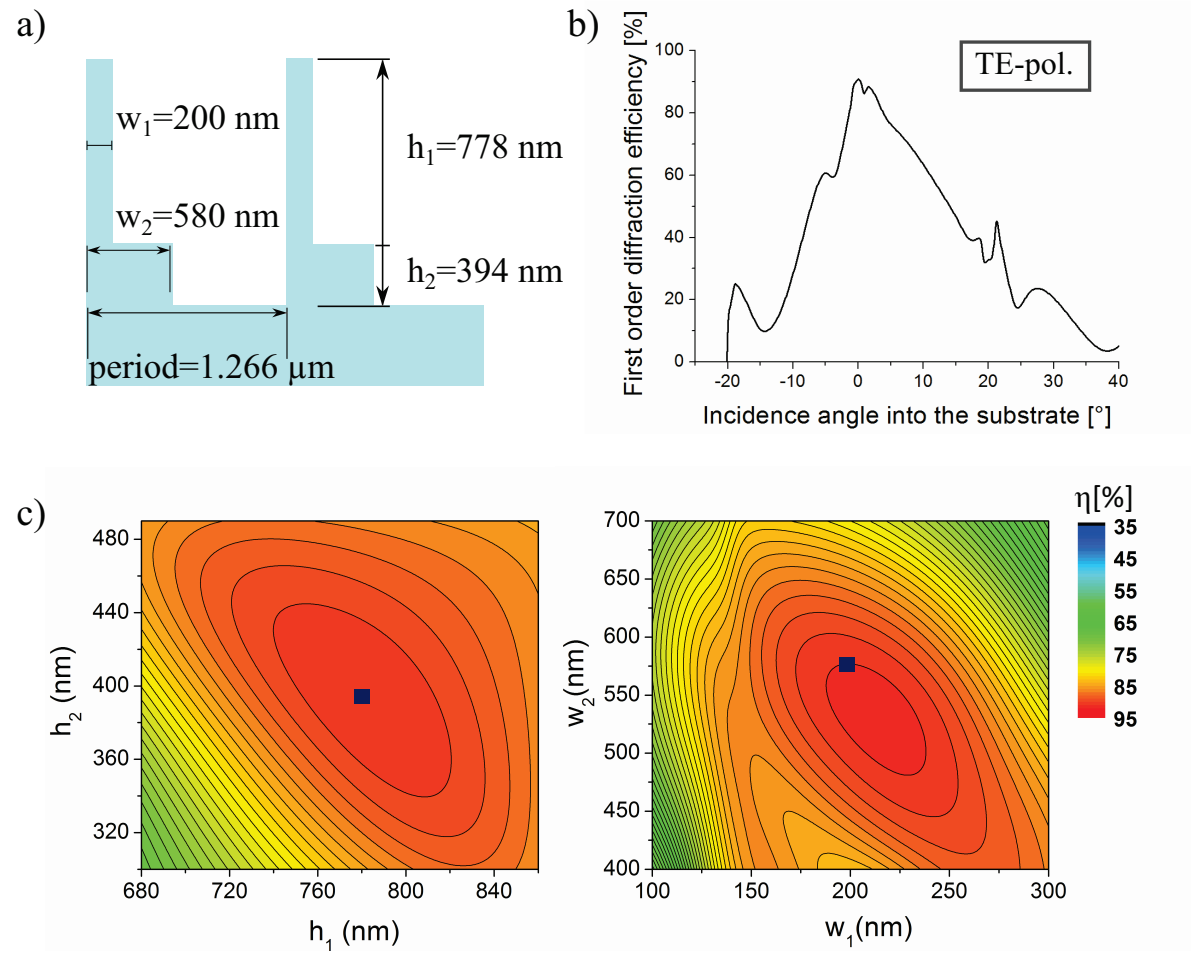

Figure 2.2: Optimized three level grating. a) Sketch in scale of the structure with the geometrical parameters values; b) Diffraction efficiency η vs. incidence angle; c) Fabrication tolerance analysis versus depths and widths of the levels. The dots indicate the geometrical parameters selected for the fabrication. The chosen values for widths w_1 and w_2 are a technological compromise between the two bar widths.

A schematic view of the designed three-level grating is provided in Fig. 2.2 a). The upper-level bar is significantly narrower (w_1 = 200 nm, h_1 = 778 nm) and deeper compared to the lower-level bar (w_2 = 580 nm, h_2 = 394 nm). The minimum feature size (200 nm) together with its relatively low aspect ratio (AR≅4) are not critical from a technological point of view.
As shown in Fig. 2.2 b), the optimized three-level structure can achieve a very high diffraction

efficiency, close to 90% for the first order at normal incidence.

The fabrication tolerance analysis of Fig. 2.2 c) shows a quite tolerant design. Nevertheless, it is more sensitive to depth than to width variations of the individual phase levels. In particular, to the concurrently decrement of the level depth h_1 and h_2, i.e. a variation of 20 nm in the levels depths cause a 5% loss in the achievable efficiency. The same efficiency loss occurs for variations of the width w_1 and w_2 larger than 80 nm.

Furthermore, the grating, optimized for 633 nm wavelength, achieves efficiencies larger than 70% in a quite large bandwidth (550-890 nm) for TE polarizations as shown Fig. 2.3 a). For the designated operation point (i.e. normal incidence, λ= 633 nm) even the TM polarization exhibits a quite high efficiency of about 74% (see Fig. 2.3 b)).

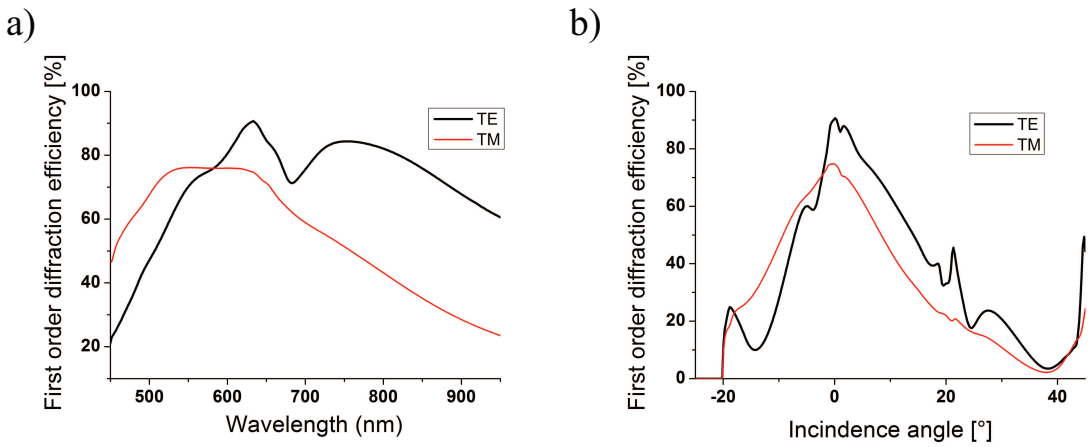

Figure 2.3: First order diffraction efficiency for TE and TM polarization. a) vs. wavelength; b) vs. incidence angle.

2.1.2 Physical model for the interpretation of the high efficiency

The achieved efficiency of about 90% is considerably high, especially if compared with a classical sawtooth blazed grating design. The high efficiency for parametric optimized multilevel gratings has been predicted by Noponen [60], but no physical interpretation of the high efficiency has been provided.

A physical model, valid for the interpretation of the high efficiency for all kind of multilevel gratings in resonance domain, probably does not exist, or the interpretation is not so straightforward. Nevertheless it is possible to find a specific model that will help to physically understand the high efficiency for a specific grating profile.

For the three-level grating, discussed in this work, the reason for such a large efficiency improvement is strictly correlated to the particular structure profile, characterized by a small width upper bar. It can be physically explained by means of an three- wave interference mechanism. This model is valid for a three-level grating that diffracts the light mainly in only three propa-

gating diffraction orders.

The interpretation is based on the virtual decomposition of the three-level grating structure into two binary sub-structures: a lower binary grating I and a second individual binary grating II, actually consisting of the bottom and the upper level of the original three-level grating, respectively, as schematically shown in Fig. 2.4.

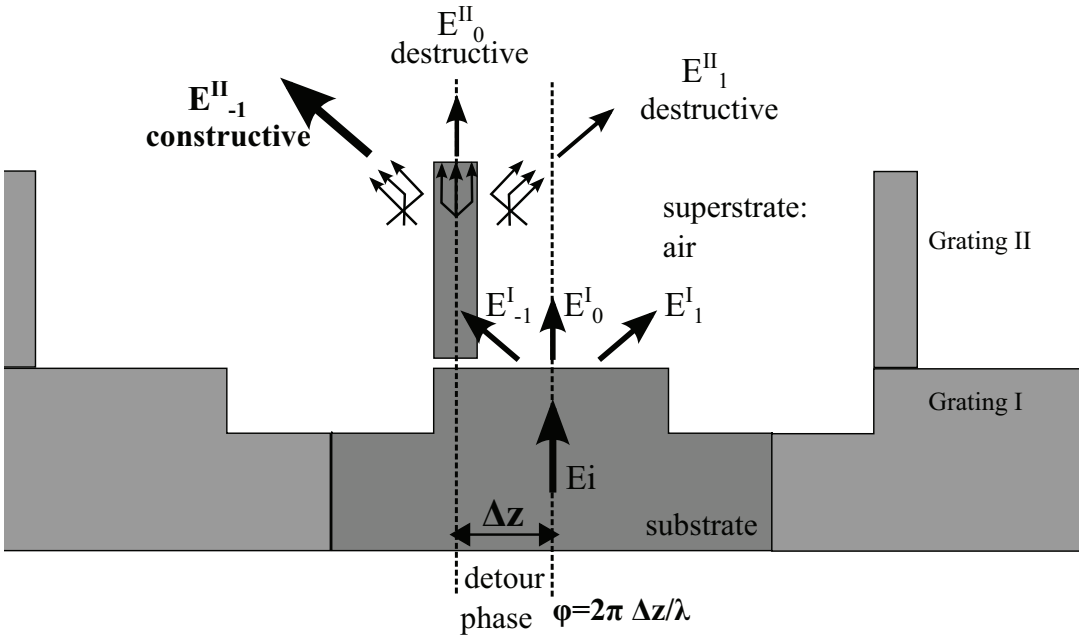

Figure 2.4: Illustration of the three-wave model for explaining the grating effect by means of two consecutive beam-splitting mechanisms.

For the sake of simplicity, the upper grating bar is assumed fully surrounded by air, i.e., as assumption, an infinitesimal air gap divides the upper and lower grating structure. In principle, such an assumption is not needed for the validity of the interpretation, but it makes the treatment easier and provides a clearer picture of the situation. Firstly, this way, one has only to deal with two kinds of one-bar-gratings, i.e. even with such trivial, most easiest types of gratings one can give a sufficient interpretation. Secondly, the upper grating exhibit an additional mirror symmetry (entrance and exit space are supposed to be air) which evokes simpler transmission matrices. Of course, this assumption implies that the transition to the upper level is treated incorrectly. But it will work well for a small width of the upper bar.

Both sub-gratings are then regarded as individual beam-splitting elements. The lower binary grating splits the incoming light into the three main transmission orders (-1, 0, +1) (as illustrated in Fig. 2.4). The second beam splitter mixes these three fields to create the final output waves.

To reach high efficiency in the blazing direction of the minus first diffraction order, the resulting interference of the three contributions has to be constructive for this order, and destructive for

the remaining two orders. The conditions required to obtain the desired interference can be mathematically derived, as shown in the following.

Considering the bottom level grating of Fig. 2.4, it works as simple beam splitter element. The normal incidence incoming light E_i at grating I is redistributed in the three output orders E_1^I, E_0^I, E_{-1}^I.

$$\begin{bmatrix} E_{-1}^I \\ E_0^I \\ E_1^I \end{bmatrix} = \begin{bmatrix} t_{-1}^I \\ t_0^I \\ t_1^I \end{bmatrix} E_i \tag{Eq.2.1}$$

where t_I^k are the amplitude coefficients for the order k, with $t_1^I = t_{-1}^I$.

The output orders of grating I are the input fields for the upper grating II, ideally suspended in air. The final output diffraction orders can be calculated by the Eq.2.2. (In the transmission coefficients notation the first and the second subscript refer to the output and input order, respectively.)

The transmission matrix $t_{1,k}^{II}$ of grating II is determined for the symmetric case, where the bar is situated in the middle of the unit cell.

$$\begin{bmatrix} E_{-1}^{II} \\ E_0^{II} \\ E_1^{II} \end{bmatrix} = \begin{bmatrix} t_{-1,-1}^{II} exp(i0\varphi) & t_{-1,0}^{II} exp(i1\varphi) & t_{-1,1}^{II} exp(i2\varphi) \\ t_{0,-1}^{II}(-i1\varphi) & t_{0,0}^{II} exp(i0\varphi) & t_{0,1}^{II} exp(i1\varphi) \\ t_{1,-1}^{II}(-i2\varphi) & t_{1,0}^{II} exp(-i1\varphi) & t_{1,1}^{II} exp(i0\varphi) \end{bmatrix} \begin{bmatrix} E_{-1}^I \\ E_0^I \\ E_1^I \end{bmatrix} . \tag{Eq.2.2}$$

Thus, the transmission matrix of grating (II) contains also a phase term, due to the detour phase $\varphi = 2\pi \frac{\Delta z}{\lambda}$ between the two grating bars, as illustrated in Fig. 2.4. The right detour phase is fundamental to achieve the interference desired conditions:

$$\begin{bmatrix} E_{-1}^{II} \\ E_0^{II} \\ E_1^{II} \end{bmatrix} = \begin{bmatrix} max \\ min \\ min \end{bmatrix} . \tag{Eq.2.3}$$

Eq.2.2 can be simplified further taking into account symmetry and reciprocity considerations (applying the *Lorentz Reciprocity Theorem* [94]) of the transmission coefficients of the grating II.

As schematically shown, in the Fig. 2.5, the number of the transmission coefficients can be reduced, and consequently Eq.2.2 can be expressed as:

$$\begin{bmatrix} E_{-1}^{II} \\ E_0^{II} \\ E_1^{II} \end{bmatrix} = \begin{bmatrix} \tau_0^{II} exp(i0\varphi) & \frac{\alpha_0}{\alpha_1} t_1^{II} exp(i1\varphi) & t_2^{II} exp(i2\varphi) \\ t_1^{II} exp(-i1\varphi) & t_0^{II} exp(i0\varphi) & t_1^{II} exp(i1\varphi) \\ t_2^{II} exp(-i2\varphi) & \frac{\alpha_0}{\alpha_1} t_1^{II} exp(-i1\varphi) & \tau_0^{II} exp(i0\varphi) \end{bmatrix} \begin{bmatrix} E_{-1}^I \\ E_0^I \\ E_1^I \end{bmatrix} . \tag{Eq.2.4}$$

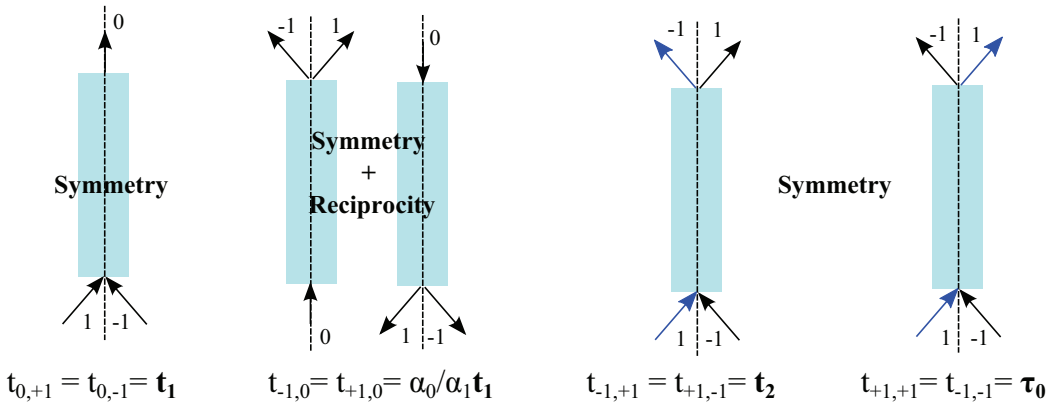

Figure 2.5: Schematic representation of the symmetry and reciprocity conditions for the transmission coefficient of the grating II.

By substituting in Eq.2.4, the calculated values of the fields E_1^I, E_0^I, E_{-1}^I, the interference conditions of the Eq.2.3 can be written as:

$$\begin{cases} E_{-1}^{II} = [\tau_0^{II} t_1^I exp(i0\varphi) + \frac{\alpha_0}{\alpha_1} t_1^{II} t_0^I exp(i1\varphi) + t_2^{II} t_1^I exp(i2\varphi)] E_i = max \quad (a) \\ E_0^{II} = [t_1^{II} t_1^I exp(-i1\varphi) + t_0^{II} t_0^I exp(i0\varphi) + t_1^{II} t_1^I exp(i1\varphi)] E_i = min \quad (b) \\ E_1^{II} = [t_2^{II} t_1^I exp(-i2\varphi) + \frac{\alpha_0}{\alpha_1} t_1^{II} t_0^I exp(-i1\varphi) + \tau_0^{II} t_1^I exp(i0\varphi)] E_i = min \quad (c) \quad . \end{cases} \qquad \text{(Eq.2.5)}$$

In order to maximize the minus first order (Eq.2.5 (a)) the phases of all three wave contributions should be similar, i.e.

$$arg[\tau_0^{II} t_1^I] \cong arg[\frac{\alpha_0}{\alpha_1} t_1^{II} t_0^I exp(i1\varphi)] \cong arg[t_2^{II} t_1^I exp(i2\varphi)] \quad . \qquad \text{(Eq.2.6 (a))}$$

The situation can be visualized in the complex plane of field vectors (Fig. 2.6), where all contributions point in the same direction leading to constructive interference for that particular order. This maximum condition implies a relation for the phases of the corresponding transmissions and the detour phase. Inspecting the relation for the plus first order (Eq.2.5 (c)) it is possible to observe that same coefficients enter that equation but now with negative detour phases. Combining both interference conditions we obtain a relation between the absolute amount of the transmission coefficients and the detour phase:

$$cos(2\varphi) \cong -\frac{\left|\frac{\alpha_0}{\alpha_1} t_1^{II} t_0^I\right|}{2\left|\tau_0^{II} t_1^I\right|} \quad . \qquad \text{(Eq.2.6 (b))}$$

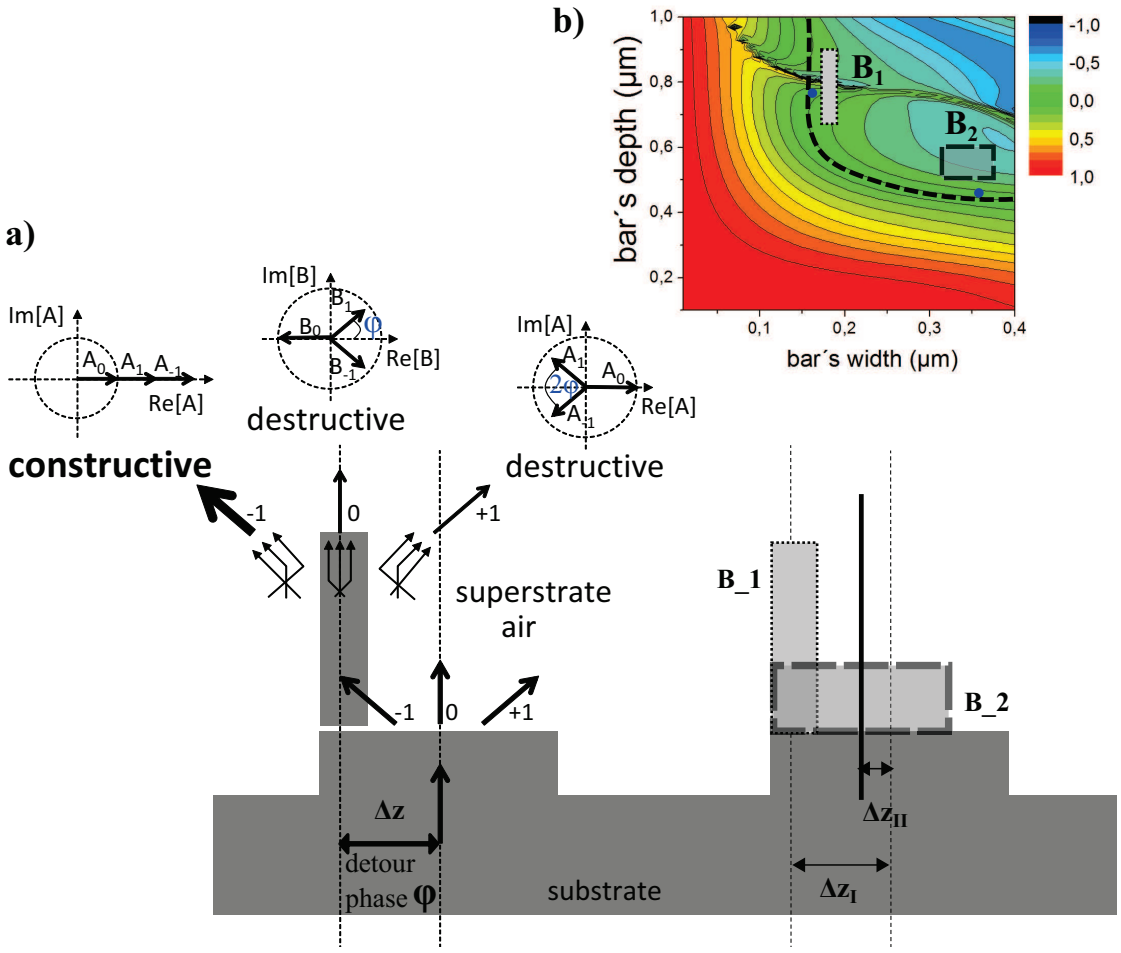

Figure 2.6: a) Illustration of phase difference between the diffraction orders (the vectors can be rotated in the complex plane, but the phase difference remains the same), and of the geometry dependency of the upper grating bar on the amount of the required detour phase. Different possible bar widths (examples B_1,B_2) are related to different detour phases. b) Difference between the 0^{th} and 1^{st} order transmission amplitudes of the upper beam-splitting bar.

Additionally, the second order wave deflection should be similar to the transmission of the first orders: $\left|t_2^{II}\right| \approx \left|\tau_0^{II}\right|$.

In principle, very different grating profiles could fulfill such conditions. In the special type of three-level grating, here discussed, the simplest situation approximately occurs, where all amounts of the three waves are very similar. In this case $cos(2\varphi) \cong -1/2$ holds, i.e. the detour phase is close to 60°. The visualization of the destructive interference of the first order in the complex field plane is shown in Fig. 2.6 a). The complex sum of three field amplitudes with very similar amounts will only vanish in case of a phase difference of $2\varphi = 120°$ between all components. A similar situation arises for the zero order transmitted field (see Eq.2.5 (b)):

$$cos(\varphi) \cong -\frac{t_0^{II} t_0^{I}}{2 t_1^{II} t_1^{I}} \quad . \qquad \text{(Eq.2.6 (c))}$$

Analogously, $2\varphi = 120°$ phase differences between each of the three field amplitudes of rather similar amount result in a destructive interference.

Now, the question arises whether this three-wave-interference mechanism can provide some understanding for the rather peculiar shape of the grating, i.e. a high aspect ratio upper bar at a low aspect ratio lower bar. As pointed out, the destructive interference results from the detour phase of between fields of the different orders with rather similar amplitudes. In the case here treated, the similar field amplitudes are generated by a roughly equal splitting behavior of both binary sub-gratings (grating I and grating II). Binary gratings with broad bars and small thickness as well as small bar width and large thickness may produce such an equal splitting behavior.

In Fig. 2.6 b) the amplitude difference of zero and first order of the upper grating II illustrates this property. The dashed, bold line corresponds to the family of binary gratings with equal amplitude splitting. In order to realize a rather large detour phase, one needs a sufficiently large shift between the upper and the lower bar. Such large shifts can only be reached for a broad width lower bar and a small width upper bar. Taking into account the similar amplitude splitting behavior, a high-aspect-ratio upper bar at a low-aspect-ratio lower bar is needed. The point in Fig. 2.6 b) very close to the beginning of the dashed, bold line (high-aspect-ratio structure) corresponds to the phase shift for the actual design.

The diffraction efficiencies have been calculated by means of this model. The diffraction orders of grating I (t_k^I coefficients in Eq.2.1) have been calculated by RCWA and used as input fields for the rigorous calculation of the diffraction of the grating II, considered suspended in air. The model results have been compared with the RCWA simulation of the three-level grating, as shown in Fig. 2.7 a). The agreement between the the diffraction results is very good. The discrepancies are due to the assumption that the upper bar is suspended in air.

To validate the model, two other three-level gratings have been optimized to achieve the maximum efficiency in the first order for the same light incidence conditions. The gratings have different periods, $p = 1.75\lambda$ and $p = 2.25\lambda$. Also for these other two gratings, the model fits in a satisfactory way with the rigorous calculations, as demonstrated in Fig. 2.7 b), c). It is worth to mention again that the model discussed here is helpful for the physically understanding of the high efficiency and the peculiar grating shape, obtained by a parametric optimization of a three-level grating in resonance domain, but from the point of view of simulation, it does not present advantages for the parametric optimization, since it is based on rigorous RCWA calculations itself.

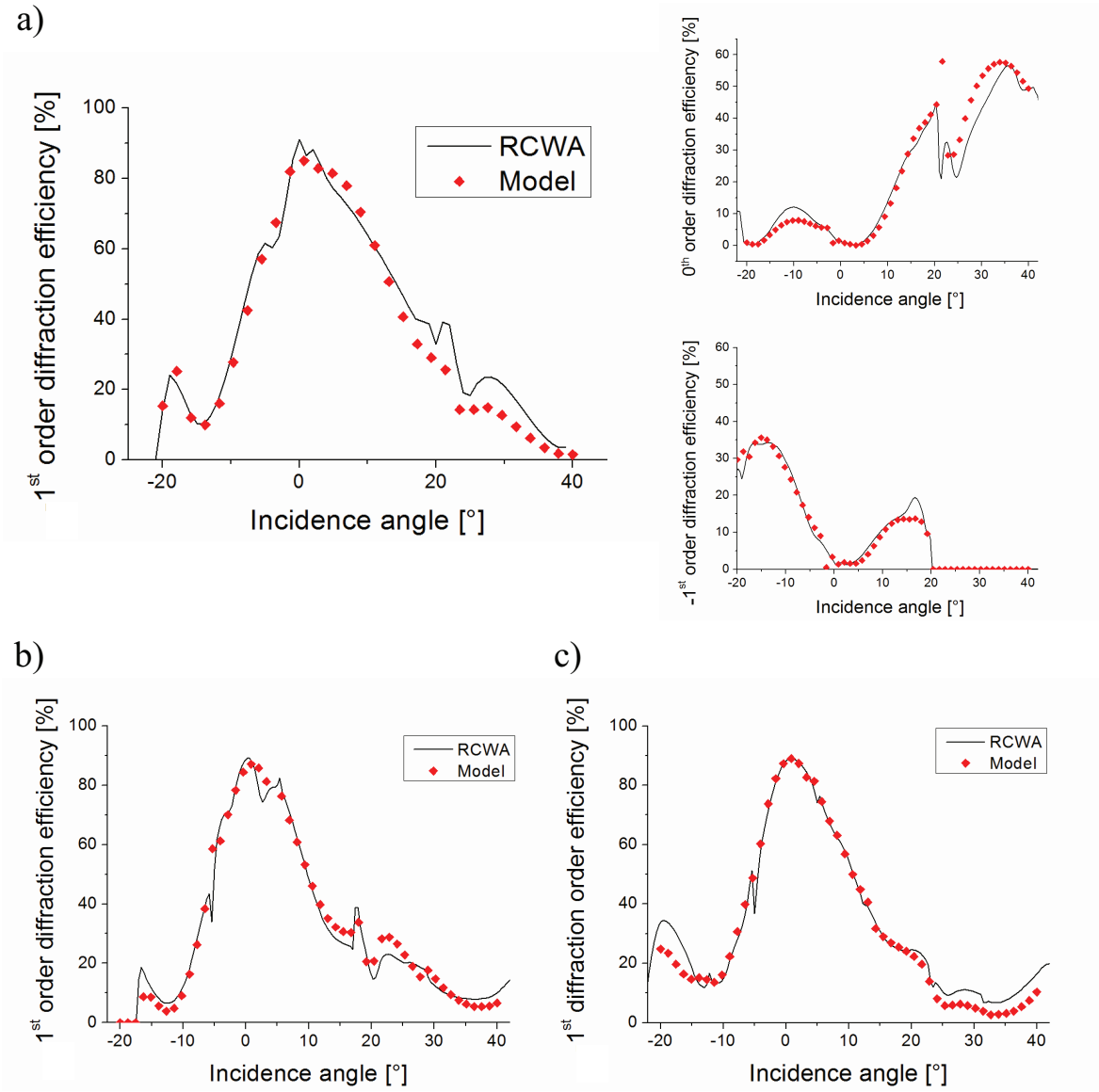

Figure 2.7: RCWA calculation and model comparison of the diffraction efficiencies of optimized three-level gratings; a) p= 2 λ (original design); b) p= 1.75 λ; p= 2.25 λ.

2.2 Effective-medium enhanced three-level grating (air to substrate)

The second blazed grating in resonance domain, analyzed in this work, is a monolithic fused silica grating. It operates at normal incidence, as in the case of the three level grating, but with opposite direction of the incident light, that in this case, is coming from air. The period of the grating is 1 μm and the operating wavelength is 650 nm.

Different kinds of structures have been optimized in order to achieve the maximum efficiency for the first diffraction order. Because of technological limitations, the minimum feature size,

allowed in the optimization, has been set again to 100 nm.

Due to the comparable small period, only binary and three-level structures have been optimized. The results of the optimization are reported in Fig. 2.8. The achieved efficiencies are quite moderate. The maximum efficiency, reach the value of 45%, 67%, and 74% for the simple binary, the two-ridges binary, and the three-level structure, respectively.

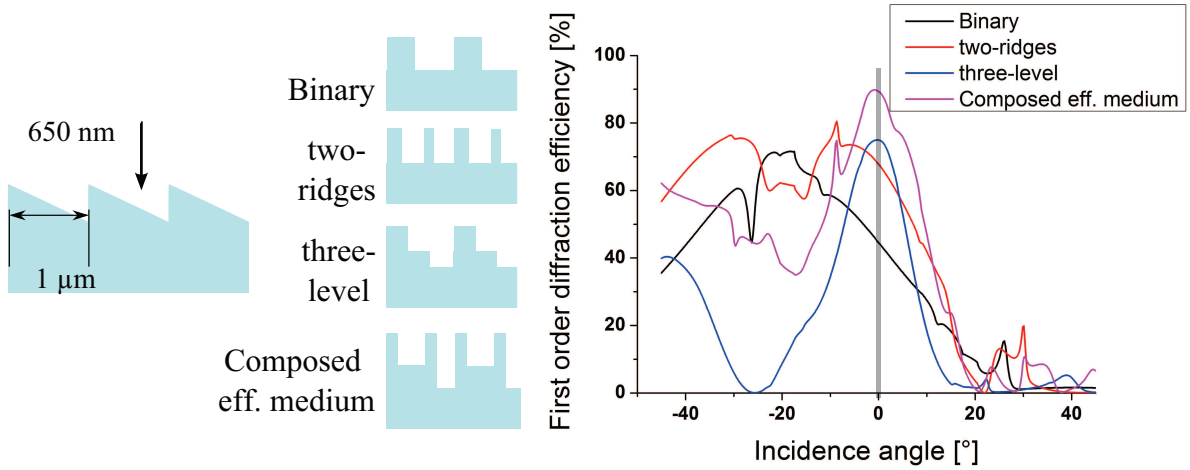

Figure 2.8: First order efficiency of different kinds of optimized fused silica gratings versus the incidence angle; Binary, two-ridges-binary, three-level and composed effective medium gratings optimized for normal incidence; wavelength: 650 nm TE polarized, p= 1 μm. The optimizations take into account fabrication constraints with a minimum CD = 100 nm for the grooves.

Therefore, the simple three-level structure is not an appropriate solution for this particular grating specifications. The reason for this can be found in the technological constrains for the optimization. If in the design the geometrical feature size limitations (CD> 100 nm, AR< 10) are not taken into account, then it is possible to optimize a three-level grating to achieve efficiencies higher than 90%. Nevertheless, the scope of this thesis is limited to gratings which can be fabricated; so new kinds of structure profiles have been investigated.

An approach to increase the efficiency can be the introduction of additional subwavelength structures in the grating profile to better control the phase profile. For example, combining a multilevel element with a simple binary structure on the upper level, generating a type of composed effective medium grating (as shown in the sketch of Fig. 2.8). By the use of such composite structure, the achieved optimized diffraction efficiency is around 90%. Nevertheless, the optimized grating geometry is extremely demanding from a technological point of view, as discussed in the following.

2.2.1 Design

The composite effective-medium grating is made of a three-level structure with an additional subwavelength binary feature on the top of the upper level, as schematically shown in Fig. 2.9

a). The optimization has taken into account some additional geometrical constrains in order to minimize the required technological effort. The height of the two ridges b_1 and b_2 is set to the same value; the lateral minimum feature size is limited to 100 nm.

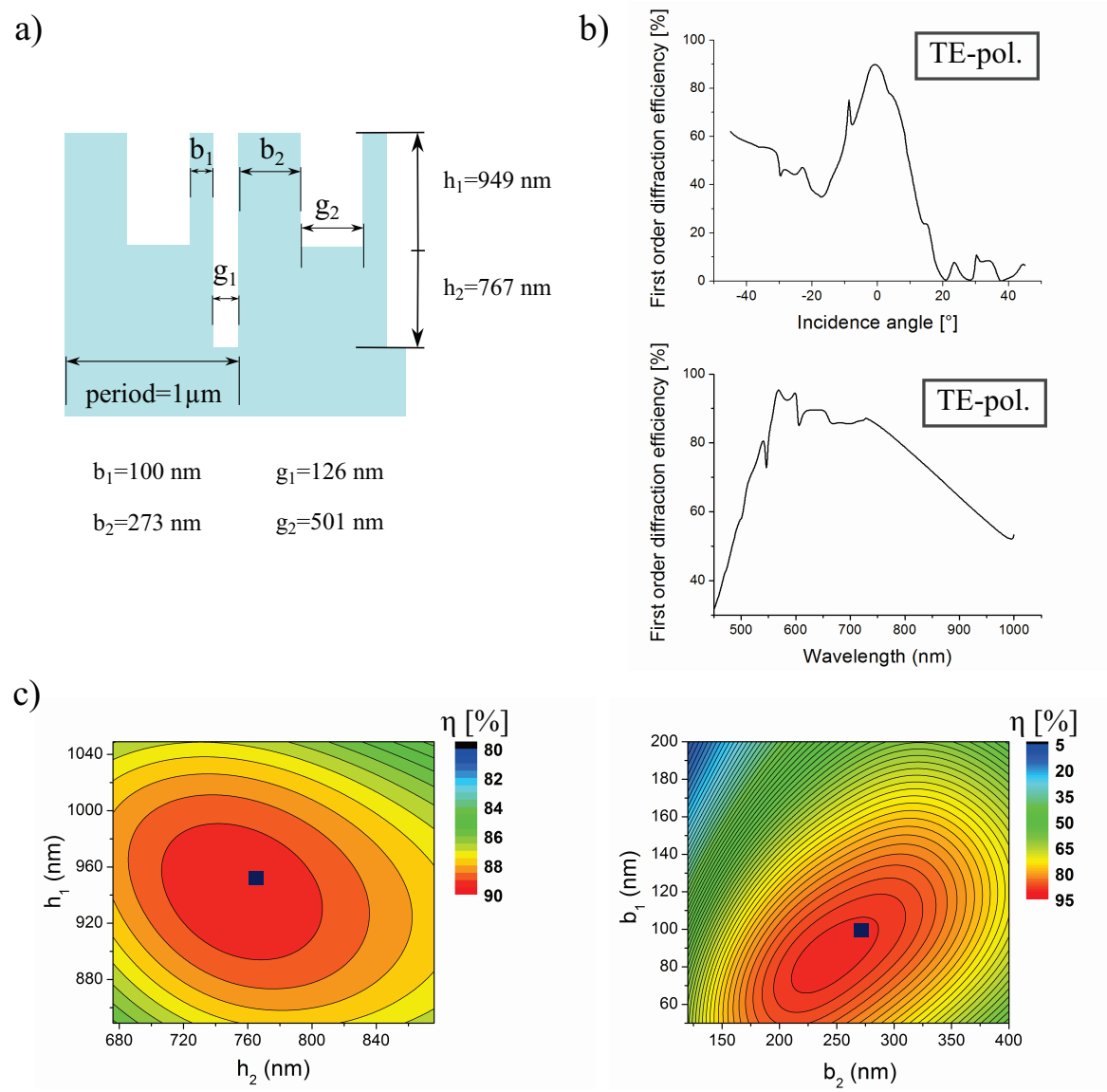

Figure 2.9: Optimized effective-medium enhanced-three level grating. a) Sketch of the structure with the geometrical parameters; b) First order diffraction efficiency η (TE) vs. incidence angle and wavelength, respectively; c) Fabrication tolerance analysis versus the level depths and the bars widths. The dots indicate the geometrical parameters selected for the fabrication.

The optimized values for the width and depth of the two bars are b_1= 100 nm, h_2= 767 nm and b_2= 273 nm, h_2= 949 nm, respectively. The AR of b_1 is close to 10 and should be considered already high for structures etched into fused silica. Furthermore, the combination of the bar b_1 with the neighboring groove g_1, with a width of 126 nm and a depth of 1716 nm (h_1 + h_2) is extremely challenging to be fabricated.

The effective-medium enhanced three-level grating achieves an efficiency slightly larger than

90% for the optimized operating point, i.e. $\lambda = 650nm, \theta = 0°$, as shown in Fig. 2.9 b). For shorter wavelengths, between 575-600 nm, the maximum efficiency reaches even higher values, close to 95%. Furthermore, the grating exhibits a wide bandwidth performance, with efficiencies are larger than 80% in a range of 550-780 nm for TE polarization and larger than 70% in a bandwidth of 490-720 nm for TM polarization.

The fabrication tolerance analysis (see Fig. 2.9 c)) shows that the design is quite tolerant with respect to the level heights (a variation of 60 nm causes 3% efficiency loss) and more sensitive to bars width, an increment of 20 nm is sufficient to lose the 3% of the efficiency.

As shown in Fig. 2.10, the grating possess another interesting property. By the variation of the width of bar b_2 it is possible to steer the incidence angle, while still maintaining the high efficiency performance. For instance, a b_2 width of 400 nm steers the optimum incidence angle to a value close to -7 degrees.

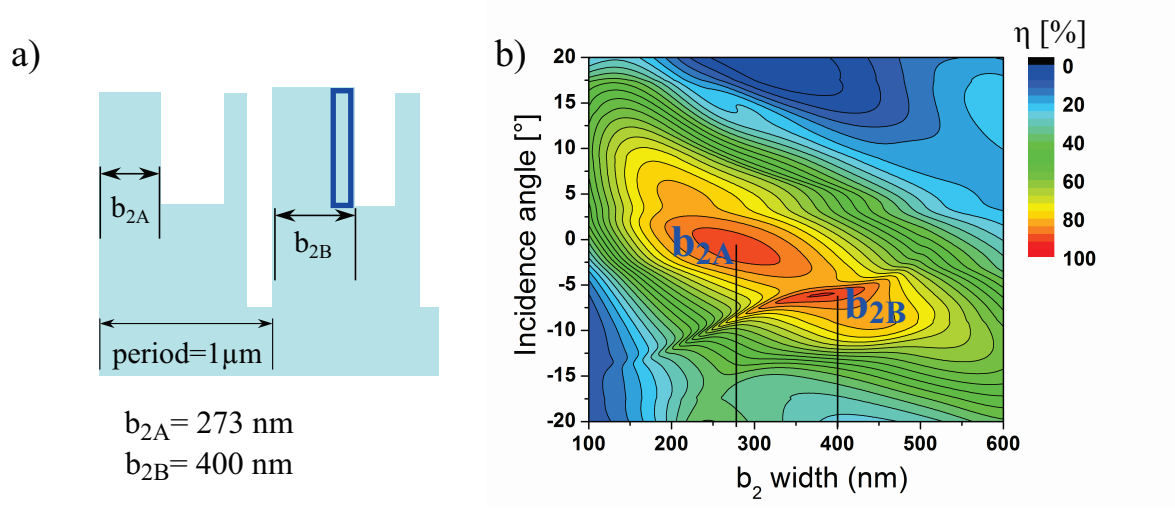

Figure 2.10: Effective-medium enhanced three-level grating: steering of the incidence angle vs b_2 width. a) Schematic illustration of the width variation of b_2; b) First order diffraction efficiency mapping vs b_2 width.

2.2.2 Modal analysis for the interpretation of the high efficiency

The blazed diffraction efficiency achieved by the effective-medium enhanced three-level grating is quite high with respect to the other kind of structures, as shown in Fig. 2.8.

To deduce the physical mechanism that leads to the high efficiency performance, it is possible to consider the grating composed of two distinct binary substructures, as schematically proposed in the sketch of Fig. 2.11. The upper grating is an effective medium grating and the bottom grating is a simple binary structure.

Firstly, the light is coupled from air to the first two-bar-layer. As shown in Fig. 2.12, this effective medium blazed (two bars binary grating) has only three propagating Bloch modes. Because of the flat phase of the normal input field (Fig. 2.12 a)), the Bloch mode 1, without

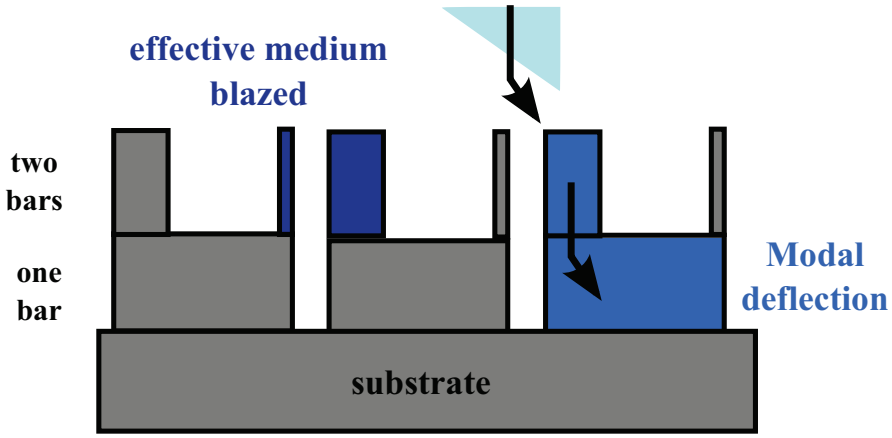

Figure 2.11: Effective-medium enhanced three-level grating: sketch of three unit cells (1 μm period): the entrance two-bar-layer acts like an effective medium blazed structure. The subsequent one-bar-layer mainly leads to a 1^{st} order deflection of the well localized, fundamental Bloch mode.

any zero, is dominantly excited ($\approx$ 65% of the total field), whereas modes 2 and 3 ($\approx$ 34% excitation together) exhibit approximately a sine and a cosine function topology of the E-Field (Fig. 2.12 b)), respectively. The modes propagate through the effective medium layer, accumulating a phase difference. If the phase difference between mode 2 and 3 attains a value of $\pi/2$ after the propagation through the effective medium layer, these modes produce an efficient deflection into the 1^{st} diffraction order:

$$\cos(\beta_1 z) - i\sin(\beta_1 z) = \exp(-i\beta_1 z)$$

with $\beta_1 = 2\pi/p$, see field distribution in Fig. 2.12 c).

The constructive interference with the 1^{st} order contribution of mode 1 leads to a maximum total efficiency in the 1^{st} order at the end of the first layer of about 70%.

A further increase of the efficiency seems to be impossible, because the dominantly excited mode 1 contains a huge amount of spurious Fourier components ($\approx$ 85%) and only a minor portion ($\approx$ 15%) takes part in creating the 1^{st} diffraction order.

Very high efficiencies are achieved with a binary blazed grating, only if the small number of propagating Bloch-modes inside the grating structure are well adapted to transform the input field into the desired output field [95, 96]. In other words, if the topology of these propagating modes does not fit well to the input and output field simultaneously, an additional mode conversion structure seems desirable.

The effective-medium enhanced three-level grating posses this required subsequent mode conversion structure. Actually, this additional mode conversion layer is here represented by the bottom level of the composite grating, i.e. it is a simple binary structure.

By this bottom level some amount of the spurious Fourier components of mode 1 can be transferred to the 1^{st} diffraction order. The fundamental Bloch mode 1 is well localized in the wider

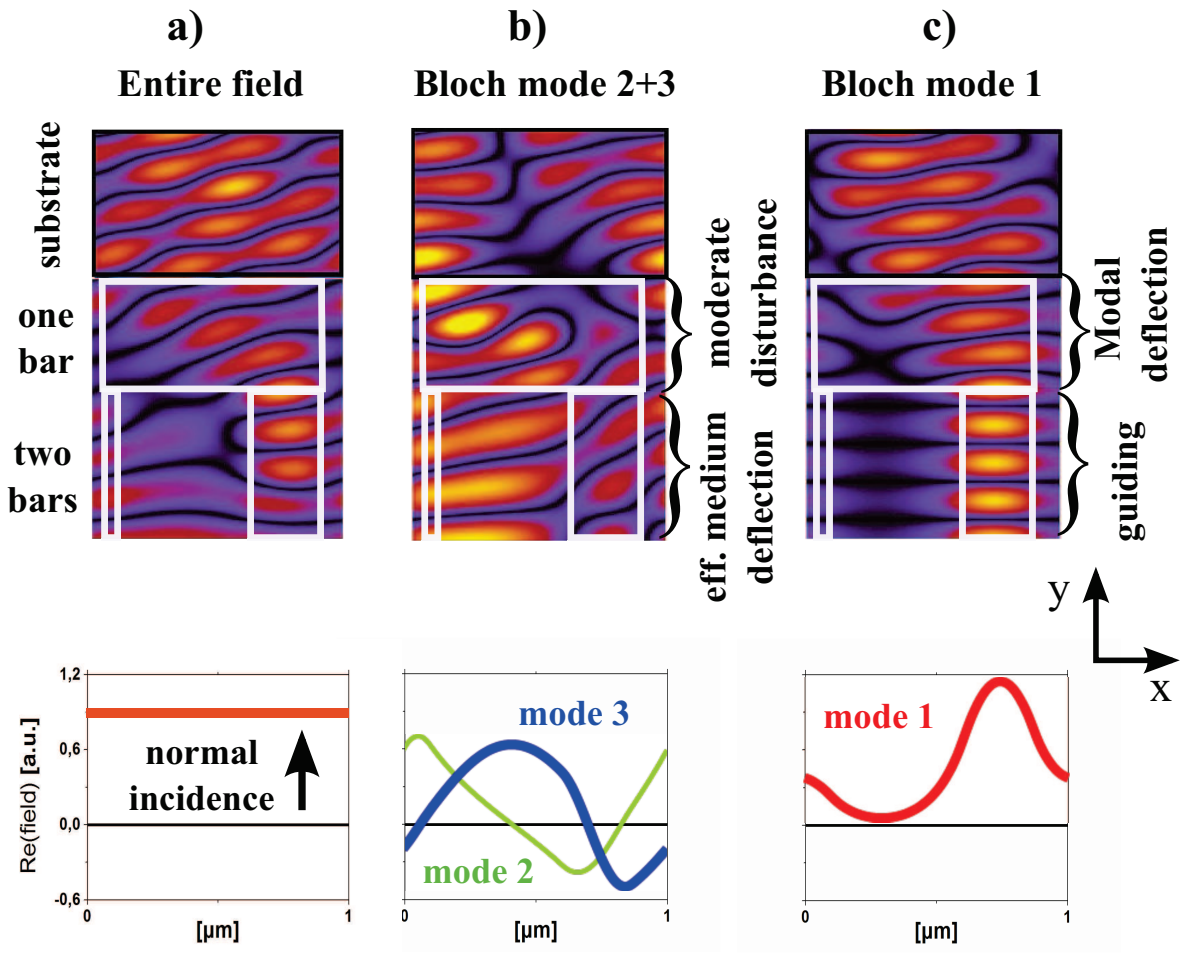

Figure 2.12: Electric field inside a unit cell: a) for a normal incident plane wave, b) for an incident light consisting of a superposition of mode 2 and 3 at the two-bar-grating entrance, c) for an incident fundamental Bloch mode at the two-bar-grating entrance.

bar of the effective medium layer (see Fig. 2.12 c)). It strikes the border of an even wider guiding bar of the second layer leading to a deflection of that light [97] and producing a much larger 1^{st} order Fourier contribution originating from mode 1. The constructive interference with the light from Bloch modes 2/3 yields a total efficiency of 90% for the composite grating. Thus, the high efficiency of the composite grating can be interpreted this way: the moderate maximum diffraction efficiency ($\approx$ 70%) of the 2 bar binary upper grating, is significantly increased to $\approx$ 90% by a subsequent bottom binary grating, acting as mode conversion layer for mode 1.

Chapter summary

In this chapter, the design of two fused silica blazed gratings working in resonance domain have been discussed. The first grating, is a simple three-level grating, parametrically optimized.

A new physical interpretation for the achieved high efficiency has been provided. The model is based on a three-wave interference mechanism in two separate, consecutive one-bar binary gratings, where the first grating leads to a splitting of the input field into the three output order with rather similar amplitudes and the second grating provides the desired phase differences for constructive/destructive interferences. The generation of the desired phases needs a large enough shift between the upper and lower grating bar leading to the very peculiar grating structure - a high-aspect-ratio upper bar at a low-aspect-ratio lower bar. The efficiencies calculated by the model are in good agreement with the result of rigorous simulations of the three-level grating.

The second optimized grating shows a new kind of grating profile. It is a composition of a three-level structure and an effective-medium additional feature. The high efficiency performance can be explained analyzing the Bloch modes of the structure. The analysis reveals that the first order response of an ordinary effective medium blazed grating is strongly increased by an additional, subsequent mode conversion layer. This grating layer converts a significant amount of the fundamental Bloch mode to the first order.

The fabrication of both gratings is quite challenging and the standard technology, discussed in the previous chapter would not be sufficient to obtain good quality structures. New technological solutions will be proposed and discussed in the next chapter.

3 New technological approaches for the fabrication of multilevel blazed gratings

In this chapter, the new techniques, purposely developed for the fabrication of the multilevel gratings discussed in chapter 2, are described.
The standard multilevel approach is introduced first and its limits are illustrated in order to explain the necessity for new approaches and their advantages for the fabrication of high efficiency multilevel blazed gratings.

3.1 Standard multistep-binary optics technology

The standard approach for the fabrication of blazed multilevel gratings is based on a multistep-binary optics approach [79]. Each single level of a multilevel grating can be considered as a simple binary structure; and the fabrication process consists in a consecutive definition and transfer of each single level into the substrate (fused silica, within this work).
This approach, discussed in general in the section 1.3.2, is described here in detail for the fabrication of the three-level and the effective-medium enhanced three-level gratings, introduced and discussed in the previous chapter.
For both kinds of gratings only two consecutive binary steps are required. In the initial step of the fabrication process, a fused silica substrate is covered first with a chromium layer followed by an electron-beam resist layer. The resist is exposed by electron beam lithography to achieve the first binary profile with the desired groove width. Using reactive ion etching (RIE), the developed resist pattern is subsequently transferred into the chromium layer. The patterned chromium then acts as a hard mask for plasma deep etching of the binary structure into the fused silica substrate [79]. Then the same process is repeated to realize the second binary grating profile on top of the first one. The sequence for the fabrication of the two levels is selected based on the geometry of the structure, in order to reduce the technological difficulties for the grating fabrication. One of the possible fabrication sequence for a three-level grating is schematically shown in Fig. 3.1. The process starts with realization of the bottom binary structure, followed by fabrication of the upper binary bar.
Also for the effective-medium enhanced three-level grating only two consecutive lithography steps are needed in order to define the geometry; the two grooves are separately exposed and

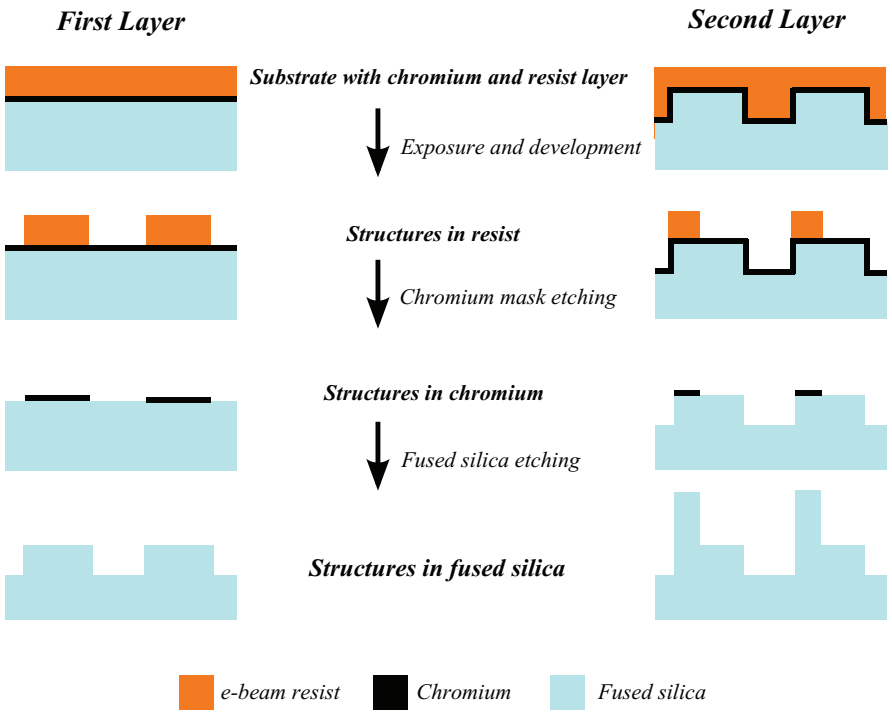

Figure 3.1: Example of a standard multilevel technological approach for the fabrication of a three-level grating. Bottom level is here transferred into substrate as first level. The upper level is the second binary fabrication step.

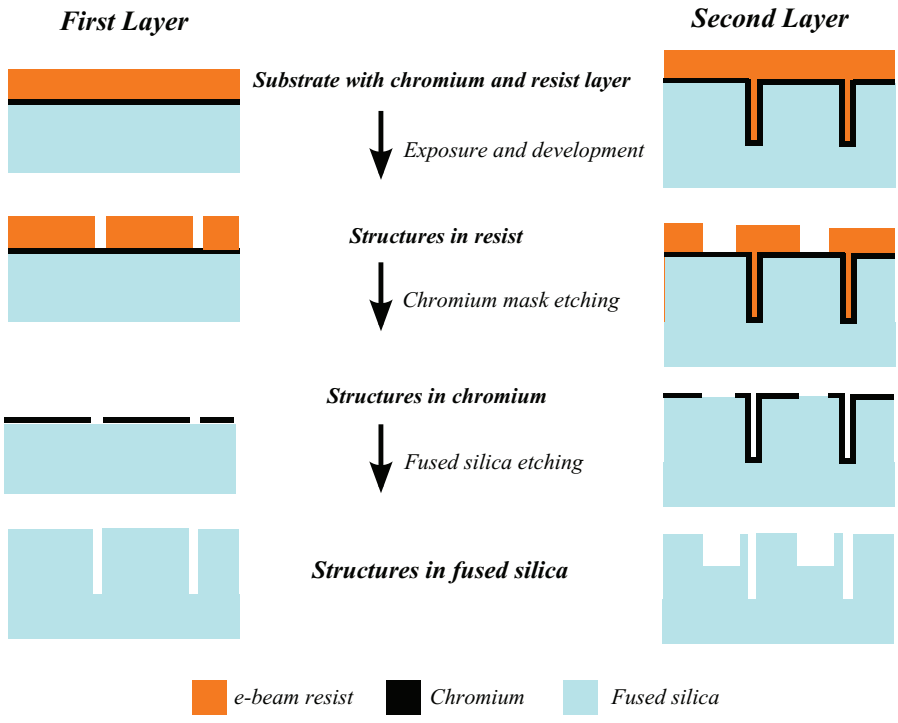

Figure 3.2: Example of a standard multilevel technological approach for the fabrication of an effective-medium enhanced three-level grating.

transferred into the substrate in two consecutive steps. One of the possible standard fabrication approaches for an effective-medium enhanced three-level grating is schematically illustrated in Fig. 3.2. Here, the smallest and deepest groove is completely transferred in the first binary fabrication step; and in the second fabrication phase, the wider groove is realized.

Limitations of the standard technology

The standard multilevel technology exhibits some limitations regarding the fabrication of accurate multilevel optical structures.

There are three main problems related to this technology, the first two concerning the lithographic processes and the last one regarding the transferring process into the substrate of high aspect ratio (AR) structures.

The first issue is due to the alignment errors that could occur between the two lithographic exposures of the different levels. This misalignment between the first etched level and the resist pattern of the second step may occur not uniformly over the sample, generating local variations and different artifacts in the profile structure, as schematically shown in Fig. 3.3 for a three-level structure.

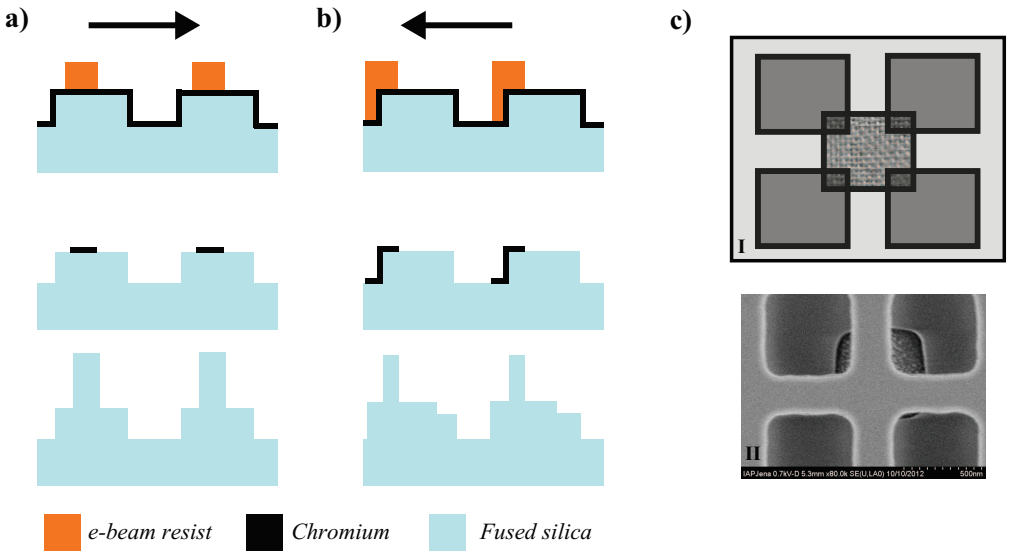

Figure 3.3: Alignment error between lithographic steps. a) and b) Schematic illustration of alignment errors in a three-level grating; c) Misalignment example in a 2D structure: the SEM picture (II) is compared with the structure design (I).

The other problem concerning the lithographic process is related to a non-planarity in the scale of the grating period of the chromium and resist layers of the second fabrication step (see Fig. 3.4 a)). The non-planarity is due to the fact that the layers are coated on the top of an already microstructured substrate. As a consequence, the profile of the upper binary grating might not be well defined and its dimensions may change across the grating area generating sizing errors

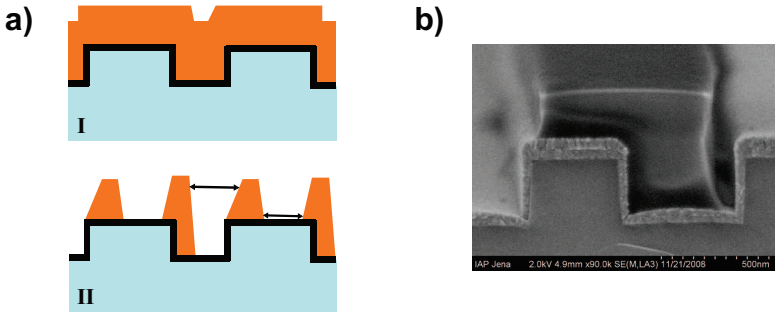

Figure 3.4: Sizing error due to the non-uniformity of the resist/chromium layer in the second fabrication step. a) Schematic view: I-non uniform resist layer for the second layer fabrication, II- non uniform resist structures; b) SEM picture of a typical sizing error.

of the local structures, as illustrated in the Fig. 3.4 b).

One technological solution to avoid this problem related to the non-uniform chromium and resist layers has been suggested by David [98]. This approach is based on the use of a very thin resist layer (50-80 nm) and stepwise etching through two successive different metal masks (Cr and Al). However, the achievable depth of the structure is limited due to the small thickness of the metal masks ($\approx 20nm$) [98].

Additionally, is it necessary to stress, that sizing and alignment errors may occur simultaneously, and a sharp distinction between the two fabrication artifacts in general is not possible.

The third limitation concerns the deviation between the achieved structure profiles, etched into the substrate, and the design based on perfectly sharp sidewalls. This is especially a limit for fused silica gratings in resonance domain due to their aspect ratio (AR). With the increase of the aspect ratio of the grating bars, the grooves strongly broaden towards the top of the structures, assuming a typical Y-shape, as recognizable from the SEM grating pictures of Fig. 3.5 (this typical profile is here called Y-shape because the groove width becomes larger on top).

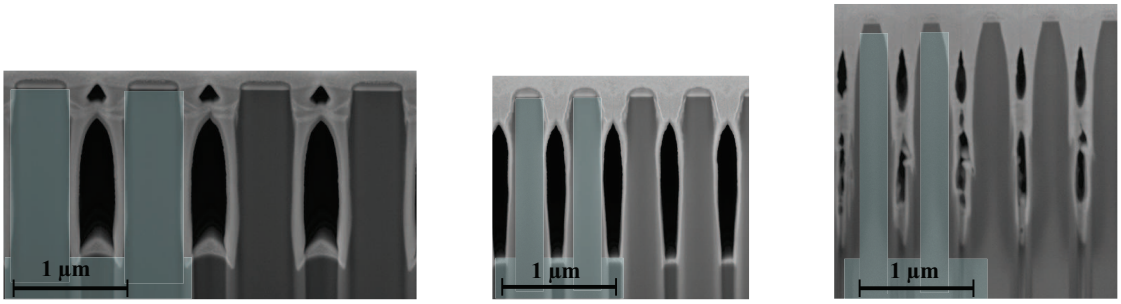

Figure 3.5: Typical sidewall profile of high aspect ratio (HAR) structures etched in fused silica. The Y-shape profile becomes more pronounced with the increase of the AR of the structures.

This Y-shape of the groove walls is related to the profile of the binary chromium mask and to its degradation during the deep etching in the fused silica substrate. For small grooves it is difficult to achieve sharp perpendicular sidewall for the chromium structures.
This difficulty is related to the optimization of the RIE etching process, that at Fraunhofer-IOF is based on a Inductively Coupled Plasma (ICP) technique. To achieve good quality sidewall in chromium, the chromium structure is usually overetched [1] against the resist mask. This means that the width of the groove in chromium is larger than the resist groove width. To compensate this effect and to obtain the desired width for the groove in chromium, a *CD bias* is introduced for the lithographic exposure, as schematically shown in Fig. 3.6.

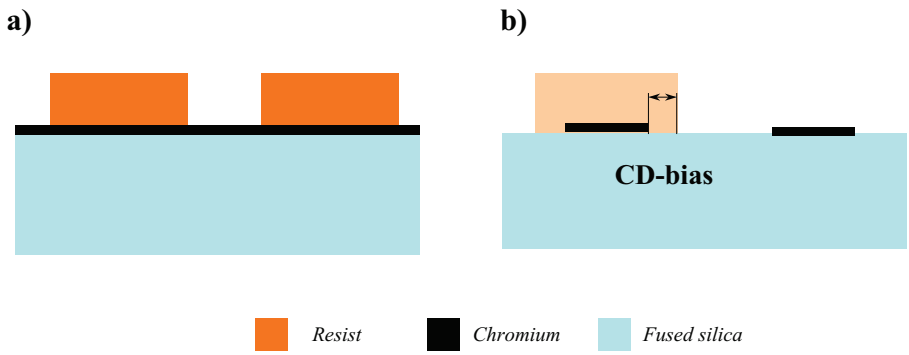

Figure 3.6: Schematically illustration of the introduction of CD-bias. a) Resist structures; b) Chromium structures: the lateral dimension of the Cr structures is reduced by a factor 2x CD-bias. For sake of clarity, one resist structure is included in the picture.

If the grating grooves are small (100-200 nm), it is not possible to use the optimal *CD bias* value, because of the minimum feature size achievable in resist (≈ 60 nm). In this case, a smaller *CD bias* is introduced and the sidewall of the chromium structures are not perfectly sharp [99]. Additionally, the chromium mask suffers of a degradation that increases with the etching depth. The resulting Y-shape of the grooves affects the achievable efficiency. However, it is possible to optimize the blazed grating structure taking into account the real fabricated shape of the bar, minimizing such efficiency losses.
Nevertheless, if such sidewall broadening effect affects already the binary structure, etched in the first step of the multilevel process, it may be very critical for the successive fabrication phases. The geometries of successive levels will be seriously compromised if the structure is characterized from features close to edge of the previous etched groove.
In resonance domain, alignment and sizing fabrication errors can have a major impact on the grating performances, because such imperfections are not negligible [100, 101] with respect to the small feature sizes of such diffractive elements. Additionally, high aspect ratio structures are quite often essential to achieve high efficiencies, especially in case of low index gratings, as

[1] overetched means that the etching process is longer than required, here, to transfer the pattern geometry from the resist mask to the chromium mask.

fused silica gratings.
Furthermore, nowadays, the diffraction gratings are moving from research to real applications; as consequence the processes employed for their fabrication must be scalable to larger areas (in the cm^2 region or beyond) delivering high and reliable optical performances [55, 59, 102]. For these reasons, the above discussed limits of the standard multilevel fabrication need to be addressed and if possible overcome.
In the following paragraphs, three new fabrication techniques are proposed and discussed as solution to address each singular problem of the standard approach. In particular, the new approaches have been proposed for successful fabrication of the gratings discussed in chapter 2.

3.2 Three-resist Layer Technology

As mentioned before, the chromium/resist layers used in the second or successive binary optics step, are coated on the top of an already microstructured substrate. Consequently, the non-uniformity of these layers over the grating area, can be avoided if the microstructured surface could be planarized.
This can be achieved in a quite simple way by introducing an additional step in the standard fabrication process.
The modified approach, called *Three-resist Layer Technology*, consists in the use of an additional layer of conventional photoresist in order to planarize the microstructered substrate (see Fig. 3.7(I)), before to proceed with the second binary fabrication step. (Planarization layers have been long used in other technological field, as in microelectronic fabrication [80]).
This way, a planar and uniformly thick chromium layer can be obtained (Fig. 3.7(II)), on which the electron beam resist can be structured with the required accuracy (see Fig. 3.7(III)). The resist pattern is transfered to the chromium by a reactive ion etching (RIE) process (see Fig. 3.7(IV)), and then the resist is removed (see Fig. 3.7(V)). The pattern geometry is transferred from the chromium mask into the photoresist by (RIE) process with oxygen plasma (Fig. 3.7(VI)).
The final etching into the substrate represents the most critical step of the fabrication process, due to the additional depth of the planarization layer (Fig. 3.7(VII))). The fabrication sequence for the different levels is decided in order to keep this etching depth as small as possible. Another option can be to additionally etch the resist planarization layer to the exact depth of the already etched level, before to proceed with the chromium deposition. This way, the etching depth is reduced again to the original designed one.

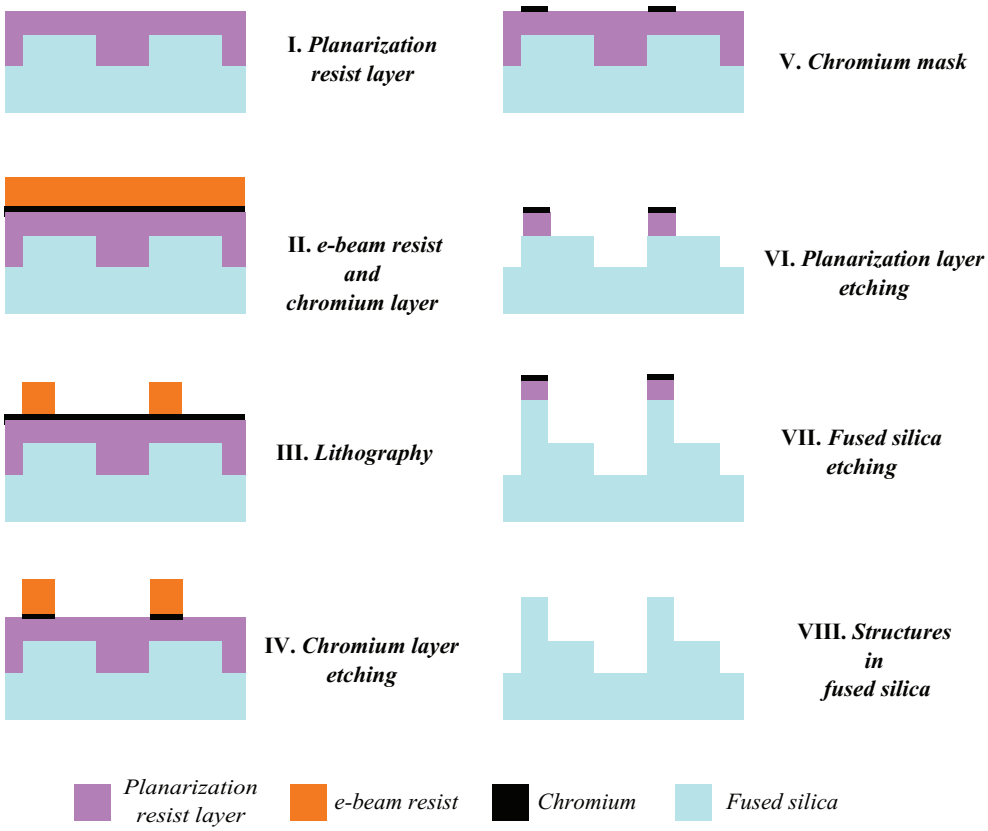

Figure 3.7: Three-resist Layer Technology: fabrication flow scheme for a three-level grating. The fabrication of the second level is schematically shown.

3.3 Relaxed Alignment Technology

The *Three-resist Layer Technology*, as discussed in the previous paragraph, is a good solution to solve the sizing errors, but it is not suited to avoid the alignment errors. This because the origin of misalignment errors lies in the non-perfect pattern overlap between different lithographic steps.

A possibility to prevent alignment errors consists in the encoding of the lateral dimension of all levels in a single mask. This is the basic idea of the *Relaxed Alignment Technology*, which will be discussed in the following. In this approach, a single coded chromium mask is used during the whole fabrication process. This coded chromium mask contains all lateral features of each level. The mask is generated by a standard process, i.e. a first lithographic exposure is used for the definition of these features in resist and then the pattern is transferred into the chromium layer. As in the standard approach, the chromium mask is used as hard mask to transfer the pattern geometries into the substrate. The difference consists in the requirement of selective etching steps to transfer the different levels of the microstructure into the substrate.

The singular level etching step is accomplished by the use of an additional resist mask, which selectively covers the coded chromium mask.
To better explain this concept, the fabrication of a three-level grating by the *Relaxed Alignment Technology* is discussed in detail in the following and schematically illustrated in Fig. 3.8.

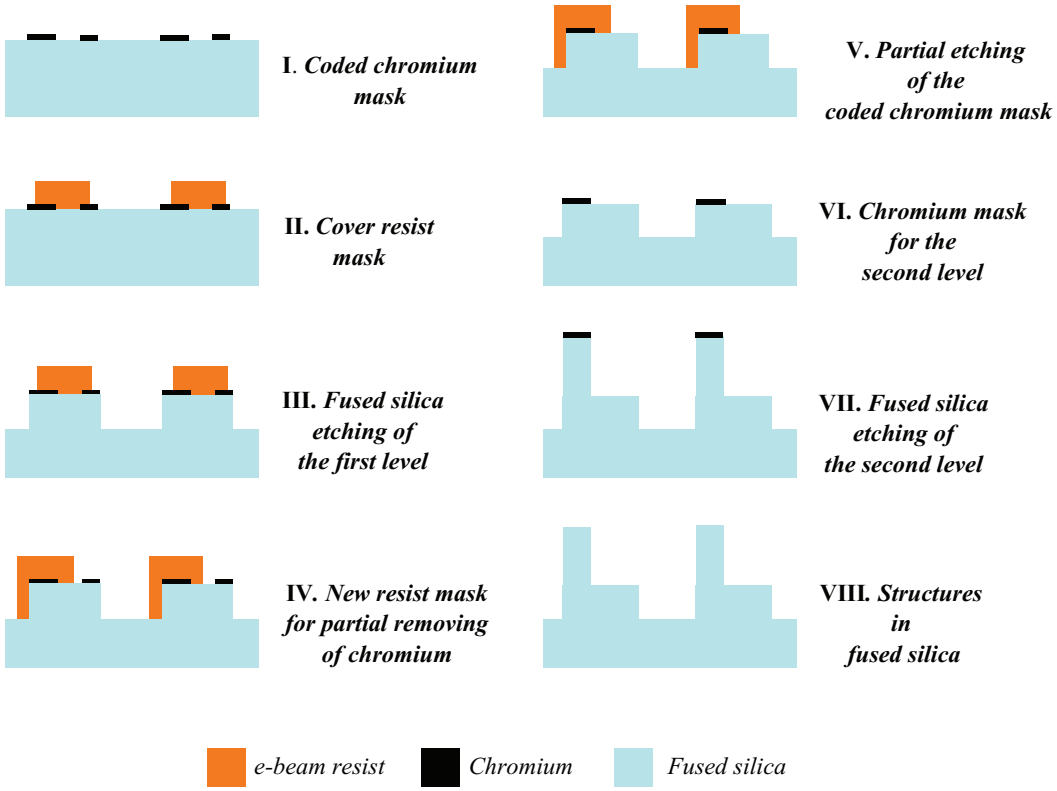

Figure 3.8: Relaxed Alignment Technology: fabrication flow scheme for a three-level grating.

All lateral information of the three level grating is coded in the initial chromium mask (see Fig. 3.8(I)). To proceed with the deep etching into the substrate of one of the two levels, it is necessary to cover a part of the coded mask. Thus, a lithography step is required to generate this cover resist mask (Fig. 3.8(II)). But, the alignment requirements for the exposure of the cover mask are not critical, because the lateral dimensions of the level which has to be etched are well defined by the already existing chromium mask. Therefore, the required alignment accuracy is relaxed to the minimum feature size of the chromium structures. The pattern is transferred into the fused silica substrate by a RIE process until the height of the first level is reached (Fig. 3.8(III)).
To further proceed with the fabrication of the three-level grating, it is necessary to remove the part of the chromium mask that is not needed anymore. An additional lithographic exposure (Fig. 3.8(V)) is used to protect the chromium pattern that has to be preserved after the next chromium etching process. This step is also not challenging with respect to the alignment

accuracy. After removing the protecting resist structure (Fig. 3.8(VI)) the second level is transferred into the fused silica substrate as well (Fig. 3.8(VII)). The last step of the fabrication process is the removal of the remaining chromium mask (Fig. 3.8(VIII)), just as it is done in the standard technology. Now, the three-level profile is completely transferred into the substrate.
The *Relaxed Alignment Technology* is a valid approach to avoid the typical alignment errors of the standard multistep-binary technology. Nevertheless, also this approach shows some limitations and additional efforts that should be considered and analyzed. For the fabrication of a three-level grating for instance, an additional lithographic exposure is required in comparison to the standard technological approach.
Additionally, the use of a combined resist-chromium mask for the etching of the second phase level limits the achievable depth for this level (Fig.3.8(III)). The reason is the relatively low etching rate selectivity of the resist with respect to the fused silica in the RIE process (typically

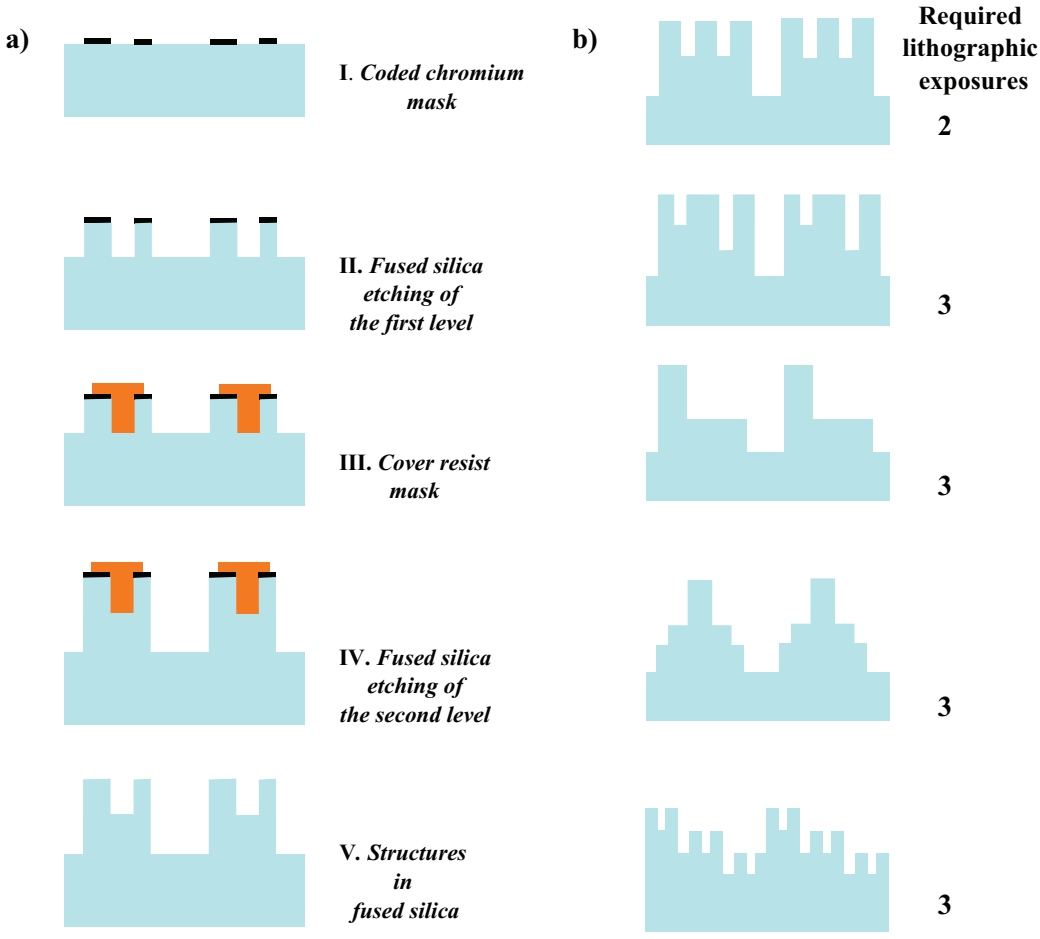

Figure 3.9: Sequence of most relevant technological steps for the fabrication of an effective medium enhanced three-level grating by Relaxed Alignment Technology approach using the same coded chromium mask for a three-level grating (see Fig. 3.8). (b) Examples of structures that can be realized by this technological approach.

$\approx$ 1..1.3). Furthermore, the resist thickness should be not larger than a few hundred nanometers in order to obtain the required resolution for diffractive elements in resonance domain.
A further limitation might arise from charging effects of the resist during the successive e-beam lithography steps due to the reduction of the chromium mask area. This charging effect could cause additional misalignment of the patterned structures. The resulting overlay error might have a similar effect than the misalignment errors in the standard approach.
Despite these limitations, the idea to use a resist-chromium mask adds a high flexibility to the profile of the structures that can be fabricated. Fig. 3.9 shows, for example, the possibility to use the same coded chromium mask for the fabrication of a three-level grating (Fig. 3.8(I)) or an effective-medium enhanced three-level grating, respectively.
By a smart variation of the sequential exposures and etching steps different structures such as binary and multilevel gratings or a combination of both can be realized. Some examples of such structures are shown in Fig. 3.9(b); e.g. effective medium, multilevel or multilevel-effective medium gratings.

3.4 Atomic Layer Deposition (ALD) Enhanced Technology

The two new alternative technologies discussed in the previous paragraphs are well suited to solve the sizing and alignment errors, but they cannot solve the problem concerning the degradation of the bar walls which occurs for demanding high aspect ratio structures.
The broadening effect at the top of the grooves significantly limits the possibility to successfully proceed with the fabrication of the subsequent level of the structure. The effective medium enhanced three-level grating discussed in 2.2.1 is for instance a typical structure geometry which requires an additional alternative technological approach in order to be successfully fabricated. For this reason, it is considered as example to describe the new technology.
Because the degradation of the walls is strictly correlated with the demanding aspect ratio of the structures, it is necessary to reduce it in order to obtain good quality sidewall profiles, as schematically described in Fig. 3.10.

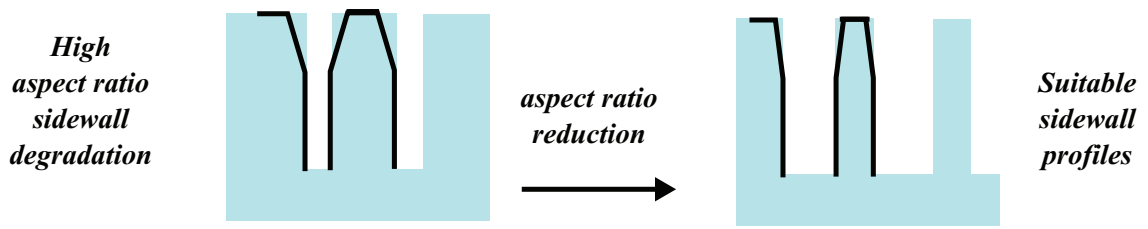

Figure 3.10: Reduction of the typical Y-shape walls profile by widening of the groove: schematic view.

The increase of the critical grooves width is the first step of the new developed approach, described in this paragraph, the so called *ALD*[2] *Enhanced Technology*, as shown in detail in Fig. 3.11.

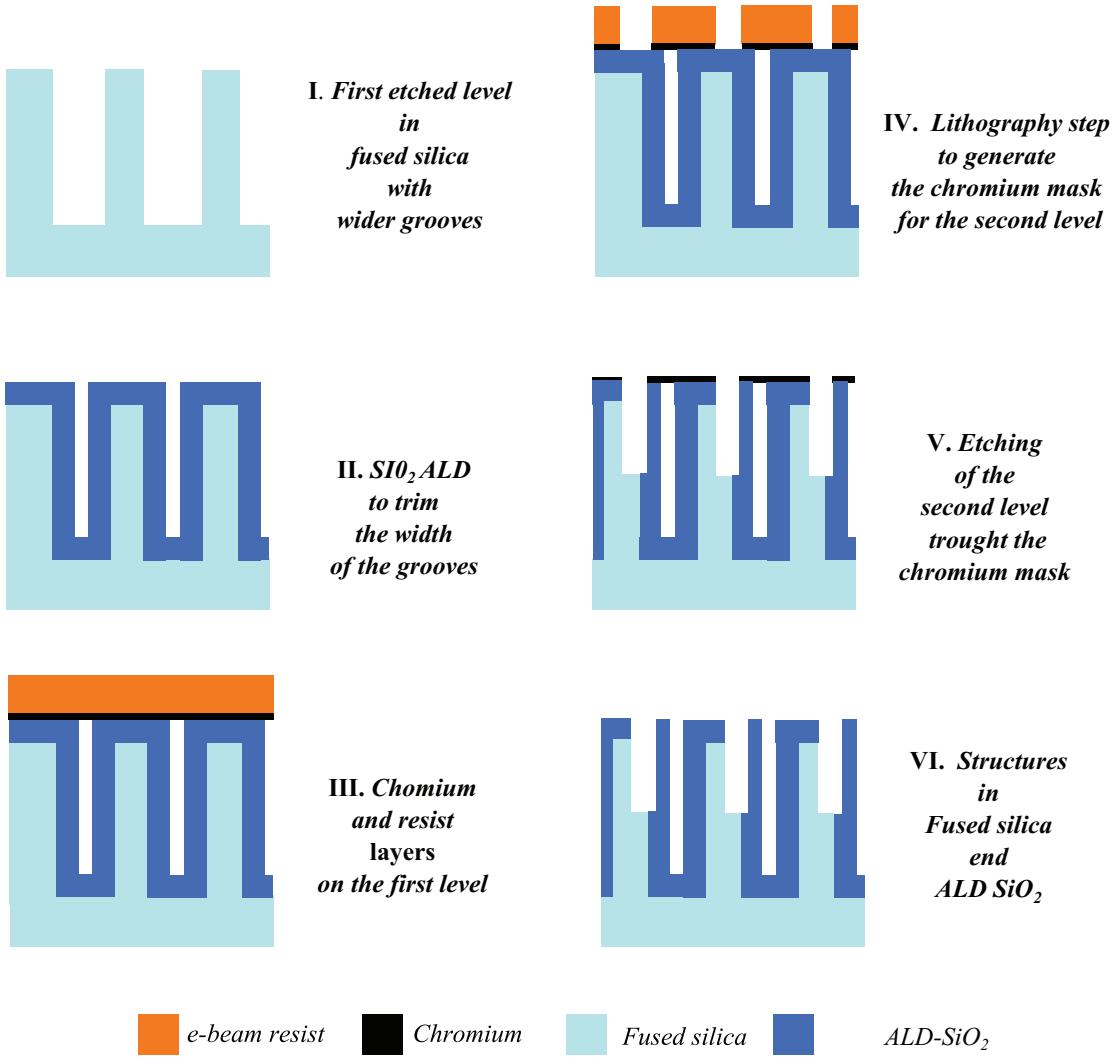

Figure 3.11: ALD Enhanced Technology: fabrication flow scheme for the second level fabrication of effective medium enhanced three-level grating.

The critical dimension of the narrow grooves is considerably increased during the first binary fabrication process (Fig. 3.11(I)). This way, the aspect ratio is reduced to a value smaller than 5, ensuring a well-etched sidewall profile. It is then possible to trim the groove width towards the designed value by ALD of SiO_2 (silicon dioxide), by adjusting the deposed layer thickness. The ALD technique [104] allows for depositing the material precisely and conformal to the topology of the original sample.

[2] ALD (Atomic Layer Deposition) is a conformal layer deposition process based on sequential, self-limiting surface reactions. Most of the ALD processes are based on binary reaction sequences [103].

In the fabrication example discussed here, the SiO_2 is deposited following the binary grating geometry, as shown in (Fig. 3.11(II)). Afterwards the fabrication of the second level is identical to the standard approach. The microstructured substrate is covered with chromium and resist (Fig. 3.11(III)). The resist is exposed by electron beam lithography, and used as mask to etch the Chromium layer (Fig. 3.11(IV)). The microstructured chromium layer is used as a mask for the deep etching into the fused silica substrate (Fig. 3.11(V)). After the removal of the chromium layer (Fig. 3.11(VI)), the grating, characterized by demanding AR structures, is obtained in fused silica.

By the addition of the ALD step in the standard fabrication process, the problems due to the Y-shaped high aspect ratio groove can be strongly reduced, allowing the fabrication of demanding AR structures with good quality sidewall profile.

Nevertheless, it is worth to mention, that the problem concerning the Y-shape groove profile is reduced by this approach, but not completely overcome.

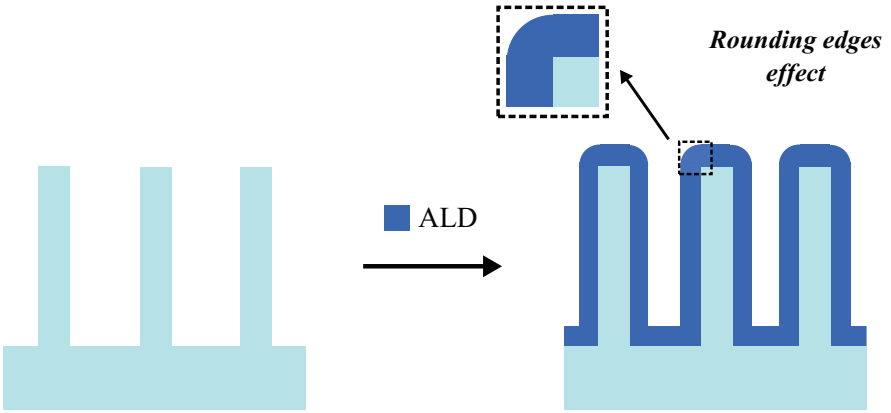

Figure 3.12: ALD rounding edges effect. The radius of curvature coincides with the ALD thickness.

On the one hand, the sidewalls of the gratings are still not perfectly sharp also in case of reduced AR structures; on the other hand, because the ALD is conformal to the coated profile, the edges of the grating bars will suffer from a kind of rounding effect. This effect, schematically shown in Fig. 3.12, will become more pronounced with the increase of the ALD thickness. The best compromise between AR reduction and ALD thickness depends on the peculiar grating profile.

Chapter summary

The standard multilevel binary optic technology exhibits some limitations for the fabrication of diffractive elements in resonance domain.

These limitations are related the non-planarity of the chromium/resist layer for the fabrication steps successive to the first one, the misalignment between different lithographic exposures and the sidewall profiles of high AR structures. In this chapter, three new technological approaches

to address and solve the single problems have been proposed.
For the non-planar layer issue, the standard approach has been modified by the introduction of a resist planarization layer, before to proceed with the other binary step fabrication.
The misalignment errors can be avoided by using a single coded chrome mask for the whole fabrication process. This coded mask contains all lateral dimensions of the grating. Resist cover masks allow the selective etching of the different levels.
To reduce the typical Y-shape profile of high AR fused silica structures, an ALD step has been introduced in the standard approach. In the first fabrication step, the critical AR is reduced, by enlarging the groove width. The ALD is than used in order to trim the groove width.
In addition, it is possible to combine the different technological approaches according to the particular geometry of the grating.
These new approaches have been developed for the successful fabrication of the two multilevel blazed gratings presented in chapter 2. The results of the fabrication of the two different gratings will be presented in the next chapter.

4 Grating fabrication results and discussion

In this chapter, the results of the fabrication of the three-level and effective-medium enhanced three-level gratings designed in chapter 2 are presented and discussed. The fabrication has been carried out by means of the standard multilevel binary optics and new technological approaches discussed in the chapter 3. The fabricated gratings have been characterized in terms of topological quality of the structures and diffraction performance. The efficiency measurements have been evaluated with respect to rigorous simulations of the original designs and of the fabricated structures.
After a short introductory section about technological capabilities available at Fraunhofer-IOF, the fabrication results obtained by the new technological approaches are compared with the results of the standard multilevel fabrication technology.

4.1 General technological specifications for the grating fabrication

The multilevel blazed gratings, discussed in this thesis, have been fabricated on 6 inch fused silica mask blanks (substrates typically used for mask fabrication in semiconductor industry). For both designs, gratings with slightly different lateral features have been realized in one singular mask blank in order to optimize the exposure data and the etching parameters for the fabrication process.
As the standard procedure, for a single binary fabrication step, the mask blank is first covered with chromium (typically 80-100 nm thick layer) and then with resist (300 nm thick layer). The resist used, the FEP 171 (Fuji-Film) [105], is a positive chemically amplified e-beam resist [106]. After a pre-exposure bake step, the resist coated sample is exposed by the electron beam system Vistec SB350 OS (Vistec Electron Beam GmbH, Jena). This is a special system developed for fast exposure of optical elements, by means of a variable-shape beam [107].
The area of each grating pattern is 15 mm x 15 mm, in order to enable a proper optical characterization. The lithographic exposure to write a single grating lasts less than 20 minutes for each lithographic step. Two kinds of alignment marks are used, in particular a first mark for the global alignment of the substrate, i.e. the mask blank, and a second one for the fine adjustment close to each grating area. The exposed gratings are then developed with OPD4262, a TMAH (tetra methyl-ammonium-hydroxide) based positive photoresist developer. The resist

pattern is used as a mask for the etching of the chromium layer. The deep etching of the grating structure into the fused silica substrate is carried out by a reactive ion etching (RIE). For the *Three-resist Layer Technology*, the resist AZ4712 (microchemical) [108] is used for the planarization layer.

4.2 Three-level grating

The three-level grating has been fabricated by three different technological approaches, i.e. standard, *Three-resist Layer* and *Relaxed Alignment* technology, described in the section 3.1, 3.2 and 3.3, respectively.
For each technological approach, two different runs have been carried out in order to confirm the suitability and the repeatability of the fabrication process.
In the following, the characterization results of all three technologies are reported and discussed.

4.2.1 Standard technology samples

The fabrication of the three-level grating (of Fig. 2.2 a)) by the standard technological approach has been realized following the fabrication flow shown in Fig. 3.1. The smoothest level (h_2= 394 nm) has been fabricated as first. Then the microstructured substrate has been covered again with chromium and e-beam resist to proceed with the fabrication of the upper smallest bar (h_1= 778 nm).
The two samples, I and II, have been first inspected by optical microscope. The gratings surfaces of sample I appears to be not homogenous; instead the sample II shows a good surface homogeneity. The spatial mapping of the diffraction efficiency of sample I, shown in Fig. 4.1, confirms a significant inhomogeneity[1] within the six fabricated gratings. Nevertheless some grating areas exhibit high efficiency around 86%. The efficiency is here defined as the ratio between first order transmitted intensity and the input intensity inside the substrate. The diffraction measurements reported in this work have an accuracy of ±0.5%.
The sample II exhibits quite uniform diffraction efficiency within each single grating area, and the maximum efficiency measured is about 88% as shown in the Fig. 4.1.
The different optical performances between the gratings were expected. The lithographic exposure data for each single grating are slightly different,resulting in different bar widths for the two level of the structure. The variation of the bar widths determines a variation in the achievable diffraction efficiency, as shown in the Fig. 2.2 c).
To understand the reason of such different performances between the sample I and sample II, further investigations have been carried out.In particular, for the sample I because of the high

[1] with diffraction homogeneity here is indicated the difference between the maximum and the minimum values achieved within a sample/grating. If this difference is higher than 5%, the efficiency is not homogeneous within the measured area.

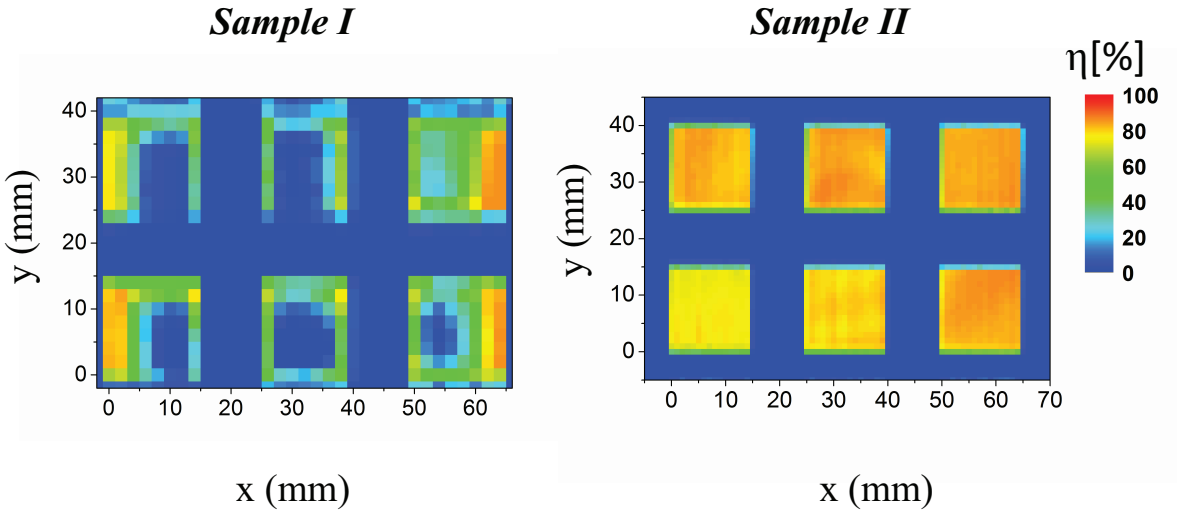

Figure 4.1: Three-level grating-Standard approach samples: spatial mapping of the first order diffraction efficiency η (x-y resolution: 2 mm for sample I; 1 mm for sample II). The Fresnel loss at the interface substrate-air is added to the measurements.

inhomogeneity in the diffraction performances within the grating area, the diffraction efficiency of one of the gratings has been measured with a finer spatial resolution. In addition, the grating area has been mapped by an Atomic Force Microscope (AFM) in order to correlate the structure profile with the achieved efficiencies. The most relevant results of the characterization are shown in Fig. 4.2.

The diffraction efficiency mapping allows to distinguish three main distinct areas. These areas are characterized by a substantial difference in the achieved efficiency, with measured values of 10%, 60% and 90%, respectively. The AFM measurements confirm that high efficiency grating areas exhibit a structure close to the designed three-level profile, even if a fabrication artifact affected the bottom level of the grating, as shown in the AFM scan section III of Fig. 4.2 b). According to the decrease of the achieved efficiency, the grating profile becomes irregular with levels not well defined and affected by heavy fabrication errors (AFM scan sections I and II). However, it is worth to mention that the bar widths and fabrication defects are overestimated in the AFM measurements, due to the convolution between the AFM tip and structure profile during the scan. Nevertheless, the low efficiencies are clearly related to a not well defined three-level profile.

The inhomogeneity of sample I has been originated during the fabrication of the second level. The causes could lie, on the one hand, on the difficulties in achieving a good exposed pattern for the second binary level exposure in areas with low and high resist thickness (as discussed in section 3.1); on the other hand, on a not accurate development process of the resist after the e-beam lithographic exposure.

Because of the homogeneous high efficiency achieved over the mask area, the sample II has been

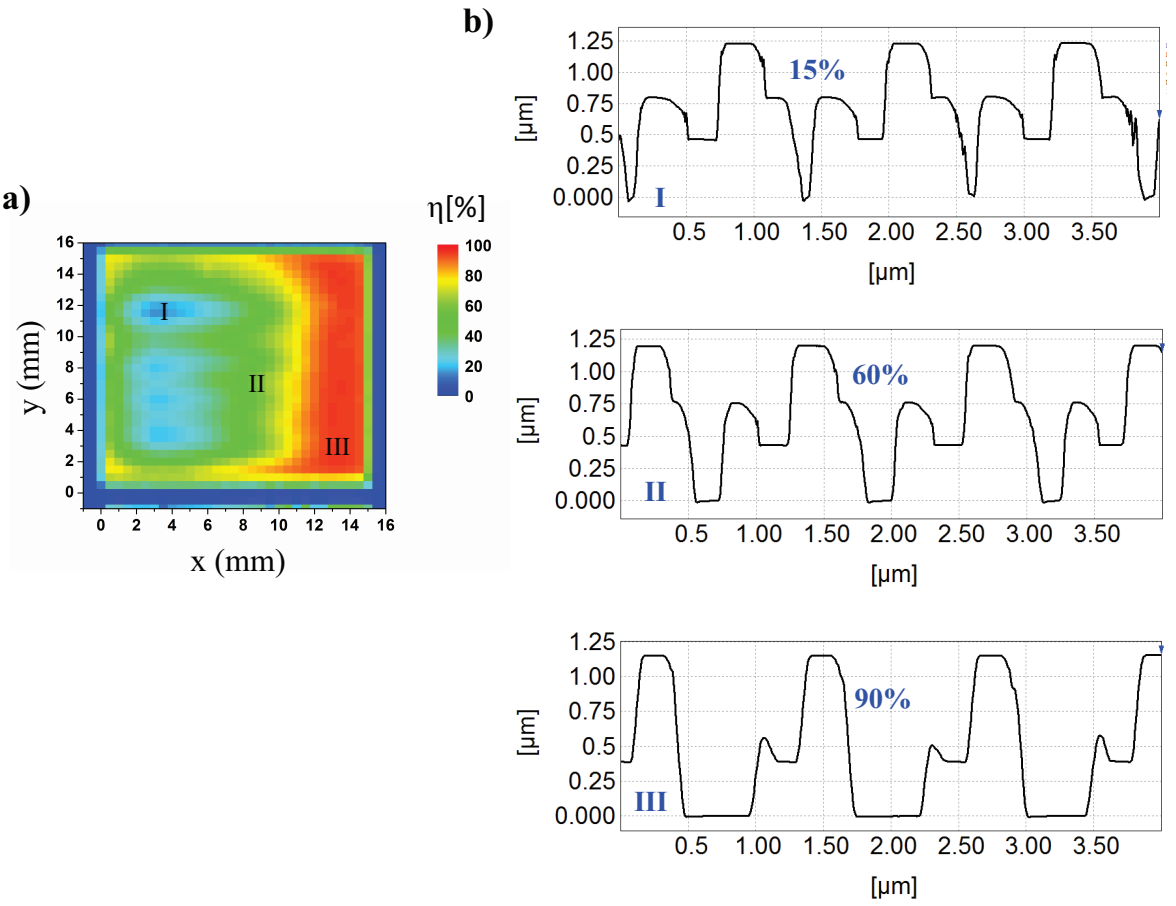

Figure 4.2: Three-level grating-Standard approach sample I. a) Detailed efficiency η spatial mapping of one grating (x-y resolution: 0.5 mm). b) AFM scans performed in the areas I, II, III with 10%, 60% and 90% achieved efficiency, respectively.

characterized in more detail. One of the gratings has been inspected by Focused Ion Beam (FIB) microscopy[2] in order to get information about the profile and the geometrical parameters of the fabricated structures. A FIB cross-section of the grating is shown in Fig. 4.3.

The profile is a well defined three-level structure, despite a slight trenching effect and the presence of a fabrication artifact. Actually, a small parasitic structure is located on the bottom level of the grating, on the opposite edge respect to the upper bar, as detectable from FIB measurement.

Furthermore, for the inspected grating, the geometrical dimensions do not perfectly fulfill the design; the upper bar w_1 is considerably wider (260 nm) with respect to the design value (200 nm), and the bottom bar w_2 is 10 nm smaller than desired. Additionally, also the depth of the upper bar h_2 (842 nm) deviates from the desired height value (778 nm). The parasitic structure is quite small; its lateral dimension is between 10 and 30 nm, its height is in the range of 80-110 nm.

[2]FIB microscopy allows to mill and then inspect a cross-section of the grating. Nevertheless, the grating is locally destroyed.

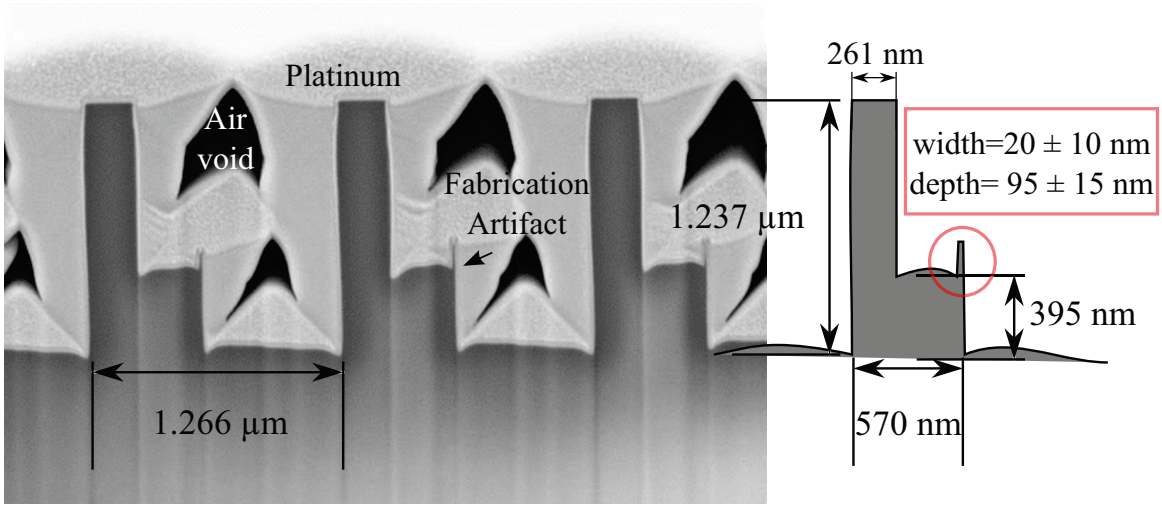

Figure 4.3: Three-level grating-Standard approach sample II: FIB cross-section of one of the fabricated gratings. A small fabrication artifact affects the structure. (The Platinum is sputtered on the sample as protective layer to allow the FIB measurement)

Nevertheless, the additional FIB/SEM measurement of a larger grating area of Fig. 4.4, shows that such parasitic structures exhibit a variation in dimensions and they are not homogeneously distributed over the sample area. In some area of the grating, the profile is a perfect three-level, without any fabrication artifact.

Furthermore, the top view of the grating area reveals an additional inhomogeneity (see holes in the Fig. 4.4), due to a particularly accentuated *trenching effect* on the bottom of the etched grooves. The trenching effect is a local enhanced etching due to the reflection of the ions from

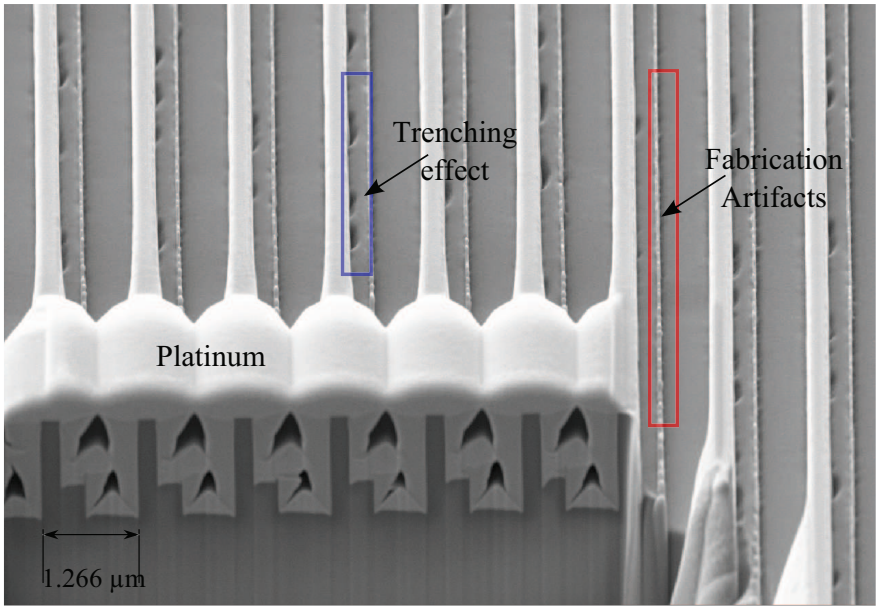

Figure 4.4: Three-level grating-Standard approach sample II: large area FIB measurement. The parasitic structures are not homogeneous within the sample area. The holes, visible in the top view of the sample, are due to an accentuated trenching effect.

the sidewalls. For a three-level grating, the trenching effect could affect the sidewalls of the bottom level groove, and the common area between the upper bar and the bottom ones.
Another one of the six gratings of sample II has been characterized in term of diffraction efficiency versus the incidence angle. The grating, chosen for the diffraction measurement, is not the most efficient one, due to its upper bar width w_1 of 240 nm, but it exhibits the most homogeneous efficiency over its area.
The measurement results are shown in Fig. 4.5 and compared with the RCWA simulation of the original design and of the FIB-measured grating profile. The measurements are in good agreement with the simulations. As expected, due to the wider lateral dimensions of the upper bar, at normal incidence the three-level grating achieves only 82% efficiency. For this reason, the measurements are closer to the simulations of the FIB-measured profile than the original design.

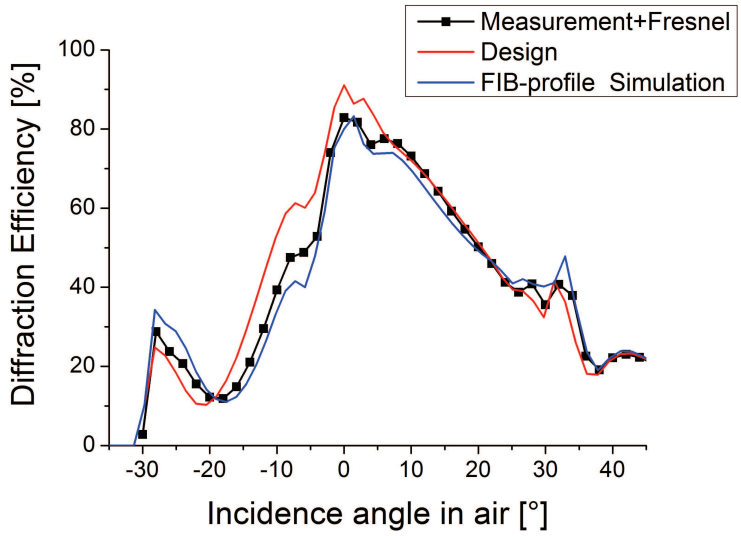

Figure 4.5: Three-level grating-Standard approach sample II: diffraction efficiency vs. incidence angle @633 nm. Comparison between the measurements and the simulation of the original design and the FIB-measured profile of the grating. Angular measurement resolution: 2 degrees.

The fabrication results of the standard multilevel technology approach demonstrates that, by an optimization of the process, three-level structures can be fabricated with high efficiency. Nevertheless, the process tends to be in-homogeneous and the grating profile might be affected by an fabrication artifact, probably due to misalignment between the lithographic exposures for the two different layers.

4.2.2 *Three-resist Layer Technology* samples

Also by the three-resist layer technology, two different three-level grating samples have been fabricated. This approach, as already explained in the section 3.2, consists in a modification

of the standard technology by an additional resist planarization layer between two consecutive binary fabrication steps.

The introduction of such planarization layer implies a higher depth for the etching of the second fabricated level; if this height is too large, the required additional etching depth could represent a limitation in achievement of good quality grating profiles.

To evaluate the impact of this factor on the grating fabrication, the two samples have been realized inverting the fabrication sequence of the two levels. The fabrication of sample I has been carried out, starting with the fabrication of the upper level of the structure (w_1, h_1). The microstructured substrate (etched h_1= 778 nm) has been then planarized with 1 μm thick AZ4712 resist layer, before proceeding with the fabrication of the bottom grating layer (w_2, h_2). For the sample II, the bottom smooth level has been transferred first into the fused silica substrate. Due to the reduced etching depth (h_2= 394 nm), only a 500 nm AZ4712 resist film has been used as planarization layer.

For both samples I and II, 40 nm chromium layer has been used for the second binary fabrication level. The sample mask layout is the same used for the standard technology. Also in this case, the six gratings differ for the slightly different lithographic exposure data, corresponding to bar width variation.

The diffraction efficiency spatial mapping of the samples I and II is shown in Fig. 4.6.

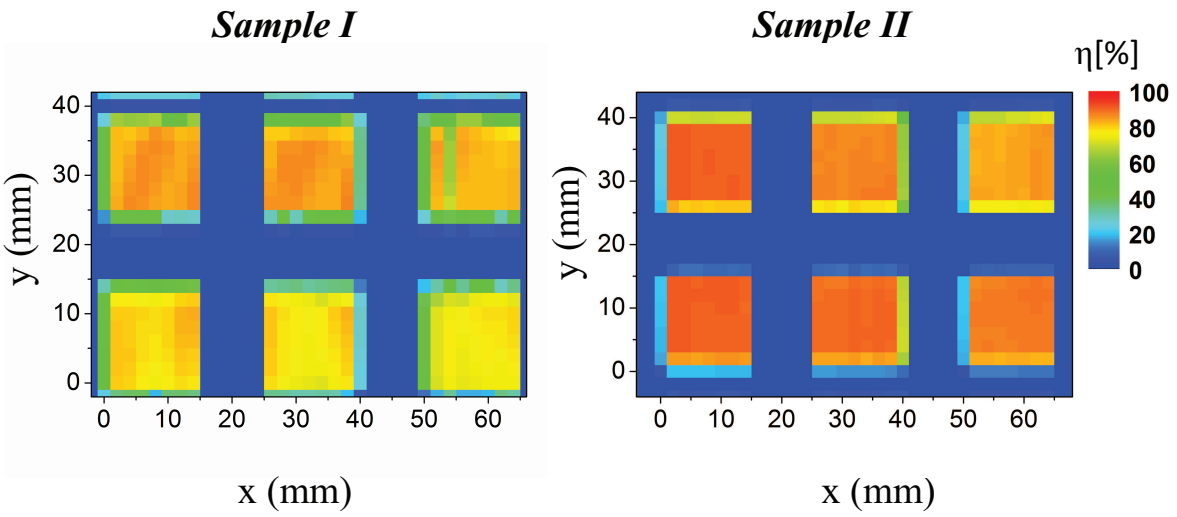

Figure 4.6: Three-level grating-*Three-layer resist* samples: spatial mapping of the first order diffraction efficiency η (x-y resolution: 2 mm). Fresnel loss at interface substrate-air are added to the measurements.

Sample I shows a good fabrication process homogeneity; except, a low efficiency strip visible in the top right grating, caused by an exposure data error in the lithographic process for the second layer. The maximum efficiency reached is about 87%, slightly less than the design.

The sample II exhibits an efficiency homogeneity of about 1% inside a single grating area. The efficiency achieves a maximum value between 82.5% and 91.5% for the least and most efficient

between the six gratings, respectively. Three of the six gratings fulfill the design diffraction performance, achieving efficiency > 90%.

The FIB cross-section of Fig. 4.7 allows to understand the reason for the different diffraction performances between the sample I and II.

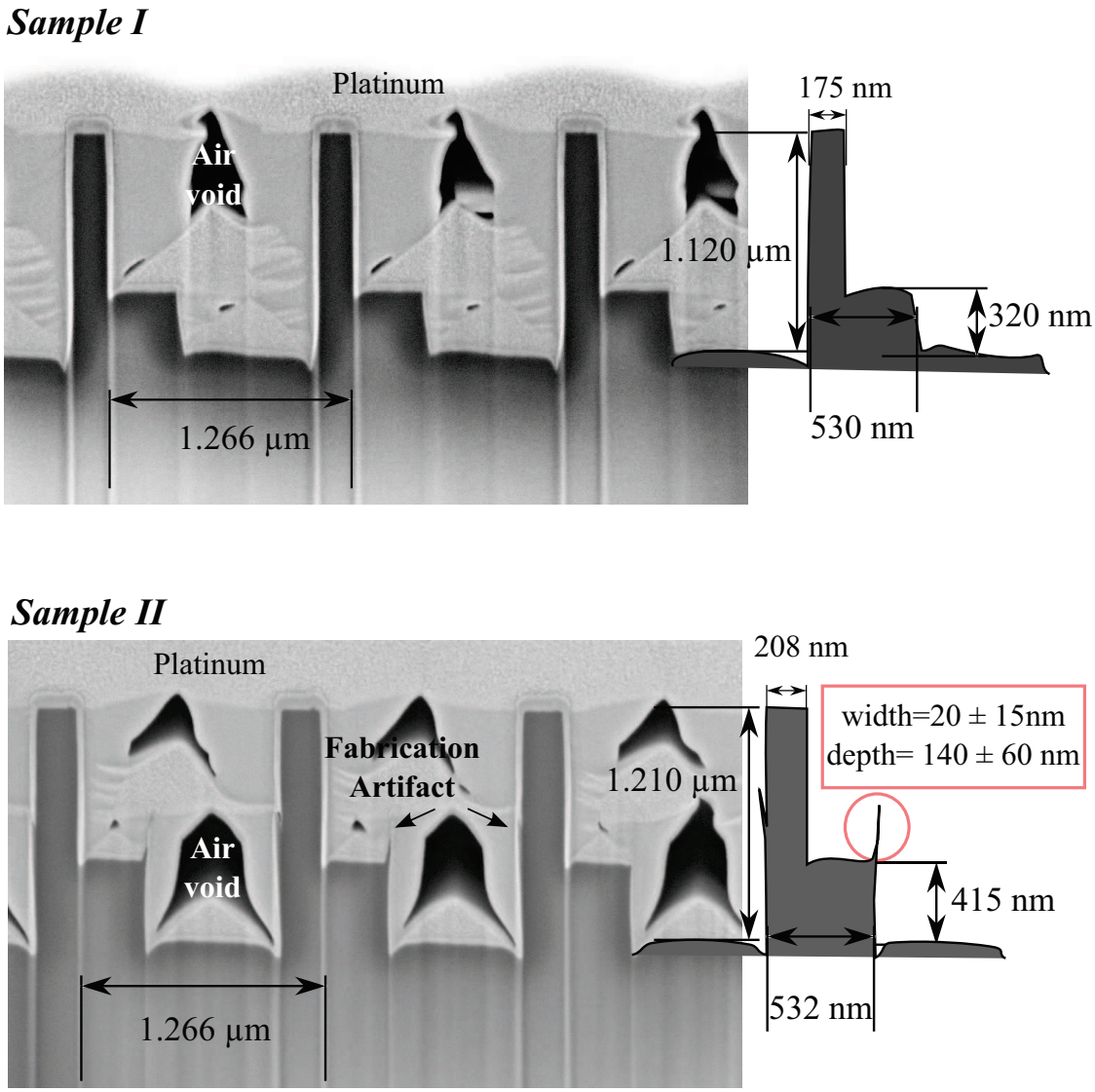

Figure 4.7: Three-level grating-*Three-layer resist* samples: FIB cross section. Sample I: The bottom level is only 320 nm deep. No fabrication artifacts. Sample II: Two parasitic structures affected the profile.

The FIB measurement of sample I, reveals that the height of the bottom level h_2, as confirmed from additional AFM characterization, is 74 nm shallower than the design, leading to loss of about 4% in the achievable efficiency (see Fig. 2.2 c)). Except the depth inaccuracy of the bottom level, the structure exhibits a perfect three-level profile, not affected by any fabrication artifact. Only a slight trenching effect modifies the sidewalls of the bottom groove.

The grating of sample II, despite the high and homogeneous efficiency measured, exhibits fab-

rication artifacts. As in the standard approach samples of Fig. 4.3, a parasitic structure lies on the edge of the bottom level, even if such defect results to be thinner and taller. And additionally, a very small artifact affects also the deepest wall of the upper bar, as indicated in the Fig. 4.7. In Fig. 4.8, larger area FIB sections of the two samples are shown.

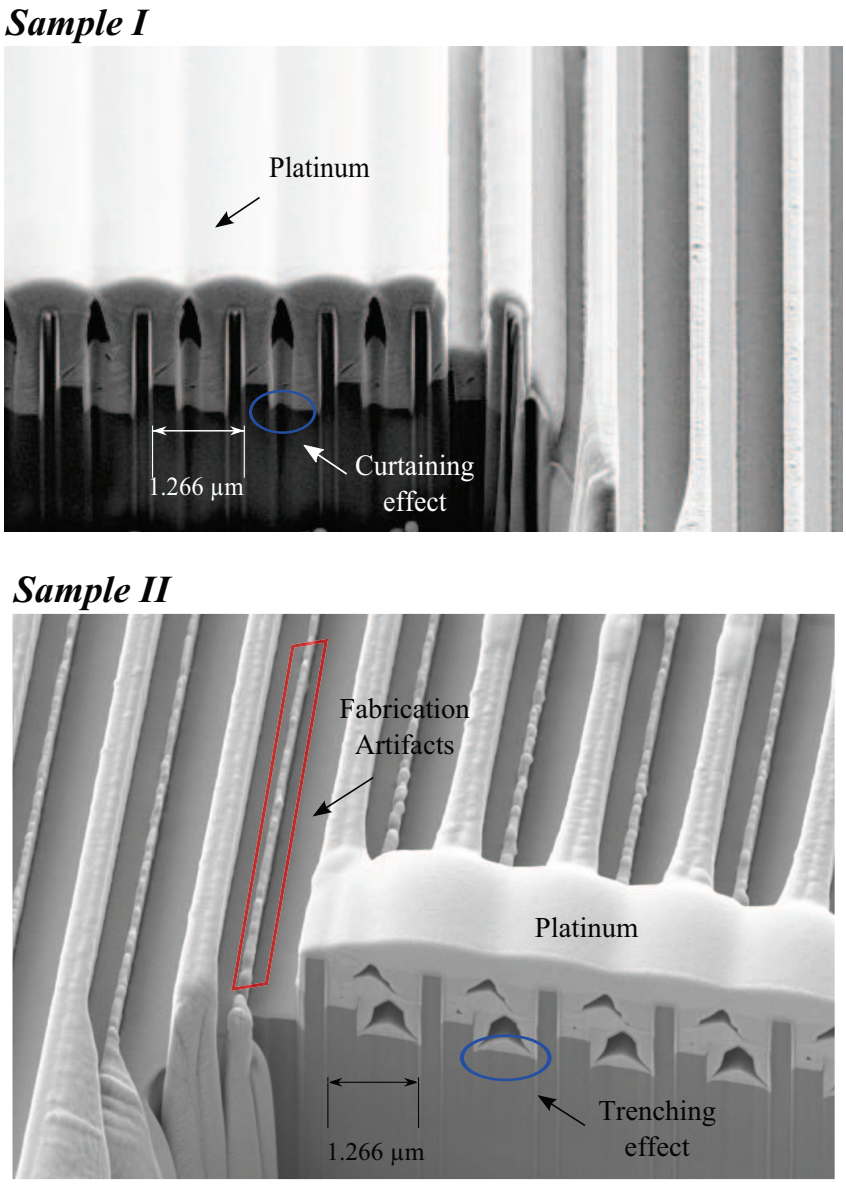

Figure 4.8: Three-level grating-*Three-layer resist* samples: large area FIB measurement. Sample I: No parasitic structures. Curtaining artifacts affect the measurement. Sample II: Parasitic structures are affecting both levels.

The grating structure of sample I is quite homogeneous and defect-free across the inspected area. It is worth to notice that in comparison to the profile shown in Fig. 4.7, a kind of convex bumps are visible at the bottom of the grating structure. These bumps are not fabrication artifacts, but they are caused by a well known FIB measurement effect, namely *curtaining effect*. This effect is due to the different sputter rate for different materials. For the measurement in

Fig. 4.8, these curtaining artifacts occur in correspondence to the air voids, as recognizable from the FIB cross-section [109].

The larger area FIB section of sample II shows a homogeneous grating surface without visible trenching effect on the top. The parasitic structures are dimensionally inhomogeneous within the area, and also some defect-free regions can be observed.

For the samples I and II, one of the most efficient and homogeneous gratings has been characterized in terms of diffraction efficiency vs. incidence angle. The measurement results are shown in Fig. 4.9 and compared with the rigorous simulations of the design and the FIB-measured profiles.

The efficiency measurement of Sample I, despite the loss of some percent in the maximum efficiency due to the not accurate etching depth of the bottom level h_1, confirm the good quality of the fabricated structures. The measurements are in good agreement with the design and the simulation of the FIB-measured profile over all incidence angles.

Also for the sample II, the results are quite satisfactory in comparison to the rigorous simulations. The discrepancies between measurements and simulations could be partially explained considering that the FIB-profile simulation cannot be very accurate for this grating due to the inhomogeneous presence of the fabrication artifacts over the grating area.

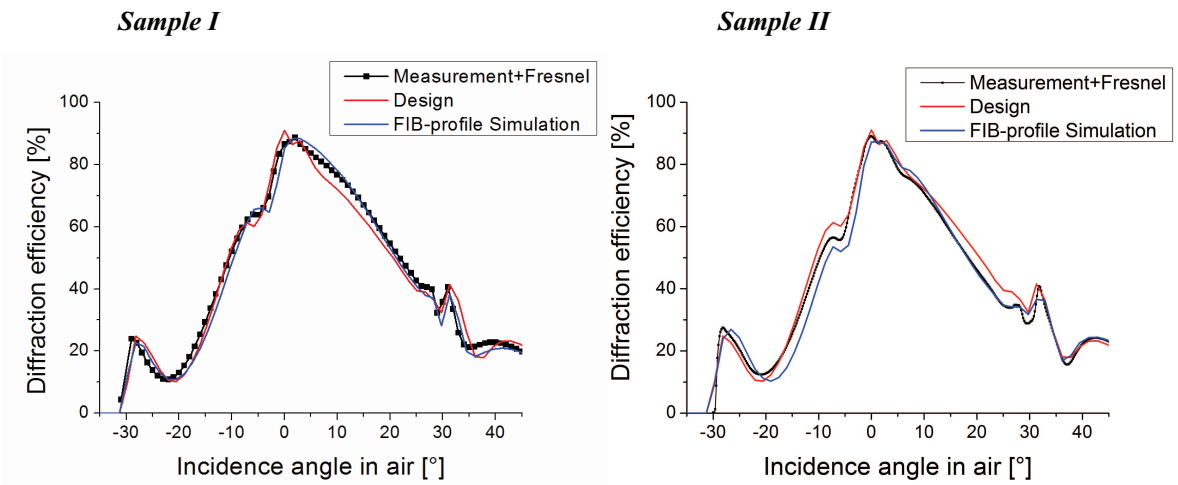

Figure 4.9: Three-level grating-*Three-layer resist* samples: diffraction efficiency vs. incidence angle @633 nm. Comparison between the measurements and the simulation of the original design and the FIB-measured profile of the grating. Angular measurement resolution - Sample I : 1 degree; Sample II : 0.2 degrees, respectively.

The results of the Three-resist Layer Technology are very satisfactory for both samples in term of achieved efficiency and homogeneity over the sample area. One of the samples is affected by a fabrication artefact presumably originated by a misalignment between the two lithographic processes of the two levels of the structure.

Nevertheless, by such an approach it has been demonstrated that the fabrication of a perfect three-level grating profile without severe fabrication artifacts, is possible also for high disper-

sive blazed elements. The results will be compared to the other technological approaches in the section 4.2.4, with particular emphasis on the origin of the fabrication artefacts.

4.2.3 *Relaxed Alignment Technology* samples

By the *Relaxed Alignment Technology*, two grating samples, I and II have been fabricated, as well. The mask layout differs from the one used for the other two technologies. Here, in order to have a larger variation of the lithographic exposure data, nine different gratings have been included on a six inch fused silica mask blank.

As discussed in paragraph 3.3, a unique coded chromium mask (containing the lateral information for both levels) is used during the whole fabrication process. The process has been realized as schematically shown in Fig. 3.8; for both samples I and II, the smoothest level (w_2, h_2), has been transferred into the substrate, as first and then followed by the upper level (w_1, h_2). The only difference in the fabrication of the two samples is that, for the sample II, the fused silica RIE etching of the smallest bar has been managed in two partial steps.

In Fig. 4.10 the results of the spatial mapping of the diffraction efficiency of the two samples I and II are shown. The gratings of sample I achieve a maximum efficiency between 77% and 94%. Therefore, in some area of the gratings the measured efficiency is even higher than the designed one. Nevertheless, except the first left grating in the middle row (where $\approx$ 90% efficiency is reached), the efficiency is not very homogeneous within the single grating area ($< 5\%$).

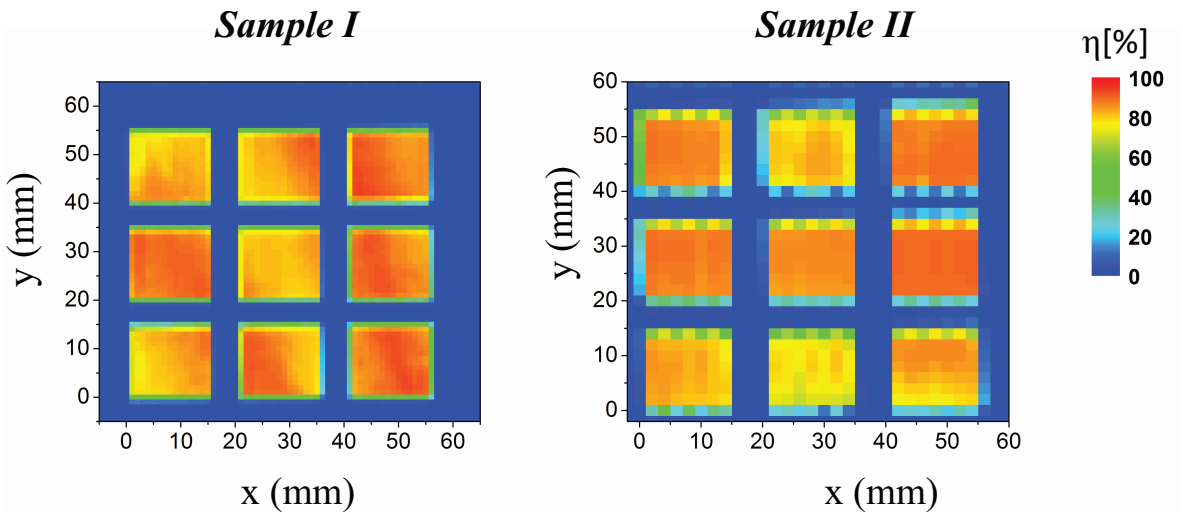

Figure 4.10: Three-level grating- *Relaxed Alignment* samples: spatial mapping of the first order diffraction efficiency η (x-y resolution: 2 mm). Fresnel loss included in the measurement.

The sample II shows a better homogeneity ($< 2\%$) within the grating areas with respect to the first fabricated sample. The maximum efficiencies reached are between 76% and 91%; the highest measured values are in agreement with the design expectations.

The FIB measurements in Fig. 4.11 surprisingly reveal the presence of the parasitic artifacts on

both samples, similar to the artifact occurring in the standard and *Three-layer Resist* approach samples. Actually, such fabrication artifacts have not been expected for these samples. The origin of these artifacts is generally found in alignment errors between consecutive lithographic steps. Even though this explanation can be valid for the other two technologies, it can not for the *Relaxed Alignment Technology* where the use of a coded chrome mask avoids misalignment errors.

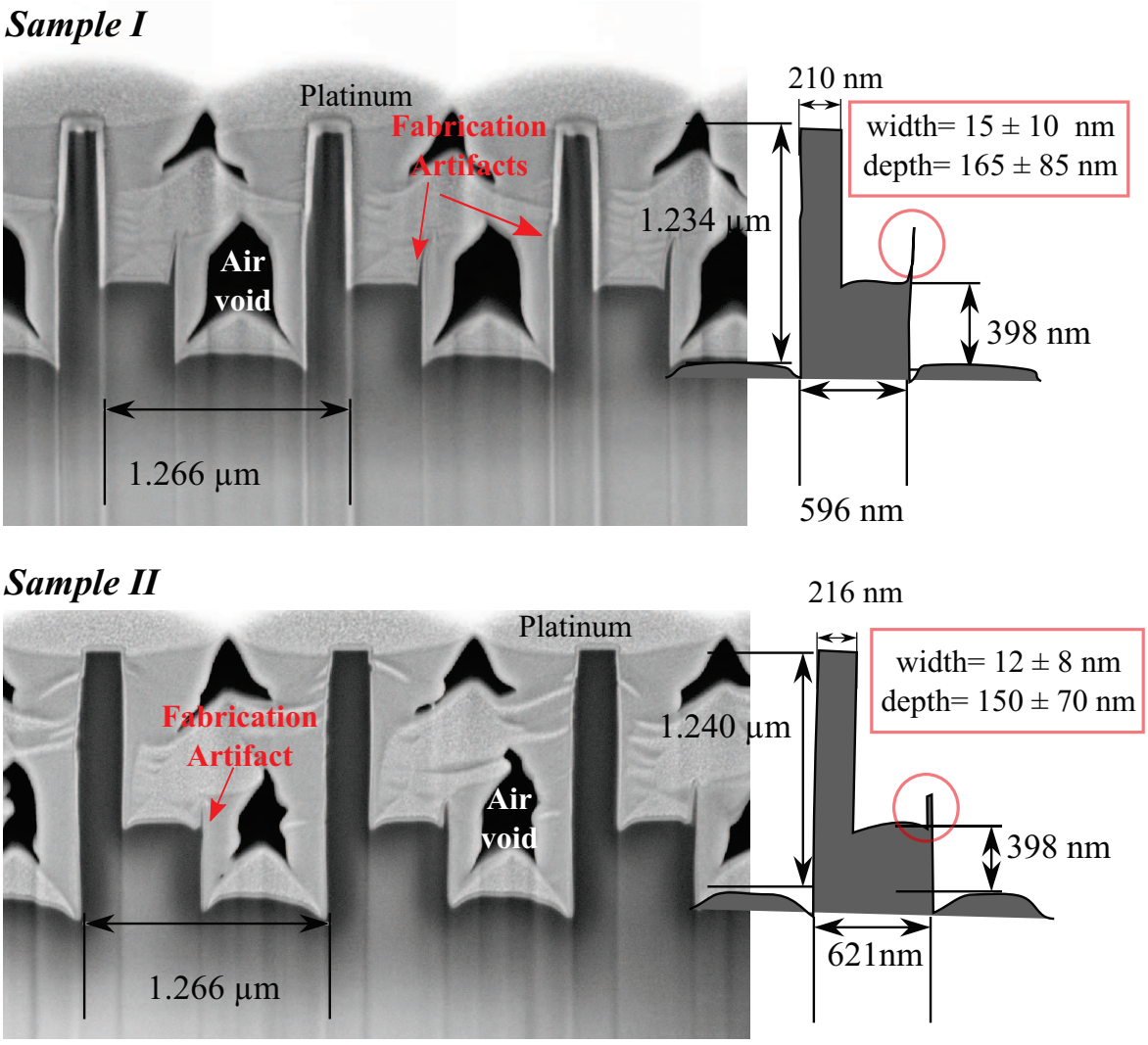

Figure 4.11: Three-level grating-*Relaxed Alignment* samples: FIB cross section. Parasitic structures are affecting both levels.

The sample I, in particular, exhibits parasitic artifacts on both levels of the grating. Also in this sample, the parasitic structures are quite thin. Furthermore, the grating profile is not perfect, especially the width of the upper bar is slightly smaller in the end part.
The FIB cross section of sample II Fig. 4.11, reveals the presence of the parasitic structures only on the bottom level. The sidewall profile is well defined. The trenching effect is probably

accentuated by the curtaining effect due to the FIB measurement.

In Fig. 4.12 larger area FIB sections of the two samples I and II are compared. Sample I exhibits a homogeneous presence of the fabrication defects over the inspected area. The trenching effect, instead is not so pronounced; the top view of the structure is uniform.

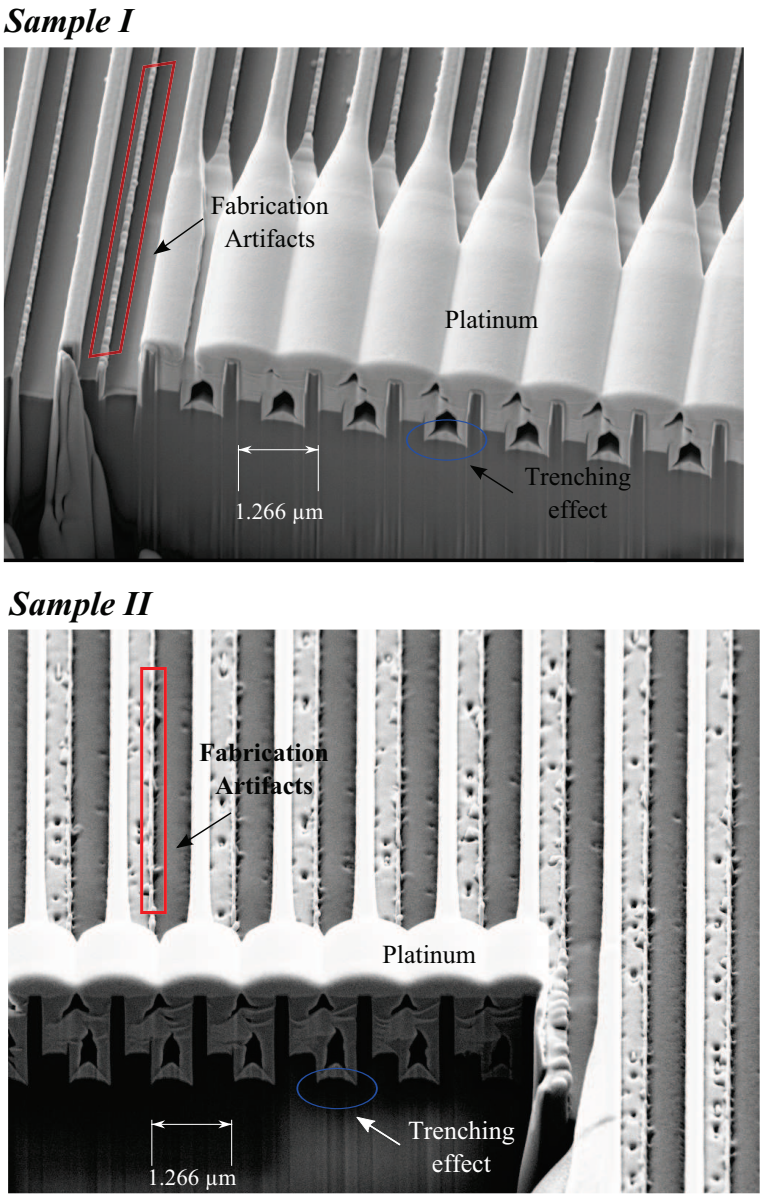

Figure 4.12: Three-level grating-*Relaxed Alignment* samples:large area FIB measurement.

Contrarily, the surface of sample II is not homogeneous. The top view reveals a pitted surface. Parasitic structures and trenching effect are not uniform within the grating area. The reason for such pronounced non-uniformity of the sample surface is not known, actually, the fabrication of sample I and II has been carried out in the same way.

Despite these fabrication irregularities affecting the gratings, the measurement of the first order efficiency versus the incidence angle, confirms good diffraction performances for both samples.

As shown in the Fig. 4.13, the results are in good agreement with the simulations. Also in this case, the accuracy of the FIB-measured profiles simulation is limited by the artifact irregularities over the grating areas.

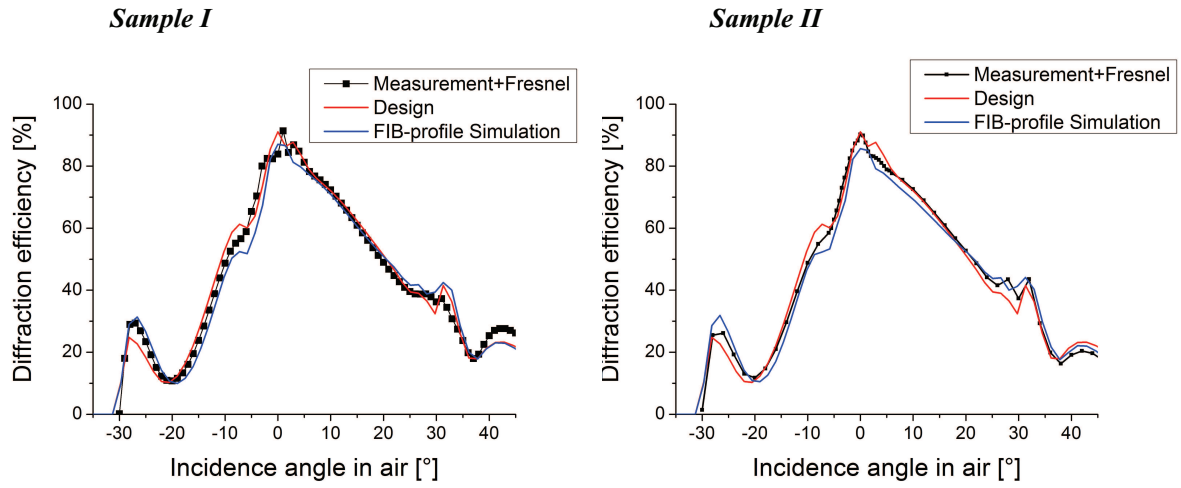

Figure 4.13: Diffraction efficiency vs. incidence angle @633 nm. Comparison between the measurement and the simulation of the original design and the FIB-measured profile of the grating. Angular Measurement resolution: 1 degree.

4.2.4 Comparison of the three technologies and discussion

The results presented and discussed in the previous sections demonstrate that all three approaches show good potential for the fabrication of high efficient three-level blazed gratings in resonance domain.

In particular, the new proposed approaches, i.e. the *Three-resist Layer* and the *Relaxed Alignment* technology, obtain better results respect to the standard approach. The new developed technologies turn out to be more robust, as confirmed by the already good performances achieved with the first samples. The efficiencies are higher and more homogeneous with respect to the standard technology samples.

Nevertheless, five of the six fabricated samples are affected by a parasitic structure on the bottom level; and additionally in two of them a very small defect is affecting the deepest wall of the upper bar. The fabrication artifacts do not compromise the high diffraction efficiency. In the simulation of the grating efficiency, the thinner upper bar defect could be neglected. The artifact in the bottom level, actually, as shown in Fig. 4.14 a), increases the maximum efficiency of the grating, at least if the dimensions are comparable to those measured for the fabricated samples.

According to the fact that the bottom level artefact is common to all used fabrication processes, the parasitic structures can not be originated exclusively by alignment or sizing problems. They are most probably due to a kind of masking effect that occurs at the side walls during the first

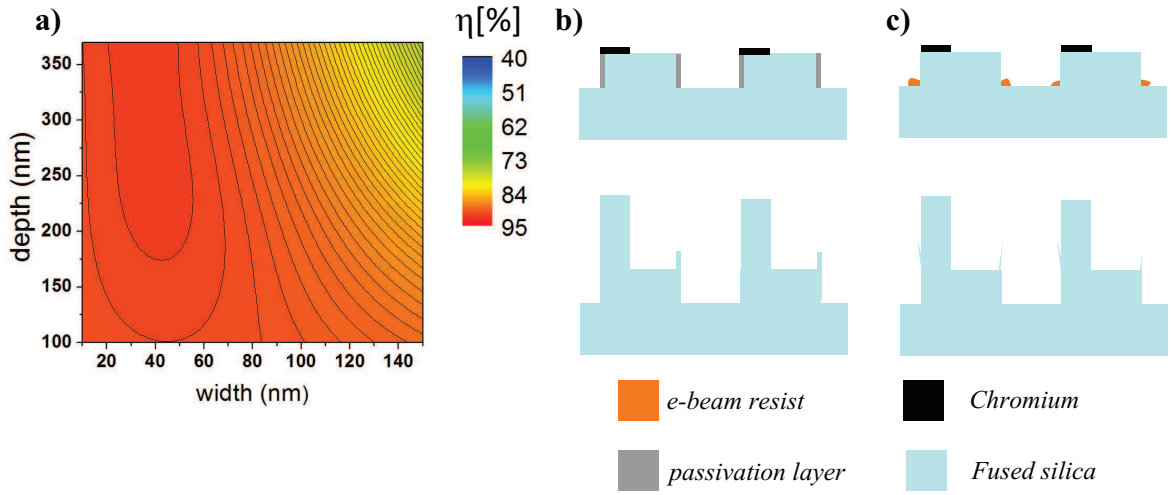

Figure 4.14: Parasitic structure: a) Influence of the bottom level artifact on the efficiency η at normal incidence of the designed three-level grating; b), c) Schematic illustration of the formation of the parasitic structures within the etching process due to a passivation layer and residual resist, respectively.

RIE etching into the substrate. Some further investigations about the origin of such fabrication defects have been carried out, especially the etching processes have been deeply characterized with several AFM measurements.

First results clarify that such parasitic structures are observable only after the last deep etching process. Their presence is related to the depth of the second etched level, i.e. larger etching depths are affected by more pronounced artifacts [101, 110].

The first hypothesis to explain such artifacts could be a kind of passivation phenomena, as schematically illustrated in Fig. 4.14 b). The deep etching into the fused silica substrate is a plasma process. During this fabrication step, a protective layer is deposed on the sidewalls. As a consequence, the presence of the layer is related to the final etched depth. This layer may act like a mask during the remaining etching time, originating the parasitic structures.

Nevertheless, the results of further etching experiments have not confirm such hypothesis. The results of one of these experiments are shown in Fig. 4.15. After the standard etching of a binary grating into fused silica through a chromium mask, the mask is removed and the grating is etched again for N-times. The formation of the passivation layer was expected, but the AFM measurements show that no parasitic structure affects the grating structure.

An other explanation for the origin of such artifacts, could be some resist residual on the sidewall of the first etched level, as shown in Fig. 4.14 c), that acts as a mask during the etching of the second level; this could better explain the irregularity of the artifacts over the grating area and especially the presence of the thinner upper bar artifact.

It has also to be mentioned, that probably the origin of this artifact is not the same for all technologies, here considered. Within the *Relaxed Alignment Technology* it is clearly related to the etching step, but within the other two approaches, it is a combination of alignment/sizing

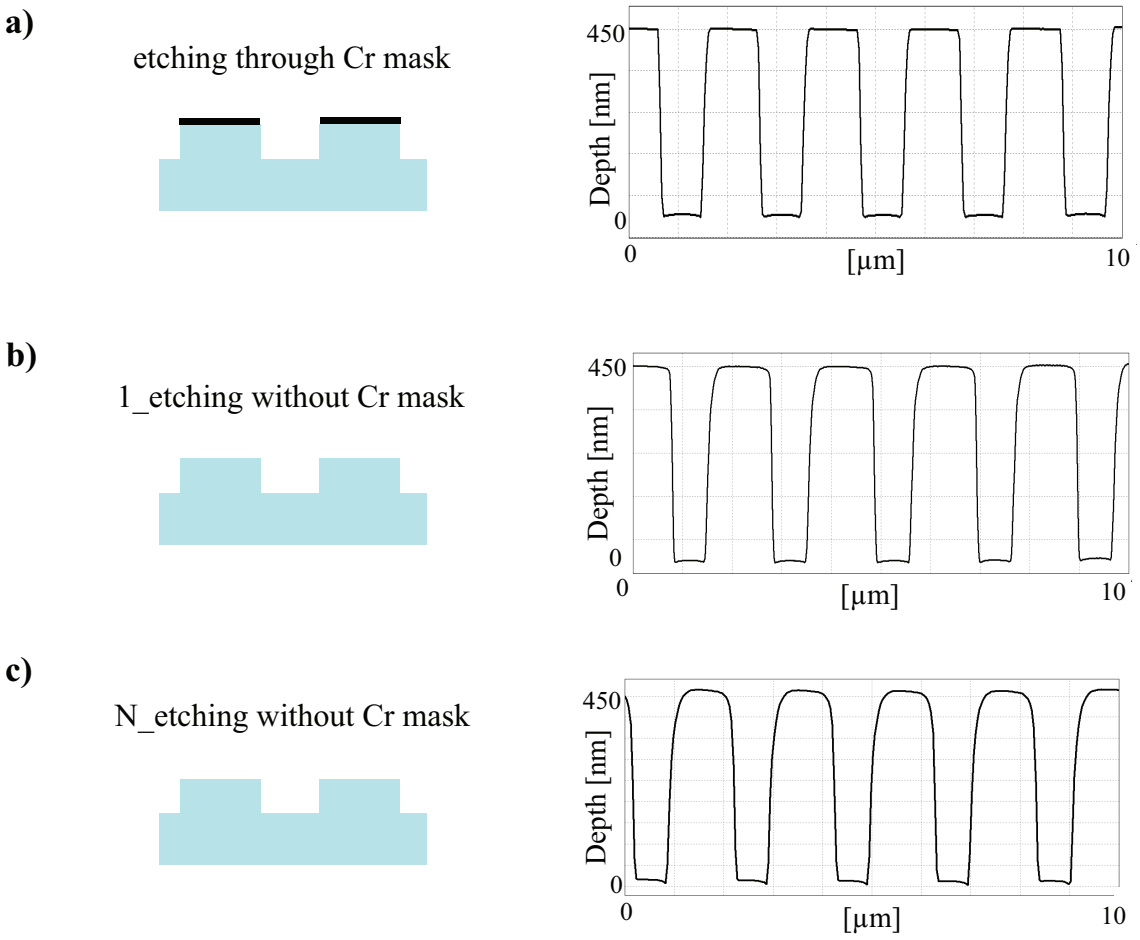

Figure 4.15: Etching experiment to confirm the formation of passivation layer. AFM measurements of the grating profile ($p = 2\mu m$). a) After the standard etching process, through a Cr mask. b) and c) after etching process without mask. No parasitic artifacts.

errors and etching depth.

Despite the presence of such artifacts, the results are quite satisfactory in terms of achieved efficiency and homogeneity. The robustness of the two new developed approaches allow to use them for the fabrication of large area blazed gratings for real applications.

4.3 Effective-medium enhanced three level grating

The profile of the effective-medium enhanced three-level grating, as already discussed in the section 2.2.1, is demanding from the technological point of view. The combination of the high aspect ratio of the smallest groove, g_1= 126 nm, and the adjacent bar, b_1= 100 nm, requires a special sidewall quality.

The fabrication of such grating is challenging and have been carried out by means of different technological approaches. But some of the fabrication processes were not successful and therefore the results will not be reported here. The first fabrication run has been carried out by the *Relaxed Alignment Technology*, but the process has been already interrupted after the first etching step (h_1= 949 nm) in fused silica. The bottom triangular shape of the smallest bar, already pronounced after the first etching, did not allow to proceed further.

Two samples have been fabricated with the standard technology, but the results did not fulfill the design specifications; as shortly discussed in the following section. Also in this case the Y-shape of the smallest groove is problematic in order to achieve high efficiency.

Only by the ALD enhanced approach it has been possible to obtain good quality and high performances gratings. Two slightly different gratings have been successfully fabricated. The first one is working at normal incidence, the second one for an incidence angle of -7 degree. The characterization results are presented and discussed. Due to the broadband performances, the diffraction efficiency has been measured for different wavelengths.

4.3.1 Standard technology samples

The gratings have been fabricated by the standard approach, following the process flow schematically illustrated in Fig. 3.2. Therefore, in the first binary step, the smallest and deepest groove $(g_1, h_1 + h_2)$ has been etched into the substrate.

In the second step, the larger bar has been patterned and transferred into the fused silica substrate. In the Fig. 4.16, the two fabrication binary steps are shown.

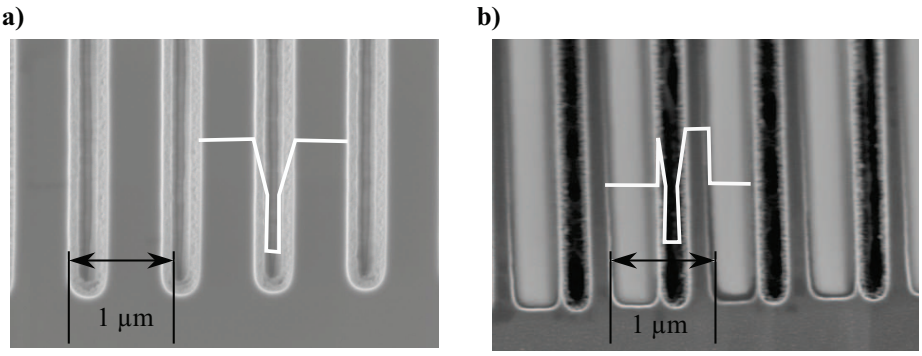

Figure 4.16: Effective-medium enhanced three level grating: a), b) SEM images of the first and second binary fabrication step, respectively.

The walls of the smallest groove exhibits the typical Y-shape, discussed in the paragraph 3.1. This shape seriously limits the second fabrication step. In the final grating profile, as shown, in Fig. 4.16 b), the smallest bar is not well defined, and the width of the larger bar is strongly reduced. Such badly defined grating profile leads to a low diffraction efficiency of only up to about 40%.

4.3.2 *ALD enhanced technology* samples

The grating fabrication has been carried out following the process described in Fig. 3.11. The lateral dimension of the groove g_1 has been relaxed and then transferred into the fused silica substrate. Afterwards, the groove width has been trimmed by the ALD deposition of SiO_2. The deposition process has been carried out at the company Beneq (Finland) [111]. The ALD layer thickness has been of 90 nm and 130 nm for the normal-incidence and for the quasi-normal incidence sample, respectively. After the ALD process, the fabrication proceeded as in the standard approach. The already microstructured mask blank has been covered with 80 nm chromium and with 300 nm FEP 171 for the second level lithography. Due to the small width (100 nm after the ALD deposition) of the first etched groove g_1, an additional planarization layer is not needed.
In one single mask blank 30 gratings have been fabricated, in order to optimize the process throughout a larger variation of the e-lithography exposure data for both levels.

4.3.2.1 Normal incidence sample

The diffraction mapping at 650 nm illumination wavelength, shown in Fig. 4.17, reveals a good homogeneity of the fabricated gratings.
The variation in the achieved efficiencies between the gratings is due to the different bars/grooves geometry, originated from the different lithographic data used for the single grating. One of the gratings reaches an efficiency close to the design, furthermore only a few gratings achieve efficiencies smaller than 70%.
The FIB characterization of the most efficient grating of Fig. 4.18, shows a well defined profile, except for the top of the bars which appears slightly distorted. Probably, on the one hand, to relax the width of the groove g_1 of 180 nm has not been sufficient to avoid the typical Y-shape profile, and on the other hand, the profile distortion is due to the rounding edge effect of the ALD process (shown in Fig. 3.12).
Furthermore both bars are wider as designed, they don't have the same height, and the total depth of the grating $h_1 + h_2$ is 35 nm too shallow compared to the design value.
The larger area FIB measurement of Fig. 4.19, shows, however, a good homogeneity over the sample's surface. The curtaining effect is recognizable in the bottom of the upper level.
The efficiency measurements are in good agreement with simulations, especially the compar-

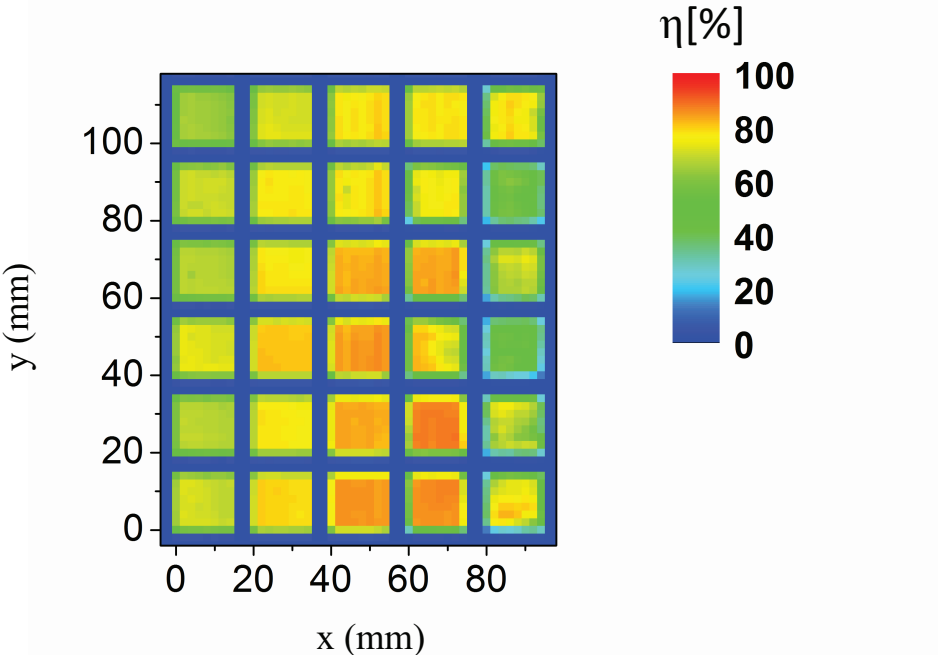

Figure 4.17: Effective-medium enhanced three-level grating-normal incidence: spatial mapping of the first order diffraction efficiency η @650 nm at normal incidence (x-y resolution: 2 mm). Fresnel losses included in the measurements.

ison with the efficiency simulation of the real fabricated grating profile shows a quasi perfect agreement, as illustrated in Fig. 4.20, a) for the characterization vs. incidence angle @650 nm, and b) for a wavelength range between 460 and 950 nm at normal incidence, respectively. Also considering a 2D efficiency mapping, see Fig. 4.20 c), over an incidence angle between -15 and 15 degree and wavelength varying between 460 and 950 nm, the results are in good agreement with the RCWA calculations. The differences between simulations and characterizations can be explained by taking into account the finite bandwidth of the laser source and the slight

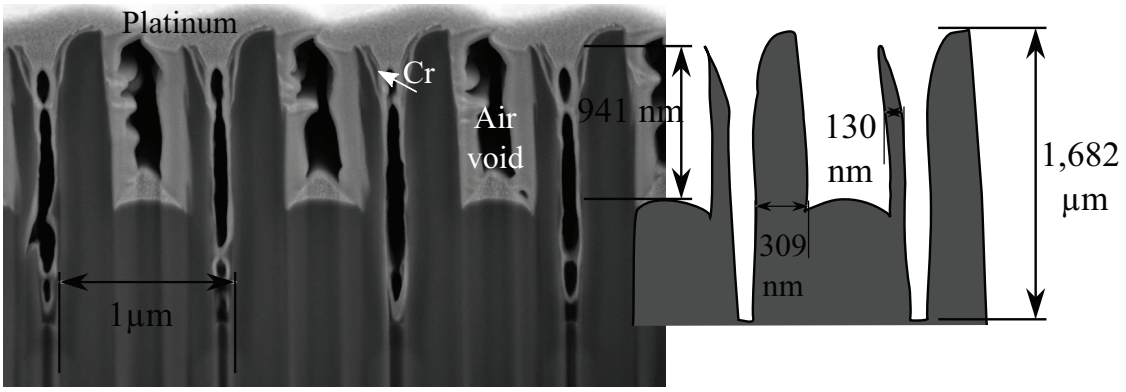

Figure 4.18: Effective medium enhanced three-level grating-normal incidence: FIB cross-section of one of the fabricated gratings. The Cr-mask is still on the top of the grating.

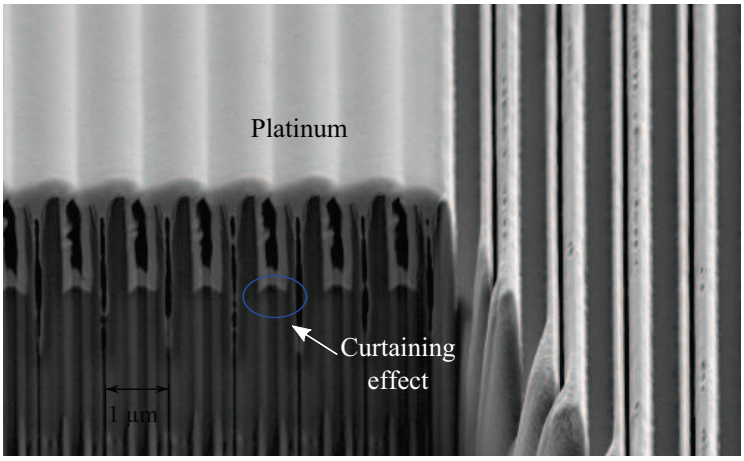

Figure 4.19: Effective medium enhanced three-level grating-normal incidence: large area FIB measurement.

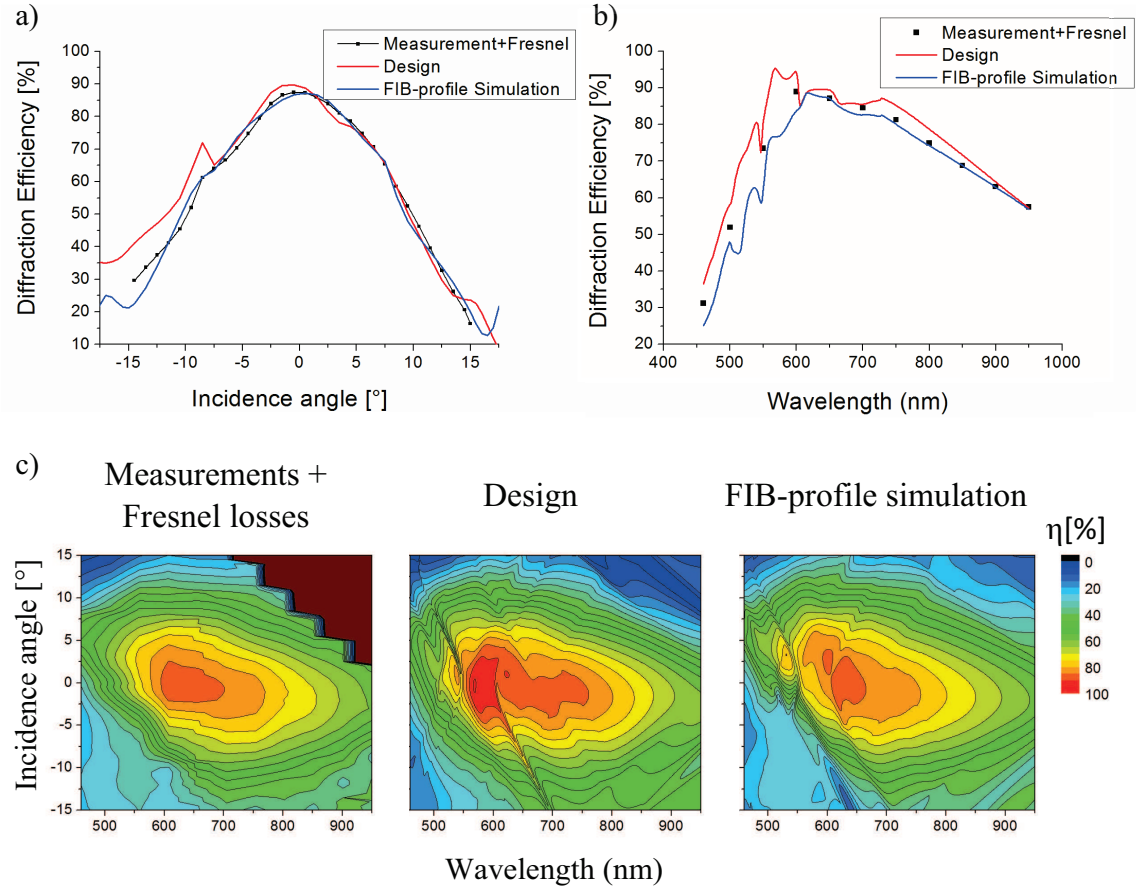

Figure 4.20: Effective medium enhanced three-level grating-normal incidence. Diffraction efficiency η . Comparison between the measurement and the simulation of the original design and the FIB-measured profile of the grating. **a)** vs. incidence angle (angular measurement resolution: 1 degree). **b)** vs. wavelength. **c)** 2D mapping-angular measurement (resolution: 0.5 degree)

profile variations of the top regions of the bars over the single grating area.
The fabricated structure profile, especially the shape and the dimensions of the two bars, are quite different for different gratings. In Fig. 4.21 the FIB cross sections of other two gratings, which achieve a lower efficiency of about 80% are shown. The profile of the wider bar of the grating in Fig. 4.21 a) is heavily distorted in the top; one part of the bar is more or less missing, and additionally the profile is not homogeneous already over a small area (4 μm). The profile of the grating shown in Fig. 4.21 b) is similar to the most efficient ones in Fig. 4.18, but the deepest groove is too small, and in some point not completely open through the all depth.

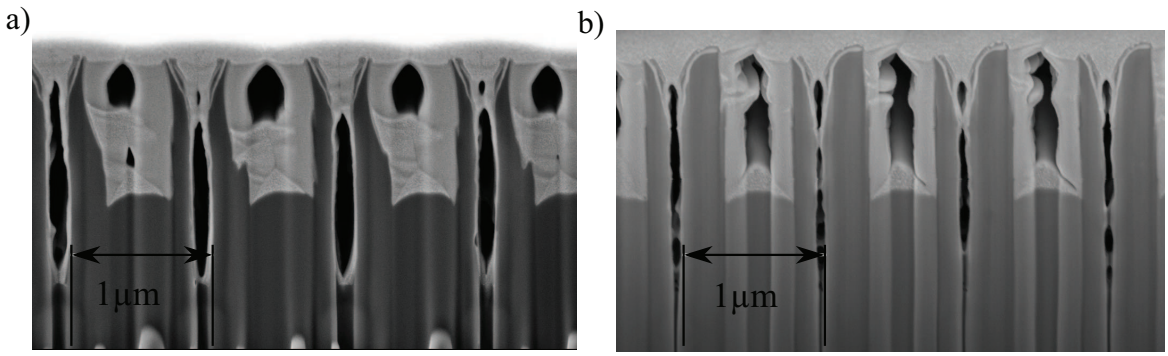

Figure 4.21: Effective medium enhanced three-level grating-normal incidence: a) and b) FIB cross-section of two fabricated gratings. Despite the different profiles, both gratings achieve the same efficiency.

The grating profile is quite irregular over the area, as a consequence the simulations for this sample cannot be very accurate. The finest profile features are not included in the simulated profile, and in addition, the simulation does not take into account the peculiarity of the measured area of the grating. The FIB simulations are related only to a 2 period grating line, directly imported from the FIB measurement. These considerations could explain some disagreements between measurement and simulations.

4.3.2.2 Close to normal incidence sample

The second grating, operating at -7 degree incidence angle, as discussed in the section 2.2.1, differs from the first one for the width of larger bar, which in this second design is wider, with a value of 400 nm.
Taking into account the results of the first sample fabricated by the *ALD Enhanced Technology*, the width of the smallest groove has been enlarged further, i.e. to 360 nm, to reduce the Y-shape of the groove's wall. Consequently, the groove width has been trimmed to the designed value g_1= 100 nm by ALD of 130 nm SiO_2.
The diffraction efficiency mapping, see Fig. 4.22, shows a good homogeneity within the grat-

ings (< 1%). Furthermore, most of the gratings achieve an efficiency higher then 90%. The maximum measured value of about 94% is even higher than the design.

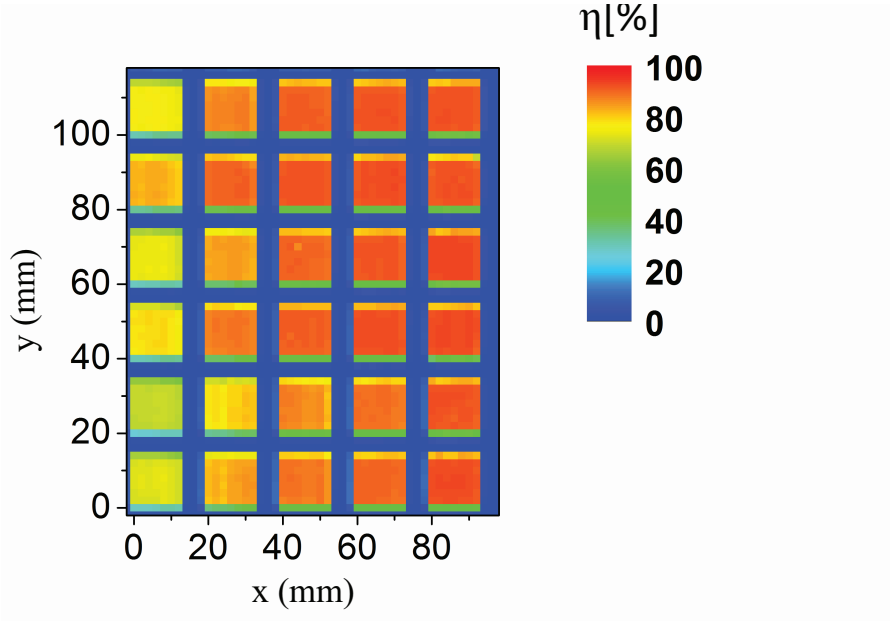

Figure 4.22: Effective medium enhanced three-level grating-close to normal incidence: spatial mapping of the first order diffraction efficiency η @650 nm for incidence angle of minus five degree (x-y resolution: 2 mm). Fresnel losses included in the measurements.

The FIB cross section of Fig. 4.23 shows the profile of one of the most efficient gratings. The typical Y-shape of the grooves walls is strongly reduced. The geometrical dimensions of the grating features fulfill the design specifications, except for the smallest bar b_1 that for the inspected grating is reduced in width and depth.

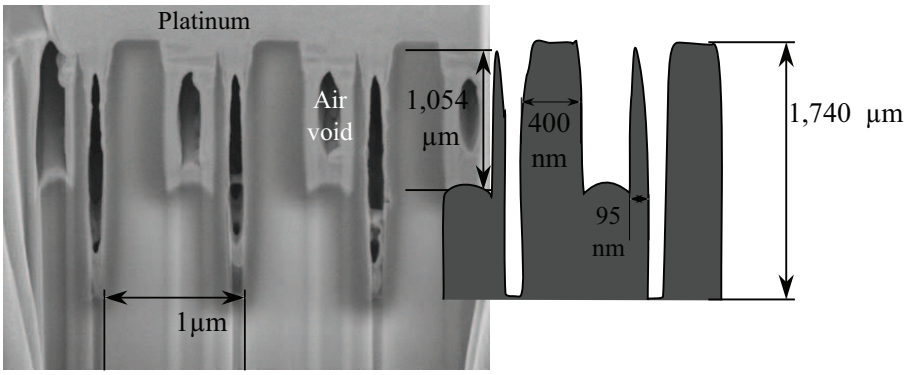

Figure 4.23: Effective medium enhanced three-level grating-close to normal incidence: FIB cross-section of one of the fabricated gratings.

A larger area FIB measurement (see Fig. 4.24) shows a good homogeneity over the grating area. No irregularities are affecting the surface.
Nevertheless, the diffraction measurements over incidence angle and wavelength of Fig. 4.25 a) and b) respectively, do show some differences with simulations. The achieved efficiencies are

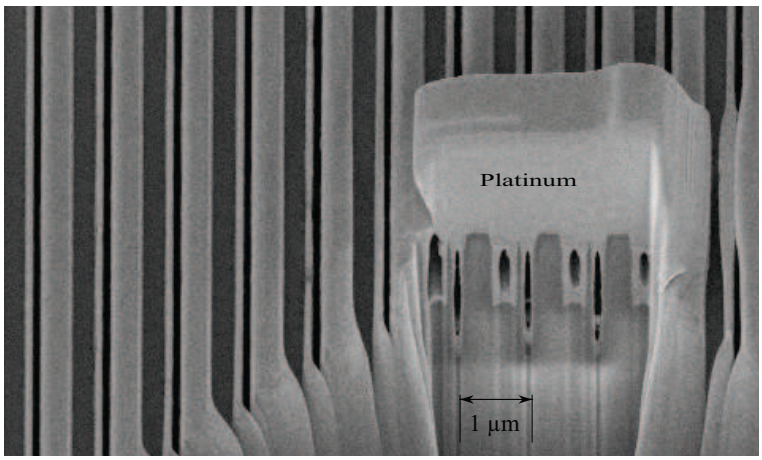

Figure 4.24: Effective medium enhanced three-level grating-close to normal incidence: large area FIB measurement.

higher than expected, especially for larger wavelengths, as clearly showed in the 2D mapping of Fig. 4.25.

The deviation between measurements and simulations could be due to the measurement resolution but also to the impossibility to characterize and consequently rigorously simulate the real fabricated structure profile over the whole measured area ($\approx 4mm^2$).

Furthermore, it has also to be considered that the refractive index of the SiO_2 coated by ALD could be slightly different from the refraction index of the bulk SiO_2. Unfortunately, the values of the refraction index of the ALD-SiO_2 are not exactly known, so in the simulations the same index of the bulk fused silica has been considered.

Furthermore, several simulations varying the dimensions of the bars and their positions vs. incidence angle and wavelength, have been carried out in order to understand the origins of the disagreement. The results have not been included in this work, because unfortunately they do not provide any additional information in understanding the higher efficiency achieved.

4.3.3 Results discussion

The ALD aided fabrication approach represents a good technological solution for the fabrication of demanding high aspect ratio structures, as successfully demonstrated for the fabrication of the effective-medium enhanced three-level gratings, discussed in this thesis.

The suggested solution to relax the lateral dimensions of the grooves before the deep etching into the substrate, can reduce the typical Y-shape of fused silica high aspect ratio structures. Nevertheless, there is a limitation in this approach due to the rounded edges typical for the ALD process. The optimal thickness of the ALD depends on the peculiar geometry of the grating.

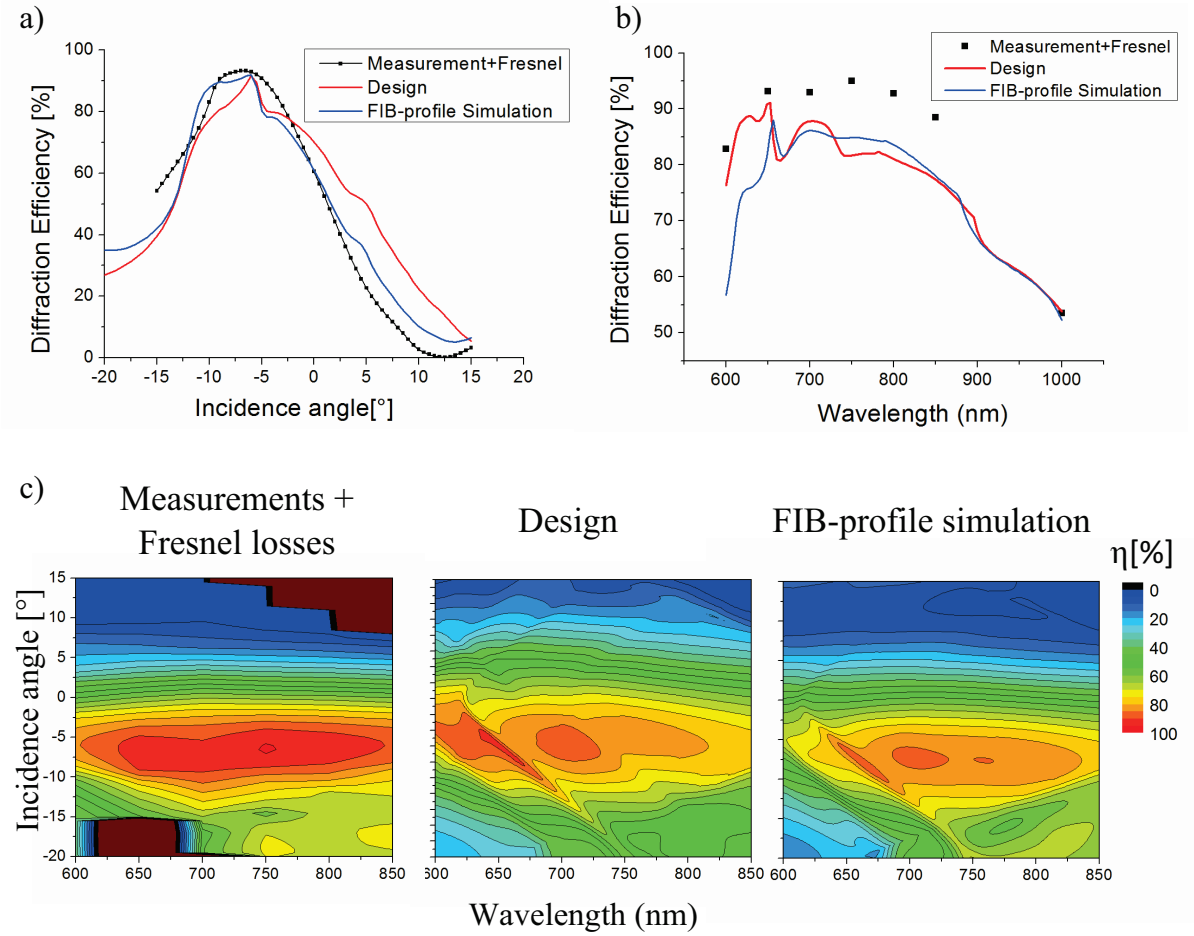

Figure 4.25: Effective medium enhanced three-level grating-close to normal incidence: Diffraction efficiency η. Comparison between measurement and simulation of the original design and the FIB-measured profile of the grating. **a)** vs. incidence angle (angular measurement resolution: 1 degree). **b)** vs. wavelength. **c)** 2D mapping-angular measurement (resolution: 0.5 degree).

Chapter summary

In this chapter, the characterization of fabricated multilevel blazed gratings in resonance domain has been presented and discussed.

The two optimized and designed gratings, i.e. three-level and effective-medium enhanced three-level grating, have been fabricated by means of different technologies, purposely developed to overcome the limits of the standard fabrication approach.

The three-level grating has been fabricated by standard, *Three-Layer Resist*, and *Relaxed alignment* technology. All approaches turn out to be suited for the fabrications of high efficiency gratings, also if the most of the gratings exhibit a fabrication artifact. This artifact is not solely due to alignment errors, but origins probably from the fused silica etching process itself (passivation layer or resist residuals, acting as a local mask for the etching). The presence of such artifact has the potential to enhance the diffraction performance of the grating, although it can generate uncontrolled scattering.

The fabrication of the effective-medium enhanced three-level grating in contrary, has been successful only for the ALD enhanced technology, due to the demanding aspect ratio. The fabricated gratings exhibit high efficiency over large bandwidth wavelength.
In conclusion, for both grating configurations in resonance domain designed and discussed in this thesis, multilevel blazed structures with very high efficiency performance have been successfully fabricated and characterized.

Conclusions

The aim of this work was the design and the fabrication of transmission blazed gratings in resonance domain. Essential requirements for the gratings were high efficiency at normal incidence, and additionally good homogeneity on relative large area ($> 10mm^2$).
To fulfil these requirements simultaneously, the work has been focused in two directions. First, different kind of structures have been investigated in order to achieve the highest efficiency possible at normal incidence. In the parametric optimization of the blazed structures the fabrication constraints have been taken into account and it resulted in optimized multilevel structures. Secondly, new technological approaches have been developed, and compared with the classical multilevel technology, to achieve homogeneous optical performances on large area fused silica gratings.
Two particular grating configurations have been chosen for the optimization of the design and fabrication. One blazed grating is working for incident light coming through the substrate, and a second grating with light coming from air, respectively.
For the case *substrate-air*, the optimized grating is a simple three-level grating, parametrically optimized as suggested by Noponen [60]. A physical model to understand the high efficiency achieved has been developed. Such a model is very intuitive and it is based on a simple three-wave interferences mechanism. The three-level grating is virtually decomposed into two binary gratings. The bottom level grating acts as simple beam splitter. The three propagating diffraction orders of this grating are the input fields of the upper level grating. It has been proven that to achieve the maximum efficiency in the first diffraction order the position of the upper level bar (with respect to the bottom level) plays a fundamental role due to the required Detour phase.
For the other configuration *air-substrate*, a simple fabricable three-level structure is not sufficient to achieve an efficiency higher than 90%. A new kind of grating design has been proposed. The grating is composed of a three-level with an additional subwavelength structure on the edge of the bottom level. This new grating design reaches high efficiencies well above 90% in a broad wavelength band. Also for this structures, it has been possible to find a physical interpretation for the high efficiency. The modal analysis of this multilevel structure shows that it can be virtually decomposed in two binary gratings, as well. The modest first order diffraction efficiency of $\approx 70\%$ of the first two-ridges grating is increased to by the bottom simple binary grating, which works actually as a mode conversion layer.

Although, in the optimization procedures the fabrication constraints have been considered, the resulting grating profiles are demanding from a technological point of view. Especially considering the limitations of the standard *Binary Optics* technology, i.e. misalignment and sizing errors in the second fabrication layer, and the difficulty of etching high aspect ratio structures in fused silica.

To overcome these limitations three new fabrication approaches have been proposed and tested for the fabrication of blazed gratings in resonance domain. In particular, the first approach, *Three-resist layer* technology, consists in a simple modification of the standard approach by adding a planarization layer in order to avoid non-flatness of resist/ chromium layers within the second fabrication step.

The second technology is devoted to completely avoid the misalignment errors that may occur between two lithographic steps. For this reason, it is called *Relaxed Alignment* technology and it consists in the use of a unique coded chromium mask for the all fabrication process. This coded mask contains all information about the lateral dimensions of all grating features.

Within the last proposed fabrication approach, *ALD-enhanced* technology, the Atomic Layer Deposition technique has been introduced in the fabrication of diffraction gratings. To reduce typical Y-shape of high aspect ratio grooves in fused silica, the groove is first etched with an enlarged width, after its width is trimmed down by ALD of fused silica.

The three new technological approaches resulted appropriate for the fabrication of multilevel structure characterized by small period ($1...5\mu m$) and submicron feature sizes, as shown from the fabrication results of the two blazed gratings, discussed here. The high efficiencies achieved, the quasi-perfect agreement with the simulations, and the comparison with the results of the standard technology confirm this assumption. Nevertheless, it is also worth to mention that for the first time a three-level resonance-domain grating, working in the visible spectral range has been successfully fabricated by the standard technology approach, as well.

In conclusion, within this research work it has been proven that it is possible to design and fabricate transmission blazed gratings in fused silica, working in resonance domain, and achieving high efficiency also for non-Littrow configuration. The optimization of the grating profile has to take into account the fabrication constrains. At the same time, the technology has to be design-based and flexible, combing also different approaches in order to find the best process for the peculiar gratings.

The technologies discussed in this work have been introduced in the fabrication chain of the CMN (Center for Advanced Micro and Nano-optics) of the Fraunhofer-IOF and successfully used for the fabrication of other three-level gratings [101, 112]. Blazed transmission gratings in resonance domain can be now used in industrial applications.

In addition, the physical interpretation for the high efficiencies, based on the analysis of the multilevel structures as a composition of simple binary gratings, shows the opportunity to in-

vestigate new kind of structure in order to achieve even higher blazing efficiency. It is possible to design the perfect blazing (diffraction efficiency = 100%) transmission grating as a multilevel structure with the upper levels wider then the bottom levels (see the attachment A).
However, further developments in the fabrication technologies are required to realize such a design. Some of the approaches developed in this work might be useful for such designs as well. Until then the blazed transmission gratings presented in this work are the most efficient design for normal incidence successfully realized up to today.

Bibliography

[1] J. Strong : The Johns Hopkins University and Diffraction Gratings. In: *J. Opt. Soc. Am.* 50 (1960), pp. 1148–1151.

[2] J. Fraunhofer : Kurtzer Bericht von den Resultaten neuerer Versuche über die Gesetze des Lichtes, und die Theorie derselben. In: *Ann. Phys.* 74 (1823), pp. 337–378.

[3] M. S. L. Lee et al. : Imaging with blazed-binary diffractive elements. In: *J. Opt. A: Pure Appl. Opt.* 4 (2002), DOI: 10.1088/1464-4258/4/5/358.

[4] E. G. Loewen and E. Popov : *Diffraction gratings and applications*, Marcel Dekker, Inc., 1997, chap. The types of Diffraction Gratings.

[5] H. Gross : Handbook of Optical Systems. In: ed. by H. Gross, vol. Volume 1, Fundamentals of Technical Optics, Wiley-VCH, 2005, chap. Grating, pp. 647–693.

[6] P. Schreiber et al. : High-brightness fiber-coupling schemes for diode laser bars. In: *Proc. SPIE 5876, Laser Beam Shaping VI, 587602*, 2005, DOI: 10.1117/12.616955.

[7] M. Oliva et al. : Twyman-Green-type integrated laser interferometer array for parallel MEMS testing. In: *Journal of Micromechanics and Microengineering* 22 (2012), DOI: 10.1088/0960-1317/22/1/015018.

[8] C. Zhou : Deep-etched fused silica gratings and applications. In: *Proc. SPIE 7848, Holography, Diffractive Optics, and Applications IV*, 2010, 78480R, DOI: 10.1117/12.869033.

[9] P. Lalanne et al. : Design and fabrication of blazed binary diffractive elements with sampling periods smaller than the structural cutoff. In: *J. Opt. Soc. Am. A* 16 (1999), pp. 1143–1156, DOI: 10.1364/JOSAA.16.001143.

[10] M. Born and E. Wolf : Principles of Optics. In: Cambridge University Press, 1999, chap. Element of the theory of diffraction, pp. 412–516.

[11] D. C. O'Shea et al. : *Diffractive Optics: Design, Fabrication, and Test*, SPIE Press, 2004.

[12] Evgeny Popov, ed.: *Gratings: theory and numeric applications*, Presses universitaires de Provence (PUP), 2012, chap. The types of Diffraction Gratings, URL: www.fresnel.fr/numerical-grating-book.

[13] R. C. Enger and S. K. Case : Optical elements with ultrahigh spatial-frequency surface corrugations. In: *Applied Optics* 22 (1983), Nr. 20, pp. 3220–3228, DOI: 10.1364/AO.22.003220.

[14] D. C. Flanders : Submicrometer periodicity gratings as artificial anisotropic dielectrics. In: *Applied Physics Letters* 42 (1983), pp. 492–494, DOI: 10.1063/1.93979.

[15] P. Lalanne et al. : Blazed binary subwavelength gratings with efficiencies larger than those of conventional échelette gratings. In: *Opt. Lett.* 32 (1998), pp. 1081–1083, DOI: 10.1364/OL.23.001081.

[16] E. Popov, L. Tsonev, and D. Maystre : Gratings-general Properties of the Littrow Mounting and Energy Flow Distribution. In: *J. Mod. Opt.* 37 (1990), pp. 367–377, DOI: 10.1080/09500349014550421.

[17] J. W. Goodman : *Introduction to Fourier Optics*, ed. by S. W. Director, Second Edition, McGraw-Hill, 1996.

[18] M. G. Moharam and T. K. Gaylord : Diffraction analysis of dielectric surface-relief gratings. In: *J. Opt. Soc. Am.* 72 (1982), Nr. 10, pp. 1385–1392, DOI: 10.1364/JOSA.72.001385.

[19] J. A. Cox et al. : Diffraction efficiency of binary optical elements. In: *Proc. SPIE 1211, Computer and Optically Formed Holographic Optics,* 1990, p. 116, DOI: 10.1117/12.17953.

[20] M. B. Fleming and M. C. Hutley : Blazed diffractive optics. In: *Applied Optics* 36 (1997), pp. 4635–4643, DOI: 10.1364/AO.36.004635.

[21] R. Magnusson and T. K. Gaylord : Diffraction efficiencies of thin phase gratings with arbitrary grating space. In: *J. Opt. Soc. Am.* 68 (1978), p. 806, DOI: 10.1364/JOSA.68.000806.

[22] G. J. Swanson : *Binary Optics Technology: The Theory and Design of Multi-Level Diffractive Optical Elements*, tech. rep., Massachusetts Inst. of Tech. Lexington Lincoln Lab, 1989.

[23] A. Wirgin and R. Deleuil : Theoretical and Experimental Investigation of a New Type of Blazed Grating. In: *JOSA* 59 (1969), Nr. 10, pp. 1348–1357, DOI: 10.1364/JOSA.59.001348.

[24] G. J. Swanson : *Binary Optics Technology: Theoretical Limits on the Diffraction Efficiency of Multilevel Diffractive Optical Elements*, tech. rep., Massachusetts Inst. of Tech. Lexington Lincoln Lab, 1991.

[25] O. Sandfuchs et al. : Rigorous analysis of shadowing effects in blazed transmission gratings. In: *Opt. Lett.* 31 (2006), pp. 3638–3640, DOI: 10.1364/OL.31.003638.

[26] O. Sandfuchs et al. : Analysis of the influence of the passive facet of blazed transmission gratings in the intermediate diffraction regime. In: *J. Opt. Soc. Am. A* 25 (2008), pp. 1885–1893, DOI: 10.1364/JOSAA.25.001885.

[27] D. Kuang and Z. Fang : Diffraction efficiency analysis of blazed grating fabricated by direct laser writing. In: *Proc. SPIE 7848, Holography, Diffractive Optics, and Applications IV, 78480P*, 2010, 78480P, DOI: 10.1117/12.866240.

[28] C. Ribot et al. : Analysis of blazed diffractive optical elements formed with artificial dielectrics. In: *J. Opt. Soc. Am. A* 24 (2007), pp. 3819–3826, DOI: 10.1364/JOSAA.24.003819.

[29] D. A. Pommet, M. G. Moharam, and E. B. Grann : Limits of scalar diffraction theory for diffractive phase elements. In: *J. Opt. Soc. Am. A* 11 (1994), pp. 1827–1834, DOI: 10.1364/JOSAA.11.001827.

[30] R. Magnusson and T. K. Gaylord : Equivalence of multiwave coupled-wave theory and modal theory for periodic-media diffraction. In: *J. Opt. Soc. Am.* 68 (1978), pp. 1777–1779, DOI: 10.1364/JOSA.68.001777.

[31] M. G. Moharam et al. : Formulation for stable and efficient implementation of the rigorous coupled-wave analysis of binary gratings. In: *J. Opt. Soc. Am. A* 12 (1995), pp. 1068–1076, DOI: 10.1364/JOSAA.12.001068.

[32] L. Li : Use of Fourier series in the analysis of discontinuous periodic structures. In: *J. Opt. Soc. Am. A* 13 (1996), pp. 1870–1876, DOI: 10.1364/JOSAA.13.001870.

[33] L. Li : New formulation of the Fourier modal method for crossed surface-relief gratings. In: *New formulation of the Fourier modal method for crossed surface-relief gratings," J. Opt. Soc. Am. A 14, 2758-2767 (1997)* 14 (1997), pp. 2758–2767, DOI: 10.1364/JOSAA.14.002758.

[34] M. A. Golub and A. A. Friesem : Effective grating theory for resonance domain surface-relief diffraction gratings. In: *J. Opt. Soc. Am. A* 22 (2005), pp. 1115–1126, DOI: 10.1364/JOSAA.22.001115.

[35] M. A. Golub and A. A. Friesem : Analytic design and solutions for resonance domain diffractive optical elements. In: *J. Opt. Soc. Am. A* 24 (2007), pp. 687–695, DOI: 10.1364/JOSAA.24.000687.

[36] W. Stork et al. : Artificial distributed-index media fabricated by zero-order gratings. In: *Opt. Lett.* 16 (1991), pp. 1921–1923, DOI: 10.1364/OL.16.001921.

[37] M. W. Farn : Binary gratings with increased efficiency. In: *Appl. Opt.* 31 (1992), pp. 4453–4458, DOI: 10.1364/AO.31.004453.

[38] M. Collischon et al. : Binary blazed reflection gratings. In: *Appl. Opt.* 33 (1994), pp. 3572–3577, DOI: 10.1364/AO.33.003572.

[39] P. Lalanne and D. Lemercier-Lalanne : On the effective medium theory of subwavelength periodic structures. In: *Journal of Modern Optics* 43 (1996), Nr. 10, pp. 2063–2085, DOI: 10.1080/09500349608232871.

[40] H. Haidner et al. : Design of a blazed grating consisting of metallic subwavelength binary grooves. In: *Opt. Comm.* 98 (1993), pp. 5–10, DOI: 10.1016/0030-4018(93)90749-U.

[41] H. Haidner et al. : Diffraction grating with rectangular grooves exceeding 80diffraction efficiency. In: *Infrared Physics* 34 (1993), Nr. 5, pp. 467–475, DOI: 10.1016/0020-0891(93)90080-Q.

[42] S. Astilean et al. : High-efficiency subwavelength diffractive element patterned in a high-refractive-index material for 633 nm. In: *Optics Letters* 23 (1998), pp. 552–554, DOI: 10.1364/OL.23.000552.

[43] M. S. L. Lee et al. : Transmission blazed-binary gratings for visible light operation: performances and interferometric characterization. In: *J. Opt. A: Pure Appl. Opt.* 5 (2003), Nr. 5, DOI: 10.1088/1464-4258/5/5/373.

[44] P. Lalanne : Waveguiding in blazed-binary diffractive elements. In: *J. Opt. Soc. Am. A* 16 (1999), pp. 2517–2520, DOI: 10.1364/JOSAA.16.002517.

[45] M.-S. L. Lee et al. : Wide-field-angle behavior of blazed-binary gratings in the resonance domain. In: *Optics Letters* 25 (2000), pp. 1690–1692, DOI: 10.1364/OL.25.001690.

[46] C. Sauvan, P. Lalanne, and M.-S. L. Lee : Broadband blazing with artificial dielectrics. In: *Opt. Lett.* 29 (2004), pp. 1593–1595, DOI: 10.1364/OL.29.001593.

[47] M. Kuittinen, J. Turunen, and P. Vahimaa : Rigorous analysis and optimization of subwavelength-structured binary dielectric beam deflector gratings. In: *Journal of Modern Optics* 45 (1998), pp. 133–142, DOI: 10.1080/09500349808231675.

[48] H. J. Hyvarinen, J. Turunen, and P. Saarikko : Efficiency optimization of blazed effective-medium gratings in the resonance domain. In: *J. Opt. A: Pure Appl. Opt.* 5 (2008), DOI: 10.1088/1464-4258/10/5/055005.

[49] H. J. Hyvarinen, P. Karvinen, and J. Turunen : Polarization insensitive resonance-domain blazed binary gratings. In: *Opt. Express* 18 (2010), pp. 13444–13450, DOI: 10.1364/OE.18.013444.

[50] M.-S. L. Lee, P. Lalanne, and P. Chavel : Blazed-binary diffractive elements with periods much larger than the wavelength. In: *J. Opt. Soc. Am. A* 17 (2000), pp. 1250–1255, DOI: 10.1364/JOSAA.17.001250.

[51] P. Lalanne et al. : Design and fabrication of blazed binary diffractive elements with sampling periods smaller than the structural cutoff. In: *J. Opt. Soc. Am. A* 16 (1999), pp. 1143–1156, DOI: 10.1364/JOSAA.16.001143.

[52] B. H. Kleemann, J. Ruoff, and R. Arnold : Area-coded effective medium structures, a new type of grating design. In: *Opt. Lett.* 30 (2005), pp. 1617–1619, DOI: 10.1364/OL.30.001617.

[53] H. Elfstroem et al. : Fabrication of blazed gratings by area-coded effective medium structures. In: *Optics Communications* 266 (2006), Nr. 2, pp. 607–703, DOI: 10.1016/j.optcom.2006.05.042.

[54] D. Michaelis et al. : Nano-Optical Gratings for Integrated Laser Interferometer Arrays. In: *CLEO/Europe and EQEC 2011 Conference Digest, OSA Technical Digest (CD)*, 2011, URL: http://www.opticsinfobase.org/abstract.cfm?URI=CLEO_Europe-2011-CK5_3.

[55] U. D. Zeitner et al. : High performance diffraction gratings made by e-beam lithography. In: *Applied Physics A: Materials Science & Processing* 109 (2012), pp. 789–796, DOI: 10.1007/s00339-012-7346-z.

[56] C. Wächter et al. : Optical design including characteristics of manufactured nanostructures. In: *Proc. SPIE 8840, Optical Modeling and Performance Predictions VI*, 2013, pp. 10.1117/12.2024055, DOI: 10.1117/12.2024055.

[57] P. S. J. Russell : Optics of Floquet-Bloch waves in dielectric gratings. In: *Applied Physics B* 39 (1986), pp. 231–246, DOI: 10.1007/BF00697490.

[58] J. Pietarinen and T. Vallius : Double groove broadband gratings. In: *Opt. Express* 16 (2008), Opt. Express, DOI: 10.1364/OE.16.013824.

[59] U. D. Zeitner et al. : High performance gratings for space applications. In: *Proc. SPIE 7716, Micro-Optics 2010*, 2010, 77161K, DOI: 10.1117/12.854951.

[60] E. Noponen, J. Turunen, and A. Vasara : Parametric optimization of multilevel diffractive optical elements by electromagnetic theory. In: *Applied Optics* 31 (1992), Nr. 28, pp. 5910–5912, DOI: 10.1364/AO.31.005910.

[61] E. Noponen and J. Turunen : Eigenmode method for electromagnetic synthesis of diffractive elements with three-dimensional profiles. In: *J. Opt. Soc. Am. A* 11 (1994), pp. 2494–2502, DOI: 10.1364/JOSAA.11.002494.

[62] E. Noponen, J. Turunen, and A. Vasara : Electromagnetic theory and design of diffractive-lens arrays. In: *J. Opt. Soc. Am. A* 10 (1993), pp. 434–443, DOI: 10.1364/JOSAA.10.000434.

[63] E. Noponen et al. : Synthetic diffractive optics in the resonance domain. In: *J. Opt. Soc. Am. A* 9 (1992), pp. 1206–1213, DOI: 10.1364/JOSAA.9.001206.

[64] T. J. Suleski and R. D. T. Kolste : Roadmap for micro-optics fabrication. In: *Proc. SPIE 4440, Lithographic and Micromachining Techniques for Optical Component Fabrication*, 2001, DOI: 10.1117/12.448025.

[65] Y. Fu, N. Bryan, and W. Zhou : Quasi-direct writing of diffractive structures with a focused ion beam. In: *Opt. Express* 12 (2004), pp. 1803–1809, DOI: 10.1364/OPEX.12.001803.

[66] C. Palmer : *Diffraction Grating Handbook*, Richardson Grating Laboratory, Rochester, NY, 2002.

[67] C. G. Blough et al. : Single-point diamond turning and replication of visible and near-infrared diffractive optical elements. In: *Appl. Opt.* 36 (1997), pp. 4648–4654, DOI: 10.1364/AO.36.004648.

[68] N. A. Vainos et al. : Excimer laser use for microetching computer-generated holographic structures. In: *Appl. Opt* 35 (1996), pp. 6304–6319, DOI: 10.1364/AO.35.006304.

[69] G. P. Behrmann and M. T. Duignan : Excimer laser micromachining for rapid fabrication of diffractive optical elements. In: *Appl. Opt.* 36 (1997), pp. 4666–4674, DOI: 10.1364/AO.36.004666.

[70] P. Nussbaum et al. : Potential of dry etching for the fabrication of fused silica micro-optical elements. In: *Proc. SPIE Vol. 3879, Micromachine Technology for Diffractive and Holographic Optics*, ed. by S. H. Lee and J. A. Cox, 1999, pp. 63–70, DOI: 10.1117/12.360533.

[71] G. A. C. M. Spierings : Wet chemical etching of silicate glasses in hydrofluoric acid based solutions. In: *Journal of Materials Science* 28 (1993), pp. 6261–6273, DOI: 10.1007/BF01352182.

[72] E.-B. Kley : Continuous profile writing by electron and optical lithography. In: *Microelectron. Eng.* 34 (1997), pp. 261–298, DOI: 10.1016/S0167-9317(97)00186-X.

[73] D. W.Wilson et al. : Recent advances in blazed grating fabrication by electron-beam lithography. In: *Proc. SPIE 5173, Current Developments in Lens Design and Optical Engineering IV*, 2003, DOI: 10.1117/12.510204.

[74] T. Shiono, T. Hamamoto, and K. Takahara : High-Efficiency Blazed Diffractive Optical Elements for the Violet Wavelength Fabricated by Electron-Beam Lithography. In: *Appl. Opt.* 41 (2002), pp. 2390–2393, URL: http://www.opticsinfobase.org/ao/abstract.cfm?URI=ao-41-13-2390.

[75] T. Fujita, H. Nishihara, and J. Koyama : Blazed gratings and Fresnel lenses fabricated by electron-beam lithography. In: *Opt. Lett.* 7 (1982), pp. 578–580, DOI: 10.1364/OL.7.000578.

[76] M. T. Gale et al. : Fabrication of continuous-relief micro-optical elements by direct laser writing in photoresists. In: *Opt. Eng. 33* 33 (1994), pp. 3556–3566, DOI: 10.1117/12.179892.

[77] T. Hessler et al. : Analysis and Optimization of Fabrication of Continuous-Relief Diffractive Optical Elements. In: *Appl. Opt.* 37 (1998), pp. 4069–4079, DOI: 10.1364/AO.37.004069.

[78] O. S. at al. : Modelling adapted to manufacturing aspects of holographic grating structures. In: *Journal Of The European Optical Society - Rapid Publications* 6 (2011), pp. 11006–10, DOI: 10.2971/jeos.2011.11006.

[79] M. Stern, in: *Microoptics: Elements, Systems and Applications*, ed. by H. P. Herzig, Taylor & Francis, London, 1997, chap. Binary optics fabrication, pp. 53–85.

[80] S. Sinzinger and J. Jahn : *Microoptics*, Wiley-VCH, 2003.

[81] S. Franssila : *Introduction to Microfabrication*, Second, Wiley, 2010.

[82] M. B. Stern : Binary optics: A VLSI-based microoptics technology. In: *Micr* 32 (1996), pp. 369–388, DOI: http://dx.doi.org/10.1016/0167-9317(95)00369-X.

[83] L. d'Auria et al. : Photolithographic fabrication of thin film lenses. In: *Optics Communications* 5 (1972), Nr. 4, pp. 232–235, DOI: 10.1016/0030-4018(72)90086-7.

[84] B. Goebel, L. L. Wang, and T. Tschudi : Multilayer technology for diffractive optical elements. In: *Appl. Opt.* 35 (1996), pp. 4490–4493, DOI: 10.1364/AO.35.004490.

[85] J. M. Finlan, R. J. Bojko, and K. M. Flood : Efficient f/1 binary-optics microlenses in fused silica designed using vector diffraction theory. In: *Optical Engineering* 34 (1995), pp. 3560–3564, DOI: 10.1117/12.215664.

[86] E. Hasman, N. Davidson, and A. A. Friesem : Heterostructure multilevel binary optics. In: *Opt. Lett. 16* 16 (1991), pp. 1460–1462, DOI: 10.1364/OL.16.001460.

[87] A. Kowalik et al. : Multi-step electron beam technology for the fabrication of high performance diffractive optical elements. In: *Microelectron. Eng.* 77 (2005), pp. 347–357, DOI: 10.1016/j.mee.2004.12.036.

[88] S. Somekh : Introduction to ion and plasma etching. In: *Journal of Vacuum Science and Technology* 13 (1976), pp. 1003 –1007, DOI: 10.1116/1.569036.

[89] G. Dahm et al. : Quartz etching for phase shifting masks. In: *Microelectronic Engineering* 27 (1995), pp. 263–266, DOI: 10.1016/0167-9317(94)00103-2.

[90] J. M. Miller et al. : Multilevel-grating array generators: fabrication error analysis and experiments. In: *Appl. Opt.* 32 (1993), pp. 2519–2525, DOI: 10.1364/AO.32.002519.

[91] M. Oliva et al. : Highly efficient three-level blazed grating in the resonance domain. In: *Optics Letters* 35 (2010), pp. 2774–2776, DOI: 10.1364/OL.35.002774.

[92] M. Oliva et al. : Highly efficient broadband blazed grating in resonance domain. In: *Appl. Phys. Lett.* 102 (2013), p. 203114, DOI: 10.1063/1.4807764.

[93] URL: www.iof.fraunhofer.de.

[94] H. A. Lorentz : The theorem of poynting concerning the energy in the electromagnetic field and two general propositions concerning the propagation of light. In: *Amsterdammer Akademie der Wetenschappen 4* 176 (1896),

[95] T. Clausnitzer et al. : An intelligible explanation of highly-efficient diffraction in deep dielectric rectangular transmission gratings. In: *Opt. Express* 13 (2005), pp. 10448–10456, DOI: 10.1364/OPEX.13.010448.

[96] H. Iizuka et al. : Role of propagating modes in a double-groove grating with a +1st-order diffraction angle larger than the substrateair critical angle. In: *Opt. Lett.* 35 (2010), pp. 3973–2975, DOI: 10.1364/OL.35.003973.

[97] T. Pertsch and C. Waetcher : Asymmetrical offon switches for crosstalk reduction in switching networks. In: *Optical and Quantum Electronics* 31 (1999), pp. 957–963.

[98] C. David : Fabrication of stair-case profiles with high aspect ratios for blazed diffractive optical elements. In: *Micr. Eng.* 53 (2000), pp. 677–680, DOI: 10.1016/S0167-9317(00)00403-2.

[99] K. Rieken : Characterization of ICP Cr Etching Processes for the Fabrication of Microoptical gratings. MA thesis, Friedrich-Schiller-Univeristy of Jena, 2013.

[100] M. Kuittinen and J. Turunen : Mask misalignment in photolithographic fabrication of resonance-domain diffractive elements. In: *Opt. Comm.* 142 (1997), pp. 14–18, DOI: 10.1016/S0030-4018(97)00325-8.

[101] M. Oliva et al. : Multilevel blazed gratings in resonance domain: an alternative to the classical fabrication approach. In: *Opt. Express* 19 (2011), pp. 14735–14745, DOI: 10.1364/OE.19.014735.

[102] U. D. Zeitner, F. Fuchs, and E.-B. Kley : High-performance dielectric diffraction gratings for space applications. In: *Proc. SPIE 8450, Modern Technologies in Space- and Ground-based Telescopes and Instrumentation II*, 2012, 84502Z, DOI: 10.1117/12.928286.

[103] S. M. George : Atomic Layer Deposition: An Overview. In: *Chem. Rev.* 110 (2010), pp. 111–131, DOI: DOI:10.1021/cr900056b.

[104] V. Miikkulainen et al. : Crystallinity of inorganic films grown by atomic layer deposition: Overview and general trends. In: *J. Appl. Phys.* 113 (2013), pp. 021301 –021301–101, DOI: 10.1063/1.4757907.

[105] URL: http://www.fujifilmusa.com/products/semiconductor_materials/photoresists/ebeam/.

[106] E. Reichmanis et al. : Chemically amplified resists: Chemistry and processes. In: *Adv. Mater. Opt. Electron.* 4 (1994), DOI: 10.1002/amo.860040205.

[107] U. D. Zeitner and E.-B. Kley : Advanced lithography for micro-optics. In: *Proc. SPIE 6290, Laser Beam Shaping VII*, 2006, p. 629009, DOI: 10.1117/12.682739.

[108] URL: http://www.microchemicals.com/products/photoresists/az_p4000.html.

[109] F. A. S. Lucille A. Giannuzzi : *Introduction to Focused Ion Beams*, ed. by F. A. S. Lucille A. Giannuzzi, Springer, 2005.

[110] M. Oliva et al. : Smart technology for blazed multilevel gratings in resonance domain. In: *Proc. SPIE 7716, Micro-Optics 2010*, ed. by H. Thienpont et al., 2010, p. 77161L, DOI: 10.1117/12.854587.

[111] URL: www.beneq.com.

[112] L. Stuerzebecher et al. : Pulse compression grating fabrication by diffractive proximity photolithography. In: *Opt. Lett.* 39 (2014), pp. 1042–1045, DOI: 10.1364/OL.39.001042.

A Perfect blazed gratings in resonance domain

The diffraction efficiencies achieved by the two blazed gratings, discussed in this work, are already very high with values >90 %. These high blazed efficiencies have been achieved with simple structures, a three-level and an effective-medium enhanced three-level grating.
By adding additional levels and additional freedom in the parametric optimization of them, it is possible achieve diffraction efficiencies of 100 % or very close to the perfect blazing efficiency. In the Fig. A.1, two examples of perfect blazed gratings are shown. The gratings are optimized for the same operating conditions of the effective-medium grating discussed in this work.

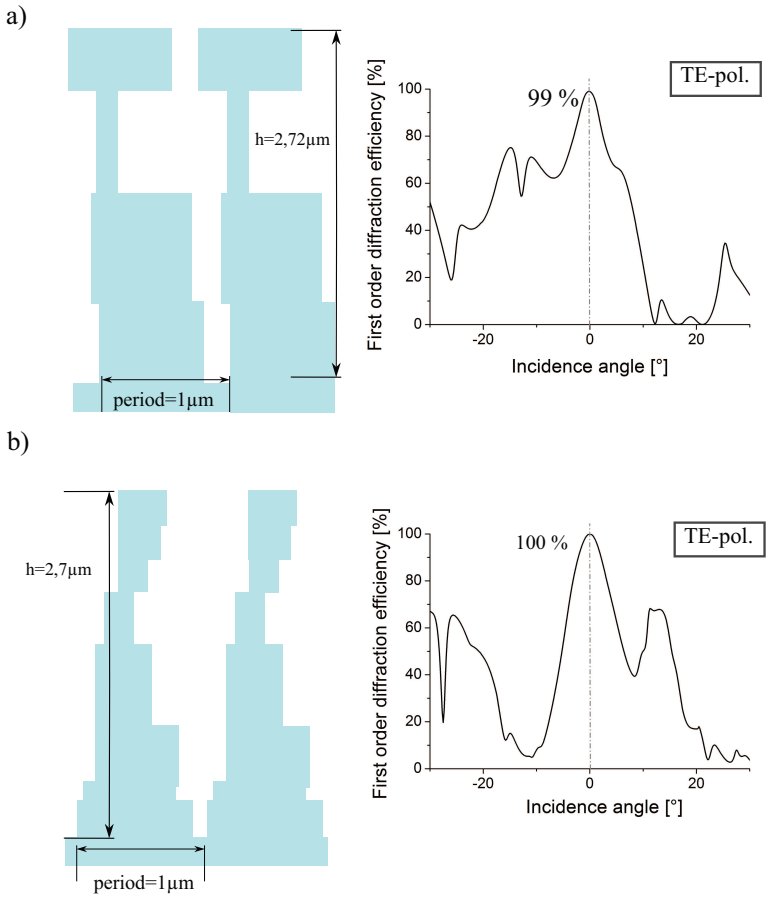

Figure A.1: Perfect blazed grating examples. a) four-level; b) eight-level. The grating are optimized at normal incidence for light coming from air. $p = 1\mu m$; $\lambda = 650nm$; TE polarization.

Both gratings are characterized by some upper levels wider as the under levels and demanding total depth of the structures. These profiles require further development in the fabrication technologies in order to fabricate such over-hanging structures.

B Publications

Peer-reviewed Journals

- M. Oliva, D. Michaelis, T. Benkenstein, J. Dunkel, T. Harzendorf, A. Matthes, and U. D. Zeitner, *Highly efficient three-level blazed grating in the resonance domain*, Opt. Lett. 35, 2774-2776 (2010)

- M. Oliva, T. Harzendorf, D. Michaelis, U. D. Zeitner, and A. Tünnermann, *Multilevel blazed gratings in resonance domain: an alternative to the classical fabrication approach*, Opt. Express 19, 14735-14745 (2011)

- M. Oliva, D. Michaelis, P. Dannberg, M. Józwik, K. Liżewski, M Kujawińska and U. D. Zeitner, *Twyman-Green-type integrated laser interferometer array for parallel MEMS testing*, J. Micromech. Microeng. 22, 015018 (2012)

- U. D. Zeitner, M. Oliva, F. Fuchs, D. Michaelis, T. Benkenstein, T. Harzendorf and E.-B. Kley, *High performance diffraction gratings made by e-beam lithography*, Applied Physics A 109, 789-796 (2012)

- M. Oliva, D. Michaelis, F. Fuchs, A. Tünnermann, and U. D. Zeitner, *Highly efficient broadband blazed grating in resonance domain*, Applied Physics Letters, 102, 203114 (2013)

- A. Savenko, I. Yildiz, D. H. Petersen, P. Bøggild, M. Bartenwerfer, F. Krohs, M. Oliva and T. Harzendorf, *Ultra-high aspect ratio replaceable AFM tips using deformation-suppressed focused ion beam milling*, Nanotechnology 24, 465701 (2013)

Conference Proceedings

- G. Lullo, R. Leto, M. Oliva and C. Arnone, *Multilevel pattern generation by GaN laser lithography: an application to beam shaper fabrication*, Proc. SPIE 6290, Laser Beam Shaping VII, 62900A (2006)

- M. Oliva, T. Benkenstein, M. Flemming and U. D. Zeitner, *AFM characterization of large area micro-optical elements*, Proc. SPIE 7389, Optical Measurement Systems for Industrial Inspection VI, 73893K (2009)

- M. Oliva, T. Benkenstein, J. Dunkel, T. Harzendorf, A. Matthes, D. Michaelis and U. D. Zeitner, *Smart technology for blazed multilevel gratings in resonance domain*, Proc. SPIE 7716, Micro-Optics 2010, 77161L (2010)

- T. Benkenstein, M Flämmich, T. Harzendorf; T. Käsebier, D. Michaelis, M. Oliva, C. Wächter and U. D. Zeitner, *Effects of metallic nanoparticle arrays in Si solar cell structures*, Proc. SPIE 8110, Thin Film Solar Technology III, 81100D (2011)

- C. Wächter, M. Müller, E. Förster, M. Oliva and D. Michaelis, *Optical design including characteristics of manufactured nanostructures*, Proc. SPIE 8840, Optical Modeling and Performance Predictions VI, 88400B (2013)

International Conference Contributions

- (poster) M. Oliva, T. Benkenstein, M. Flemming and U. D. Zeitner, *AFM characterization of large area micro-optical elements*, Proc. SPIE 7389, Optical Measurement Systems for Industrial Inspection VI, 73893K (2009)
- (oral) M. Oliva, T. Benkenstein, J. Dunkel, T. Harzendorf, A. Matthes, D. Michaelis and U. D. Zeitner, *Smart technology for blazed multilevel gratings in resonance domain*, Proc. SPIE 7716, Micro-Optics 2010, 77161L (2010)
- (oral) V. Eichhorn, D. Jasper, F. Krohs, P. Bøggild, S. Fahlbusch, M. Oliva, O. Krause, H. Hascke and S. Fatikow,*NanoBits: Exchangeable and customizable scanning probe tips as a versatile tool for nanoscale applications*, 7th International Workshop on Microfactories, 24-27 OCT. 2010, Daejeon, Korea (2010)
- (oral) M. Oliva, D. Michaelis, T.Benkenstein, J. Dunkel, T. Harzendorf, A. Matthes, U.D. Zeitner, *A novel approach for design, interpretation and fabrication of high efficient three-level grating*, EOSAM 2010, 26 - 29 October 2010, Parc Floral de Paris, France (2010)
- (oral) U.D. Zeitner, M. Oliva, D. Michaelis, M. Józwik, M. Kujawińska*Nano-optical grating interferometer for SMART InspEction system High Speed and multifunctional testing of MEMS and MOEMS (SMARTIEHS)*, EOSAM 2010, 26 - 29 October 2010, Parc Floral de Paris, France (2010)
- (oral) D. Michaelis, M. Oliva, T. Benkenstein, T. Harzendorf, A. Matthes, and U. Zeitner, *Nano-Optical Gratings for Integrated Laser Interferometer Arrays*, CLEO/Europe and EQEC 2011, Munich (2011)
- (oral) M. Oliva, D. Michaelis, F. Fuchs, U.D. Zeitner, *Effective-medium enhanced three-level grating in resonance domain*, DO2012, 27.02-1.03 2012, Delft (2012)
- U. D. Zeitner, M. Oliva, F. Fuchs, D. Michaelis, T. Benkenstein, T. Harzendorf and E.-B. Kley, *High performance diffraction gratings made by e-beam lithography*, META 12, 19-22 April, Paris (2012)
- U. D. Zeitner, F. Fuchs, M. Oliva, E.-B. Kley, *Recent Advancements of High-Performance Gratings for Spectroscopic- and Laser-Applications*, EOS Conference on Manufacturing of Optical Components, Munich (2013)

C Acknowledgments

Here, I would like to thank all people who helped me with and during this research work. I hope to be able with words to describe my whole gratitude to each one of them.

First, my thanks to Prof. Andreas Tünnermann to follow and supervise my research work; to Dr. Andreas Bräuer for his support and his German-Italian friendship, and Dr. Uwe Zeitner for giving me the opportunity to be part of the CMN-Optics with its high-end technology. Furthermore I thank him for his scientific support and several discussions during my PhD.
A special thanks goes to Dr. Dirk Michaelis, for his precious support since the begin of my PhD, suggesting me the right research direction. He showed me how discover the beauty of the Physics of gratings and I learned from him to be more accurate, correcting my innate *Italian style*.
A sincere thanks to Dr. Frank Fuchs for his RCWA software tool, MOOSE, used for the optimization of the gratings; for his patience to proof several versions of my Dissertation and to tolerate my uncountable questions; for the several scientific and friendly discussions and for his perfect Italian accent! A big thanks to Torsten Harzendorf, for his precious help with the technological issues, especially about the development of the *Relaxed Alignment Technology*, and to be for me not only a good colleague but also a good friend. I thank also Lorenz Stüzerbecher to be a very good office colleague and friend and for our technological/scientific discussions about gratings but also about Italian coffee! I thank him also for the Latex and Inkscape tips.
Many thanks to all colleagues from CMN-Optics, in particular Andrè Matthes for the etching, Tino Benkestein for the preparation of the samples, and Kathrin Rieken for the numerous FIB measurements and for our relaxing thee-pauses. I thank also all IAP colleagues working together with the CMN-Optics and the A3-department of IOF.

Ringrazio il Prof. Claudio Arnone per essere sempre un punto di riferimento, con cui scambiare punti di vista e idee.
Un grazie enorme alla mia amica Michela, per conoscermi cosi bene da trovare sempre le parole adatte (spesso dure!) per scuotermi e motivarmi in ogni situazione! E per avermi fatto notare e cercato di smussare la mia estrema testardaggine!
Ringrazio di cuore tutti i miei amici a Jena, che hanno reso il periodo del dottorato ancora più bello. In particolare un sentito grazie a Dania, Alessandro e Vito per avermi sopportato, supportato, consolato, motivato in ogni momento. Un grazie anche a Daniela e Ilaria per il loro tele-sostegno dall'Italia.
E non ci sono abbastanza parole per ringraziare la mia famiglia, in particolare mia sorella Marianna, per il loro supporto incondizionato, pur soffrendo la mia mancanza.

The last thanks goes to two persons that, also if for completely different reasons, delayed a bit my work. But, they gave me the chance in two fundamental phases of it, at begin and at end, to severely test my motivation and my love for these gratings.

Vielen Dank!

D Short Curriculum Vitae

Personal Data

Name	Maria Oliva
Nationality	Italian
Date and place of birth	09/01/1980 - Caltanissetta (Italy)
Adresse	Grietgasse, 10 - 07743 Jena
email	maria.oliva@iof.fraunhofer.de

Education

Current–03/2014	MBA student at HHL-Leipzig Graduate School of Management
12/2014–02/2010	PhD student at University of Jena - Faculty of Physics
09/1998-11/2005	Master Degree in Electronic Engineering, University of Palermo, Italy
07/1998-09/1993	Scientific High School Degree, Liceo Scientifico *A. Volta*, Caltanissetta, Italy

Work Experience

Current–07/2007	Researcher at Fraunhofer Institute IOF, Jena CMN-Optics, Center for Advanced Micro - and Nano-Optics
06/2007-05/2006	Research Assistant at Polytechnic University of Turin, Italy Department of Physics
05/2006-11/2005	Research Engineer at University of Palermo, Italy Opto and Bio-Electronics Lab

Jena, January 22, 2015

E Ehrenwörtliche Erklärung

Ich erkläre hiermit ehrenwörtlich, dass ich die vorliegende Arbeit selbständig, ohne unzulässige Hilfe Dritter und ohne Benutzung anderer als der angegebenen Hilfsmittel und Literatur angefertigt habe. Die aus anderen Quellen direkt oder indirekt übernommenen Daten und Konzepte sind unter Angabe der Quelle gekennzeichnet.

Bei der Auswahl und Auswertung folgenden Materials haben mir die nachstehend aufgeführten Personen in der jeweils beschriebenen Weise unentgeltlich geholfen:

1. Dr. Dirk Michaelis für seine Hilfe mit den physikalischen Modellen für die Interpretation der Effizienz.
2. Torsten Harzendorf für die Idee der *Relaxed Alignment Technology*.

Weitere Personen waren an der inhaltlich-materiellen Erstellung der vorliegenden Arbeit nicht beteiligt. Insbesondere habe ich hierfür nicht die entgeltliche Hilfe von Vermittlungs- bzw. Beratungsdiensten (Promotionsberater oder andere Personen) in Anspruch genommen. Niemand hat von mir unmittelbar oder mittelbar geldwerte Leistungen für Arbeiten erhalten, die im Zusammenhang mit dem Inhalt der vorgelegten Dissertation stehen.

Die Arbeit wurde bisher weder im In- noch im Ausland in gleicher oder ähnlicher Form einer anderen Prüfungsbehörde vorgelegt.

Die geltende Promotionsordnung der Physikalisch-Astronomischen Fakultät ist mir bekannt.

Ich versichere ehrenwörtlich, dass ich nach bestem Wissen die reine Wahrheit gesagt und nichts verschwiegen habe.

Jena, den January 22, 2015